DETERMINATION OF MAXIMUM STRESSES AND FACTORS OF SAFETY IN A SIMPLE LANDING GEAR MECHANISM DURING RETRACT AND LANDING

Prepared for:

Professor McGrann
ME 481, Computer Aided Engineering
Watson School of Engineering, Binghamton University

Prepared by:

Matthew Grenier

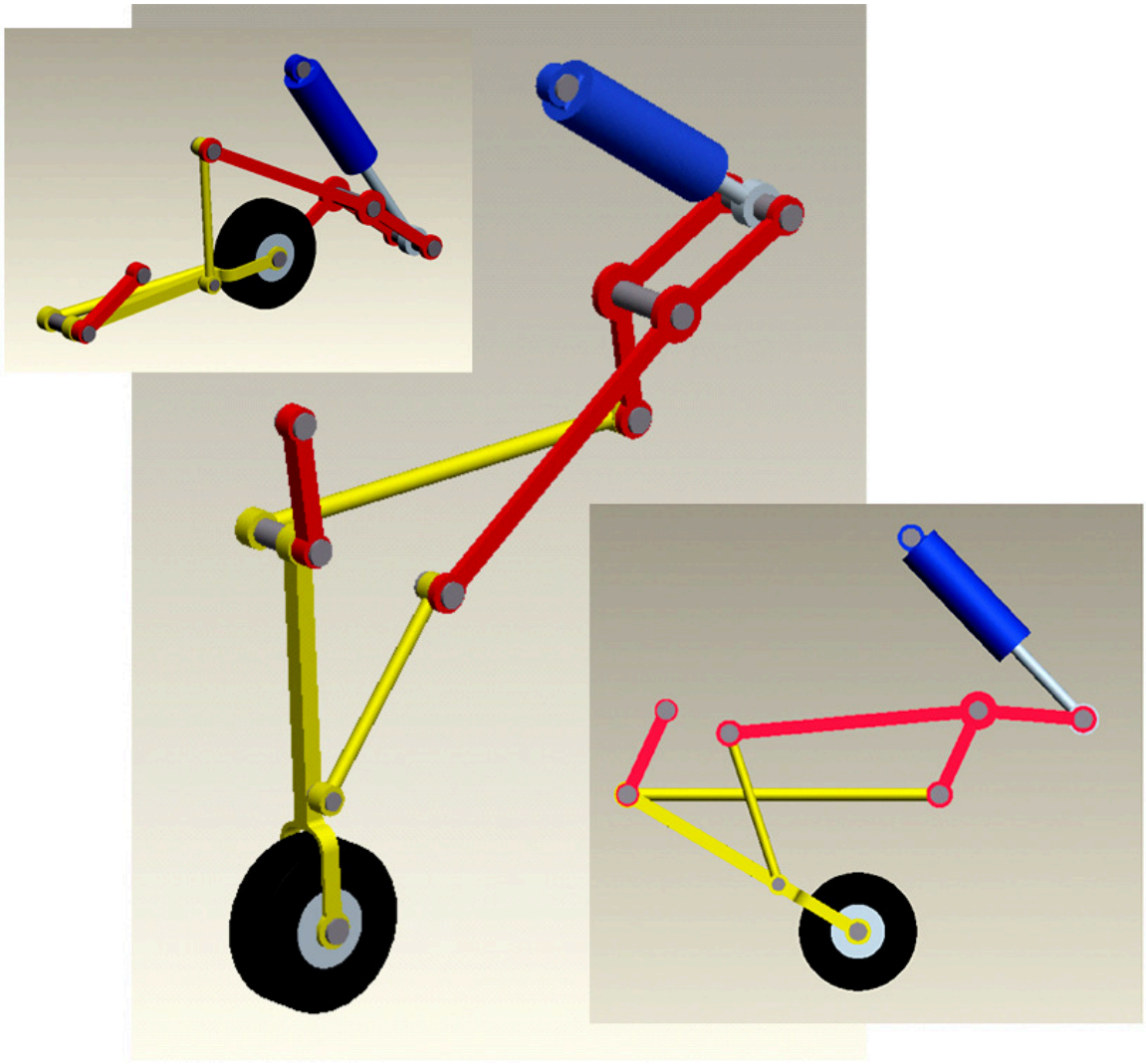

December 6, 2008

TABLE OF CONTENTS

LIST OF ILLUSTRATIONS **1**
EXECUTIVE SUMMARY **2**
INTRODUCTION **3**
Project Description 3
Project Scope 3
SIMULATION MODEL **4**
Landing Gear Design 4
Material Properties 5
Pin Connections 6
Piston Driver 7
DATA COLLECTION **9**
Dynamic Gear Retract Simulation 9
Gear Retract FEA 13
Static Landing Simulation 18
Landing FEA 20
DATA VERIFICATION **21**
Acceleration Verification 21
Stress Verification 28
CONCLUSIONS **32**
Factors of Safety 32
Recommendations 33
REFERENCES **34**
APPENDIX A-1: DESIGN DRAWINGS **36**
APPENDIX A-2: PIN CONNECTION REACTION FORCES **56**
APPENDIX A-3: GEAR RETRACT FEA RESULTS **66**
APPENDIX A-4: LANDING FEA RESULTS **74**
APPENDIX A-5: ACCELERATION VERIFICATION MATLAB CODE **82**

LIST OF ILLUSTRATIONS

Figures

Figure 1 – Configuration Provided 4
Figure 2 – Mechanism Created 4
Figure 3 – Pin Connections 6
Figure 4 – Piston Position vs Time 7
Figure 5 – Pin Connections at Pin E 9
Figure 6 – Connection E1 Reaction Measures 10
Figure 7 – Connection Reactions (Pin E) 11
Figure 8 – Magnitude of Net Reaction Vectors (Pin E) 12
Figure 9 – FEA Constraints and Loads on Pin E 14
Figure 10 – FEA Results (Pin E) 15
Figure 11 – FEA Constraints (Pins A and H) 17
Figure 12 – FEA Constraints (Pin D) 17
Figure 13 – FEA Constraints (Pin B) 17
Figure 14 – Landing Gear Deployed and Retracted 21
Figure 15 – Piston Retracted and Deployed with Rotation of Link CDFG 22
Figure 16 – Piston Dimensions 23
Figure 17 – Link CDFG Unit Vectors 24
Figure 18 – Verification Positions 25
Figure 19 – Velocity Measured in Pro/Mechanism 26
Figure 20 – Velocity Calculated in MATLAB 26
Figure 21 – Acceleration Measured in Pro/Mechanism 27
Figure 22 – Acceleration Calculated in MATLAB 27
Figure 23 – Normal Stress in Z Direction 28
Figure 24 – Shear Force and Bending Moment Diagrams for Pin B 29
Figure 25 – Pin B Idealization Cutout 30
Figure 26 – Pin B Stress Verification FEA 30
Figure 27 – ZZ Normal Stress vs Z Position Along Pin B Axis* 31

Tables

Table 1 - Material Properties 5
Table 2 – Maximum Pin Stresses (Gear Retract) 16
Table 3 – Reaction Components (Landing) 19
Table 4 – Net Reaction Magnitudes (Landing) 19
Table 5 – Maximum Pin Stresses (Landing) 20
Table 6 – Pin Factors of Safety (Gear Retract and Landing) 32

EXECUTIVE SUMMARY

The project presented in this report required that a simple landing gear mechanism be designed in accordance with the sketches and configuration constraints provided by Professor McGrann. A model of the landing gear mechanism was created in *Pro/Engineer* and both a dynamic gear retract simulation and a static landing simulation were carried out. The scope of the project was limited entirely to the determination of maximum stresses and the subsequent factors of safety for the pins joining the various links of the landing gear mechanism.

The dynamic gear retract simulation was carried out in *Pro/Mechanism* and involved controlling the movement of the landing gear piston using a position-controlling servo motor. The static landing simulation was carried out in *Pro/Mechanism* and involved applying an approximated landing force for an F-16 Fighting Falcon to the bottom of the landing gear tire while the mechanism was fixed in its deployed state. The approximated landing force applied was 194,000 pounds. In both simulations the connection reaction forces at each pin were measured and plotted (dynamic simulation) or tabulated (static simulation).

Finite Element Analysis was performed in *Pro/Mechanica* to determine the maximum stresses on each pin of the landing gear mechanism. The maximum forces measured in *Pro/Mechanism* were used as the loads applied to the pins in *Pro/Mechanica*. *Von Mises* stresses were displayed from the FEA results and allowed the multidimensional stress states of the pins to be compared to the yield tensile strength of AISI 4340 steel.

The maximum stress observed during the retract of the landing gear was 1663 lbf/in^2 on Pin E while the maximum stress observed during landing was 2345000 lbf/in^2 on Pin J. To evaluate the likelihood that the pins in the landing gear mechanism would fail in response to the maximum stresses observed the factor of safety for each pin was calculated. Based on the factors of safety calculated from the dynamic gear retract simulation it was apparent that the design of the landing gear mechanism was adequate for retracting the landing gear at the rate imparted by the position-controlling servo motor. The lowest factor of safety calculated for retracting of the landing gear was 135 for Pin E while the highest was 2715 for Pin A.

The factors of safety calculated from the static landing simulation were more troubling. Pins E and J had factors significantly less than one, which indicated that they yielded in response to the landing force applied to the bottom of the tire. Based on the shock loading of the landing gear and the need to endure repeated landings 10 was recommended for the factor of safety. This factor was also recommended given that 1) the total cost of an F-16 Fighting Falcon and payload could easily exceed 20 million dollars and 2) considerable harm could be caused to the pilot or others on the ground should the front landing gear collapse during landing.

Finally, it was recommended that Pins A, D, E, F, G, and J all be redesigned to achieve the recommended factor of safety and provide adequate assurance that the pins will not fail during landing. It was suggested that this be achieved by increasing the typical diameter of the pins. It was also recommended that more extensive redesign take place in order to reduce stress concentrations, especially on Pins D, E, G, and J, and that a shock absorber be incorporated to reduce the stresses on the pins.

INTRODUCTION

This report presents the design of a landing gear mechanism and the analysis of motion and stress in that mechanism. This introduction provides a description of the project and its scope.

Project Description

The project was presented by Professor McGrann of the Watson School of Engineering at Binghamton University as part of the course ME 481, *Computer Aided Engineering*. The project required that a simple landing gear mechanism be designed in accordance with the sketches and configuration constraints provided by Professor McGrann. A model of the landing gear mechanism was created in *Pro/Engineer Wildfire 3.0* for the purpose of dynamically simulating the gear retract motion and analyzing the stresses on the pins in the mechanism. The steps followed during the project are presented in the following list;

1. Create all components of the landing gear mechanism using the provided sketches
2. Assemble the components, modifying the design of each component as necessary to prevent interferences and obey configuration constraints (use subassemblies for the piston and cylinder as well as for the tire and wheel)
3. Look up material properties and assign to all components
4. Build a dynamic simulation model in *Pro/Mechanism* to determine the forces at each pin for the complete range of piston movement, verify the results for one pin by verifying the acceleration of that pin using mathematical calculation
5. Perform Finite Element Analysis (FEA) in *Pro/Mechanica* to determine the maximum stresses on each pin, verify the results for one pin using mathematical calculation
6. Approximate the peak vertical force expected to occur on the bottom of the tire during the landing of a United States Air Force F-16 Fighting Falcon
7. Build a static simulation model in *Pro/Mechanism* to determine the forces at each pin resulting from the peak vertical force experienced during landing
8. Perform Finite Element Analysis (FEA) in *Pro/Mechanica* to determine the maximum stresses on each pin resulting from the peak vertical force experienced during landing
9. Calculate factors of safety for each pin for both the dynamic gear retract simulation and the static landing simulation

Project Scope

The scope of the project was limited entirely to the determination of maximum stresses and factors of safety for the pins joining the various links of the landing gear mechanism. In the dynamic simulation, the stresses on the pins were the result of the components having mass and being accelerated during the movement of the driving piston as the landing gear was retracted. In the static analysis, the stresses on the pins were the result of a peak landing force being applied to the bottom of the tire. Other considerations, such as the stress on the links, deformation of the links, or deformation of the pins, were outside the scope of the project.

SIMULATION MODEL

This section discusses the design of the landing gear mechanism and the development of the model used for the dynamic gear retract simulation and the static landing simulation.

Landing Gear Design

The components of the landing gear mechanism were created using sketches and configuration constraints provided by Professor McGrann. The provided configuration of the landing gear mechanism is illustrated in Figure 1. The constraints that accompanied Figure 1 are presented in the following list;

1. The location of the ground points A, D, and H cannot be altered
2. The dimensions of the tire and wheel cannot be altered
3. The vertical distance from point A to point J cannot be altered
4. The distance from point A to E must be the same as the distance from point D to F
5. The distance from point E to F must be the same as the distance from point A to D
6. The overall width of the assembly should be equal to approximately two widths of the tire

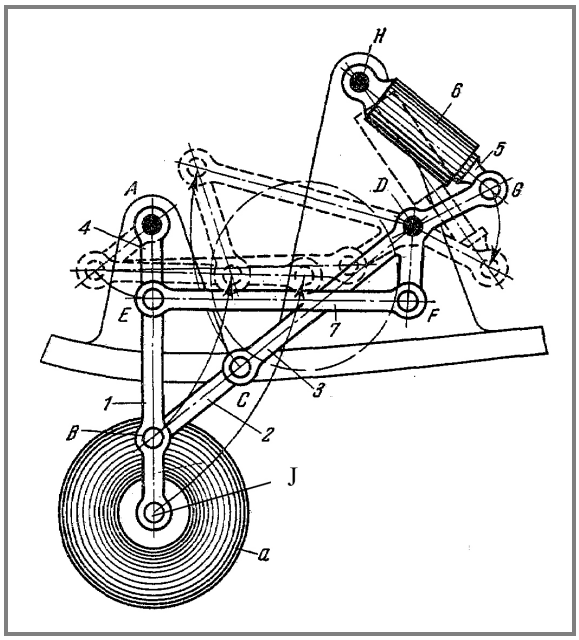

Figure 1 – Configuration Provided

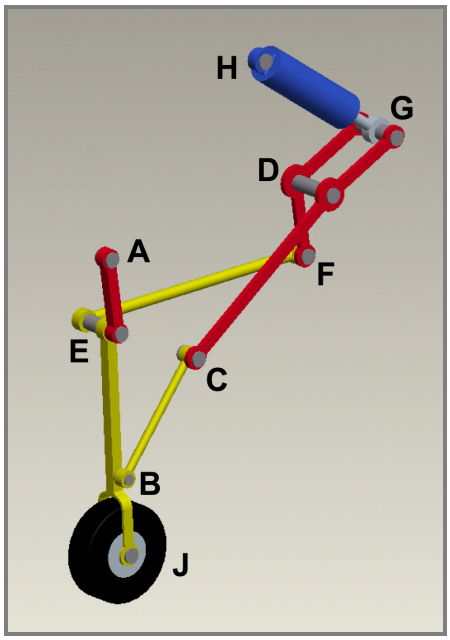

Figure 2 – Mechanism Created

The landing gear mechanism created from the provided sketches and configuration constraints is illustrated in Figure 2. The design of each landing gear component was modified as the assembly was created to prevent interferences. The links in the landing gear mechanism were named by the line segment convention (Link 4 in Figure 1 is called Link AE in Figure 2). It is important to note that there were two separate links (FDG and CDG) intersecting Pin D. Both of these links rotated simultaneously about Pin D and were therefore collectively referred to as Link CDFG. For details concerning the landing gear design refer to *Appendix A-1: Design Drawings*, which includes an exploded assembly view, bill of materials, and detail drawings of all the landing gear components.

Material Properties

The material properties for the landing gear components are listed in Table 1. The properties listed include density, ultimate tensile strength, yield tensile strength, modulus of elasticity, and Poisson's ratio. Density and yield tensile strength were the properties most significant to the project. The density gave mass to the landing gear components which, when accelerated during the piston movement, applied forces to the pins. Because it was not desirable for any of the pins to yield, the yield tensile strength was used in the calculation of factor of safety as the maximum allowable stress. Because the pins were the only components for which factor of safety was calculated the yield tensile strength of the AISI 4340 steel is the most significant yield strength listed in Table 1. To determine which components of the landing gear are composed of which materials refer to the bill of materials in *Appendix A-1: Design Drawings*.

Table 1 - Material Properties

Material	$\rho \cdot 10^4$	TS	σ_Y	E	v_p
Steel AISI 4340	7.34544	269	225	28400	0.300
Aluminum 6061-T651	2.52646	45	40	10000	0.330
Stainless Steel 316L-SS	7.47645	809	42.1	28000	0.250
Solution Styrene Butadiene Rubber (S-SBR)	4.00656	----	----	----	----
Air	.022864	----	----	----	----

$\boldsymbol{\sigma_Y}$ = Yield Tensile Strength (ksi) – **E** = Modulus of Elasticity (ksi) – $\boldsymbol{v_p}$ = Poisson's Ratio
$\boldsymbol{\rho}$ = Density ($lbf \cdot s^2/in^4$) – **TS** = Ultimate Tensile Strength (ksi)

Material properties for the steel, aluminum, and stainless steel in Table 1 were obtained from *MatWeb.com*. The density of the S-SBR was not obtained directly via research. The density was calculated using the properties of the landing gear tire. Using the *Goodyear Aircraft Tire Data Book* the weight of the tire (part number 461B-3563-TL) was found to be 16.1 pounds. This desired weight of the tire, and the known volume of the tire as measured in *Pro/Engineer*, were used to calculate the necessary density of the S-SBR.

Air appears as a material in Table 1 because a solid component was created in Pro/Engineer to represent the volume of air inside the landing gear tire. According to the *Aircraft Tire Data Book* the rated pressure of the tire is 315 lbf/in^2. It was decided that the density of the air would be calculated for pressure and temperature conditions of 300 lbf/in^2 and 70°F respectively. The ideal gas equation $pv=RT$ and R, the gas constant for air, were obtained from *Fundamentals of Engineering Thermodynamics* by Moran and Shapiro. Handling unit conversions carefully allowed the specific volume (v) of air to be calculated for the stated conditions. Inverting the specific volume yielded the density. It was found after applying the material properties that the air volume added a relatively insignificant one pound to the overall weight of the tire.

Pin Connections

The pins and links of the landing gear mechanism were assembled using *pin connection* constraints. This type of constraint was used because it indicated to *Pro/Mechanism* the presence of a *revolute joint* with one rotational degree of freedom. This means that *Pro/Mechanism* understood that each link was only allowed to rotate about the pins it was attached to and could not move sideways along the shafts of those pins.

The pin connections that made up the landing gear mechanism are named and indicated in Figure 3. Multiple connections at the same pin were denoted using numbers. For example, there were three connections named E1, E2, and E3 all at Pin E. It is important to note that there was only one connection at each of the pins A, B, and H. There was only one connection at Pins A and H because they were grounded to the frame of the aircraft. There was only one connection at Pin B because it was fixed to Link EBJ. In order to measure the forces at each pin it was necessary to measure the reaction forces at each one of the connections shown in Figure 3. This will be discussed in detail in the section *Dynamic Gear Retract Simulation*.

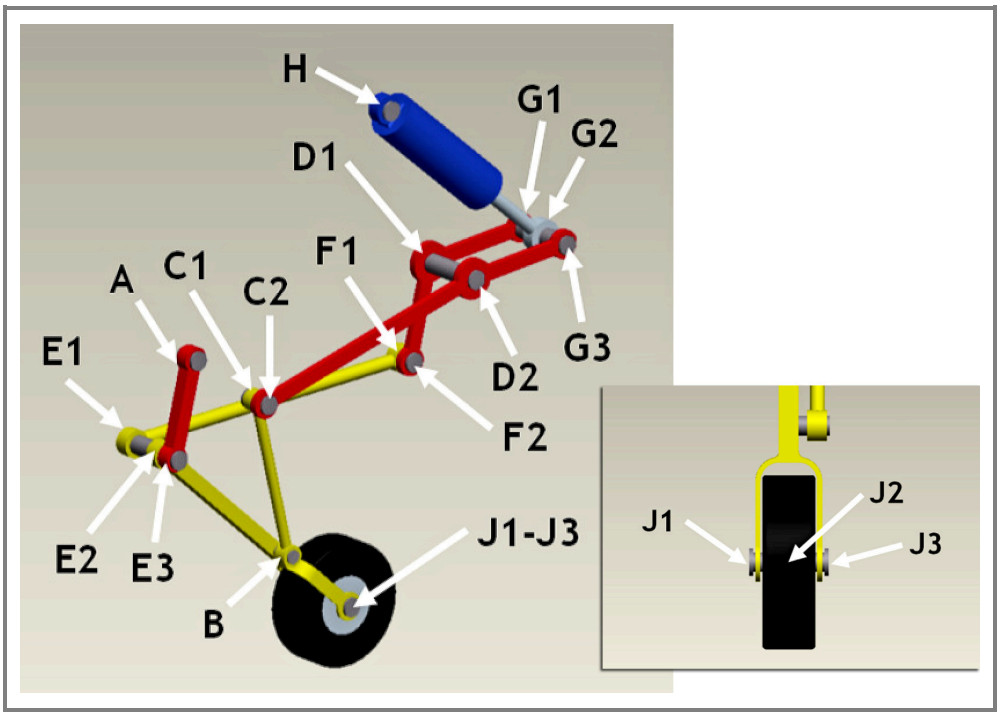

Figure 3 – Pin Connections

It is important to note that *pin connection* constraints were not used within the subassemblies for the piston and cylinder or for the tire, wheel, and air. Generic *mate* and *align* constraints were used within the tire subassembly. The *pin connection* constraint named J2 in Figure 3 was used to connect the tire subassembly to Pin J. The constraint used in the piston and cylinder subassembly will be described in detail in the section *Piston Driver*.

Piston Driver

The source of the landing gear movement in the dynamic gear retract simulation was the movement of the piston inside the cylinder. The piston and cylinder were joined using a *slider* constraint within the piston subassembly. The *slider* constraint was used because it indicated to *Pro/Mechanism* the presence of a *prismatic joint* with one linear degree of freedom. This means that *Pro/Mechanism* understood that the piston could move back and forth within the cylinder but could not rotate. The minimum and maximum limits on the piston position were set to correspond to the deployed and retracted states of the landing gear mechanism.

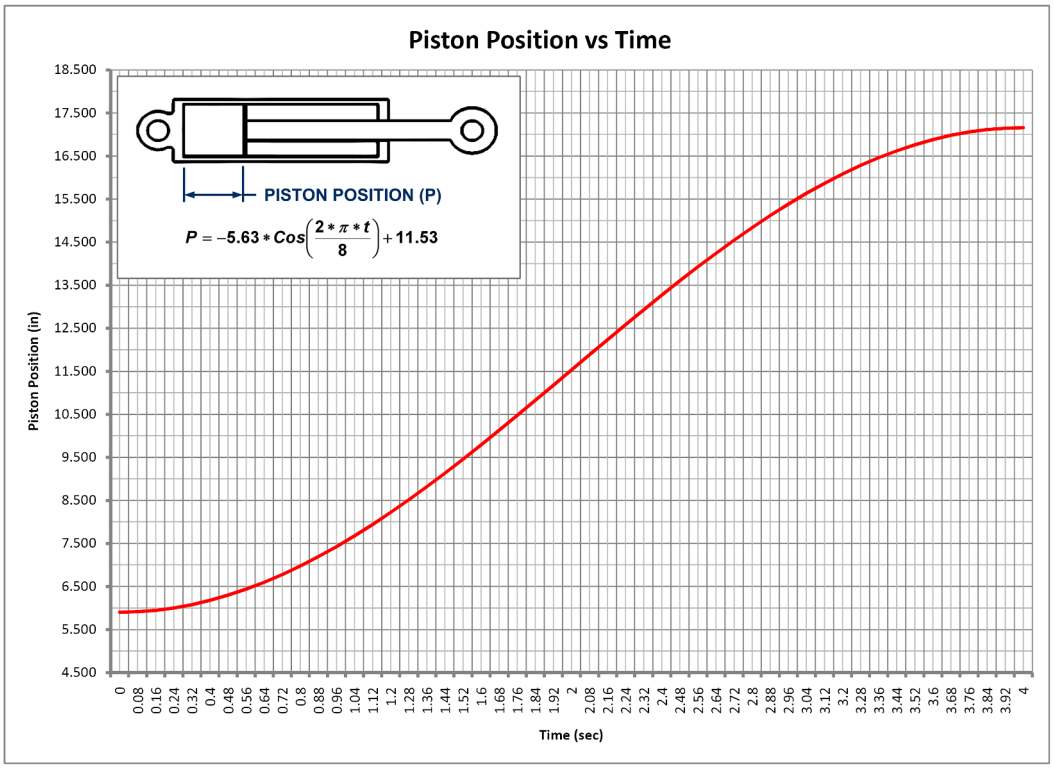

Figure 4 – Piston Position vs Time

To control the movement of the piston in *Pro/Mechanism* a position-controlling servo motor was assigned to the slider constraint between the piston and cylinder. The servo motor was assigned a cosine drive profile almost identical to that shown in Figure 4. It is important to note that the drive equation in *Pro/Mechanism* was slightly different than that shown in Figure 4 because the references used to measure the piston position were slightly different than those indicated in Figure 4. This means that in *Pro/Mechanism* the drive profile was the same as in Figure 4 except that it was translated upward slightly. Regardless of this fact, the cosine drive profile and equation depicted in Figure 4 are correct given the accompanying illustration of how the piston position was measured.

A position-controlling servo motor was selected because the position of the piston was the most straightforward attribute of the piston to control. The cosine drive profile in Figure 4 was selected because the piston velocity (the derivative of the piston position) starts at zero, peaks halfway through the piston movement, and ends at zero. The start and end of the drive profile in Figure 4 represent the minimum (retracted state) and maximum (deployed state) positions of

the piston in the cylinder. A time of four seconds was chosen for the entire gear retract motion. It is important to note that the retracted state of the piston corresponds to the deployed state of the landing gear mechanism. Similarly, the deployed state of the piston corresponds to the retracted state of the landing gear mechanism. This is illustrated in Figure 14.

To ensure adequate understanding of the drive equation in Figure 4 its derivation will be described. The 5.63 term in the equation represents the amplitude of the cosine function and is equal to half the distance between the minimum and maximum values that the function reaches. The amplitude 5.63 was chosen because it is equal to half the difference between the minimum and maximum piston positions. With the proper amplitude achieved it was necessary to translate the entire cosine function upward by 11.53, which is equal to the amplitude plus the minimum piston position. This translation ensured that the cosine function would never drop below the minimum piston position and never rise above the maximum piston position.

When the cosine function has a positive amplitude it starts at its maximum value. When the cosine function has a negative amplitude it will start at its minimum value. Both of these statements assume that the cosine function has not been phase shifted. To make the drive profile start at the minimum piston position at time zero the 5.63 amplitude was negated and the phase shift was made to be zero. Phase shift refers to the translation of the cosine function left and right across the time axis. For there to be no phase shift the constant added to the $2\pi t/8$ term inside the cosine function had to be zero.

All terms of the drive equation have been established except for the period of the cosine function, or how much time it takes the cosine function to complete one cycle. If the term inside the cosine function were t instead of $2\pi t/8$ the function would take 2π seconds to complete one cycle. The term multiplying t has the effect of squeezing the cosine cycle when it is greater than one or of expanding the cosine cycle when it is less than one. It was desired that the drive profile complete one half cycle in 4 seconds, or one full cycle in 8 seconds. Because 8 seconds is more than 2π seconds the cosine cycle had to be expanded to achieve the desired period. This means the term multiplying t had to be less than one. The relationship between the period and the term multiplying t is given by the following; when 2π is divided by the term multiplying t the result is the period. Using this relationship the term multiplying t was calculated to be $2\pi/8$, which is less than one. This completes the derivation of the drive equation which creates the drive profile in Figure 4. This equation will be referred to in the *Acceleration Verification* section because it was used during the project to derive an equation for the relationship between the movement of the piston and the rotation of Link CDFG.

It was stated in the *Project Description* that a dynamic simulation model was created to determine the forces at each pin for the complete range of piston movement as well as a static simulation model to determine the forces at each pin resulting from the peak vertical force experienced during landing. In the dynamic model the piston was driven according to the drive profile in Figure 4 and the forces at each pin were determined over the entire range of movement (resulting in plots of force versus piston position). In the static model the same forces were measured but the piston position was fixed in its retracted state and the landing force was applied to the bottom of the tire. This resulted in a table of force values for that fixed position of the piston, rather than a plot of force versus piston position. This will be discussed further in the section *Static Landing Simulation.*

DATA COLLECTION

This section discusses the collection of force and stress data in *Pro/Mechanism* and *Pro/Mechanica* for the retract and landing simulations. The simulation model was fully constructed by creating the individual components of the landing gear mechanism, assigning material properties, connecting the pins and links with pin connections, and establishing a position-controlling drive profile for the piston. Simulations were then run in *Pro/Mechanism* to determine forces at the connections and in *Pro/Mechanica* to determine maximum stresses.

Dynamic Gear Retract Simulation

As mentioned in the section *Pin Connections*, in order to measure the forces on each pin it was necessary to measure the reaction forces at each of the 18 pin connections in the simulation model. Reaction forces are the equal and opposite forces experienced at a connection by the pin and the link at that connection. For the pins at which there were more than one connection it was necessary to consider the effects of the reaction forces at each one of the connections. Pin E will serve as an example of how reaction forces were measured and how the data was interpreted during the dynamic gear retract simulation. Pin E and the three links that terminate at Pin E, resulting in connections E1, E2, and E3, are shown in Figure 5. The design of Pin E is evident in Figure 5 in that it was capped on either end to prevent the links from sliding off the pin. Pin E also incorporated a spacer between two of the links by having an enlarged cross section between those links. While these design details were not important for measuring reaction forces they did have an impact on the stresses observed.

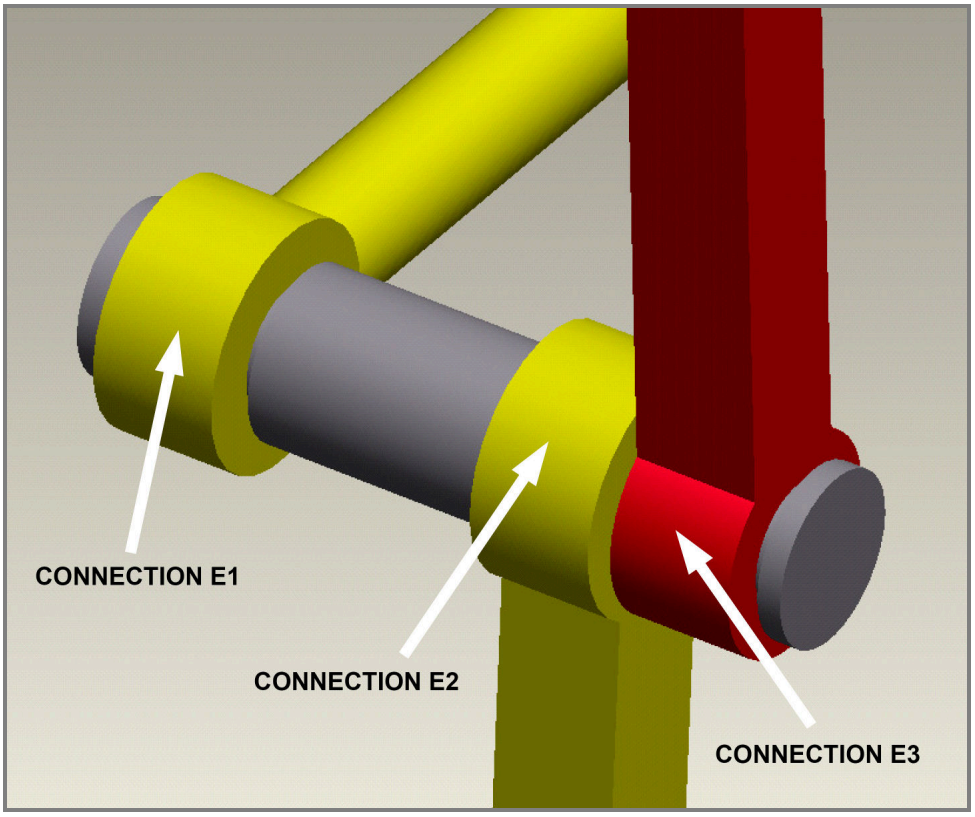

Figure 5 – Pin Connections at Pin E

While preparing for the *Pro/Mechanism* simulation it was important to determine exactly how reaction forces should be measured at each of the pin connections. In *Pro/Mechanism* it is possible to measure the magnitude of the net reaction force or to separately measure the X and Y components of that net reaction force. In deciding which measurements to take it was important to remember that force is a vector and consists of both magnitude and direction. When the magnitude of a net reaction force was measured it lacked information about the direction in which that net reaction force was acting. This was satisfactory for a pin at which there was only one connection because there was only one reaction force at that pin. When considering a pin at which there were multiple reaction forces, such as Pin E, it was imperative to know the directions in which each of the reaction forces were acting because those forces might add or subtract from one another. The conclusions were that 1) at pins at which there are only one connection a measure of net reaction force is satisfactory, and 2) at pins at which there are multiple connections measures of X and Y reaction forces are necessary.

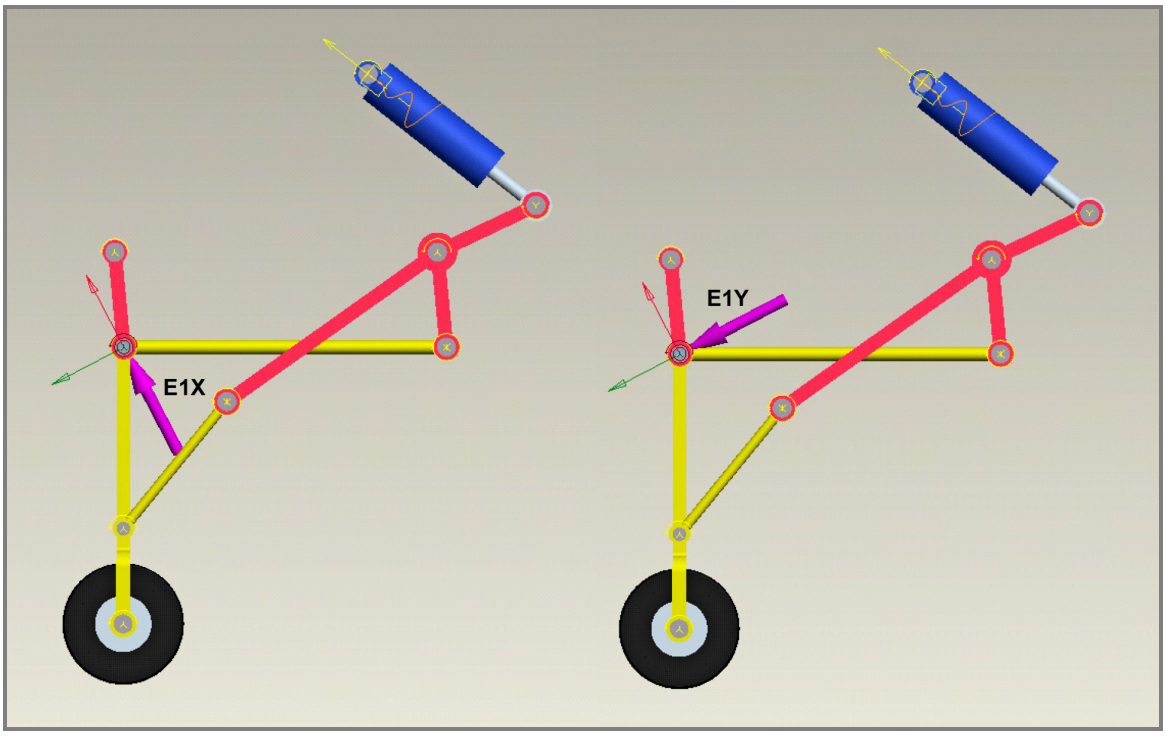

Figure 6 – Connection E1 Reaction Measures

To create the connection reaction measures in *Pro/Mechanism* a pin connection, the type of measurement (net magnitude, X component, Y component), and the coordinate system to measure with respect to were specified. The body on which to measure the forces exerted was also specified. Figure 6 illustrates measures created for the X and Y reaction forces at connection E1. The magenta arrow in Figure 6 indicates the positive direction. Both the X and Y reaction forces at connection E1 were measured with respect to the coordinate system of Pin E. This means that as the landing gear mechanism moved the E1X and E1Y reaction forces were always measured with respect to the same coordinate system. Care was taken to make sure that the magenta arrows for E2X and E3X pointed in the same direction as that for E1X, and similarly for the Y directions. Similar reaction measures were established for all of the other pin connections in the simulation model.

In a couple cases the magenta arrows for two reaction measures (such as for F1Y and F2Y) pointed in opposite directions. This was noted and all of the force values for one of the two measures were negated after the simulation was run. Running the simulation simply required creating an analysis that used the servo motor described in the section *Piston Driver* and an initial condition in which the landing gear was fully deployed. The simulation retracted the landing gear according to the drive profile in Figure 4 and the resulting tables of connection reaction force data were exported to Microsoft *Excel* and plotted.

Two types of plots were created from the reaction force data exported from *Pro/Mechanism*. The first type of plot was a single plot containing each of the components for each of the connections on a single pin. Figure 7 illustrates a plot of connection reactions for Pin E. Note that there are six separate reaction force curves, an X and Y component for each of the three connections E1, E2, and E3. At the request of Professor McGrann, all of the reaction forces were plotted versus the position of the piston rather than versus time. The callouts in Figure 7 referring to FEA loads will be ignored presently because they are related to Figure 8.

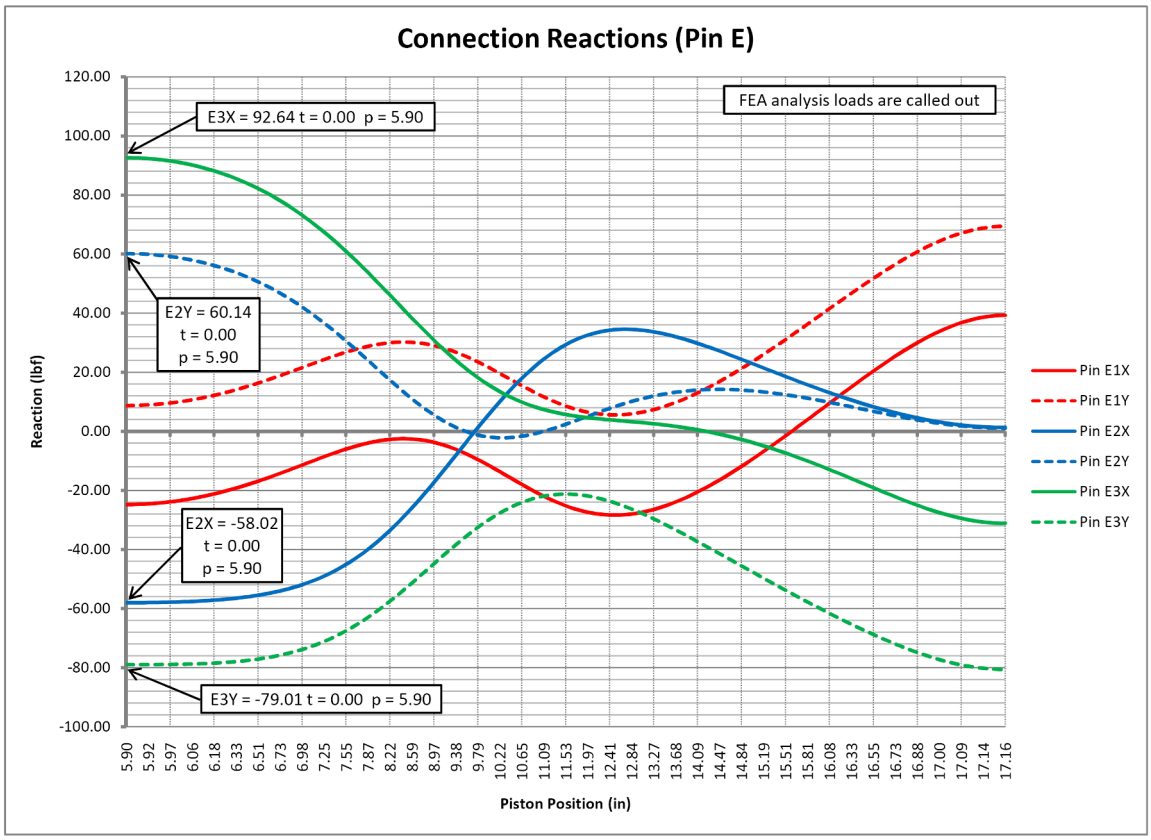

Figure 7 – Connection Reactions (Pin E)

The second type of plot created from the reaction force data was a single plot containing the net reaction forces for each of the connections on a single pin. Figure 8 illustrates a plot of the magnitude of the net reaction vectors for Pin E. The data presented in Figure 8 was created from the data presented in Figure 7. For example, a value for E1 in Figure 8 was created by squaring a value of E1X, squaring a value of E1Y, adding them together, and taking the square root. This procedure is the calculation of the magnitude of the vector resulting from the addition of the E1X and E1Y component vectors.

Though Figure 8 does not provide insight concerning the directions in which the net reaction forces are acting, it does indicate where the quantity of force acting on Pin E at each of the three connections E1, E2, and E3 is at a maximum.

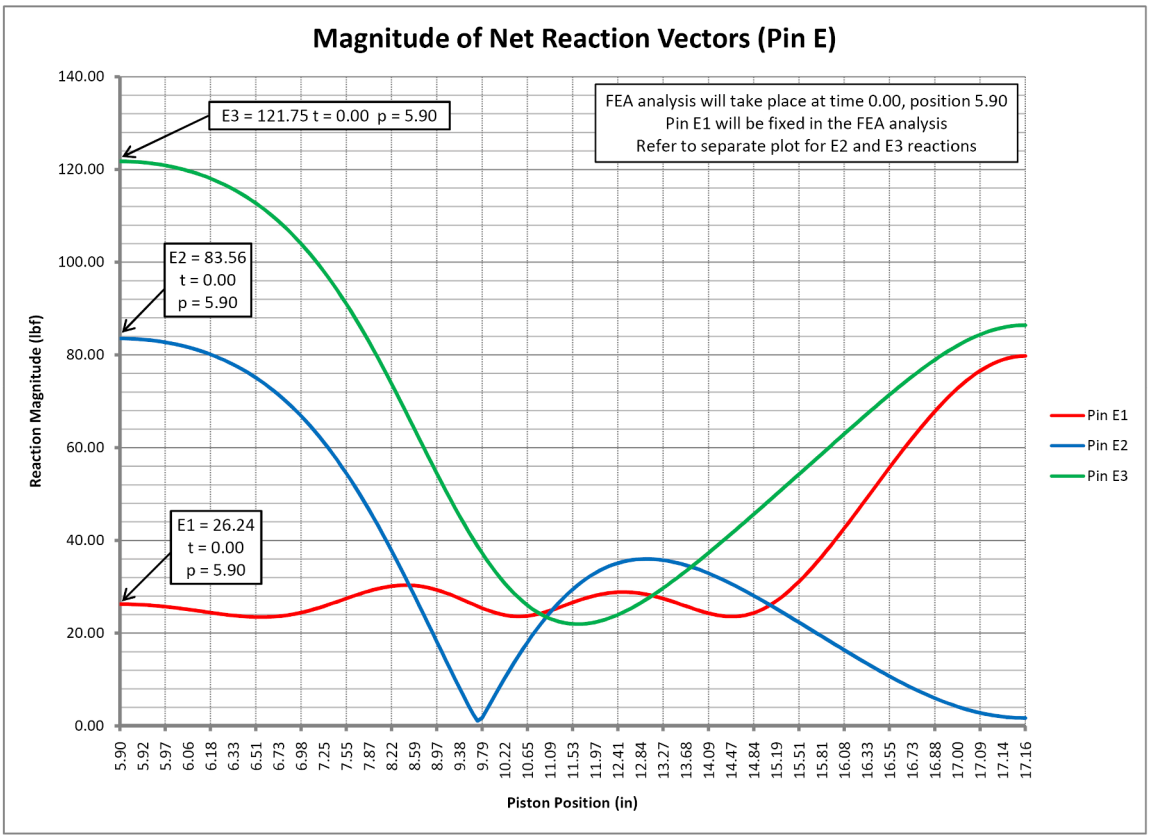

Figure 8 – Magnitude of Net Reaction Vectors (Pin E)

With the reaction force data summarized in two types of plots it was possible to determine at what point the stress analysis should take place for each pin. Because the purpose of the stress analysis was to determine the maximum stresses the point selected for each pin had to correspond to the maximum forces experienced by that pin. By analyzing Figure 8 it was apparent that the stress analysis for Pin E needed to take place when the piston position was at its minimum or when the time was equal to zero. The values of the three net reaction forces were called out at this point, as shown in Figure 8. Even though the E1 net reaction force was not at its maximum at this point the E2 and E3 net reaction forces were both at their maximum values. Because the stress analysis needed to take place at *one* point (force values could not be picked from different points on the plot) the point indicated on Figure 8 was the ideal point for Pin E to undergo stress analysis.

It is important to note that Figure 8 was only utilized to select the point at which the stress analysis would take place, it was not utilized to determine the values of the forces that were applied during the stress analysis. The forces that were applied to Pin E during the stress analysis are shown called out in Figure 7 at the same point shown in Figure 8. The values of the connection reactions in Figure 7 were utilized for the stress analysis because the directions of those reaction forces were known at each connection.

Note that Figure 8 indicates that connection E1 was fixed in the stress analysis and that in Figure 7 there are no callouts for the E1X or E2X connection reactions. This is related to how the stress analysis was carried out and is explained in the section *Gear Retract FEA.*

The previous discussion utilized Pin E as an example of how reaction forces were measured and how the data was interpreted. Pin E will continue to serve as an example in the discussion on stress analysis. For the force plots of connection reactions and net reaction magnitudes of all the pins refer to *Appendix A-2: Pin Connection Reaction Forces*. Remember that for pins A, B, and H only the net reaction magnitude was measured because there was only one connection at each of those pins. There is only one plot in the appendix for these three pins.

Gear Retract FEA

As stated in the *Project Description*, data collection continued by performing Finite Element Analysis in *Pro/Mechanica* (using the reaction forces measured in *Pro/Mechanism*) to determine the maximum stresses on each pin of the landing gear mechanism.

As presented in ME 481, *Computer Aided Engineering*, FEA is a numerical technique which represents a problem as a system of simultaneous algebraic equations and provides results as approximate values at a discrete number of points. The procedure in FEA is to divide a body into many smaller bodies that are joined at common points, surfaces, or boundaries, creating a mesh. The stress equations for each of the smaller bodies are combined and solved simultaneously for the entire body. The first mesh created in an FEA does not provide sufficient results. The mesh is typically refined over several passes until optimal results are achieved, a process called convergence.

To conduct an FEA in *Pro/Mechanica* a body must be both constrained and loaded. At least one displacement constraint must be applied to the body to allow it to resist movement when loads are applied. At least one load must be applied to the body for stresses to result. Displacement constraints or loads can be applied to portions of a surface, such as portions of a pin shaft, by defining *surface regions* and applying the constraints or loads to those regions. Figure 9 shows Pin E with three surface regions defined to represent the portions of the pin that were in contact with the three links that connect to Pin E (the surface regions are indicated by the red lines). The surface regions effectively represented the three pin connections E1, E2, and E3. Because Pin E was not in contact with any other components except at the pin connections one of the surface regions needed to be constrained. The reaction forces were then applied to the two surface regions that remained unconstrained.

Returning to Figure 8, it was stated that connection E1 was fixed in the Finite Element Analysis. This was decided because connection E1 had the smallest net reaction magnitude of the three connections at the point chosen for the FEA. The E1 surface region was fixed by applying a displacement constraint. This effectively eliminated the net reaction force at connection E1 and allowed the FEA to take place. Though eliminating the reaction forces at one connection was not favorable it can be argued that eliminating the net reaction force with the smallest magnitude reduces the possibility of adverse effects on the analysis results. Because connection E1 was fixed in the Finite Element Analysis Figure 7 does not include callouts for connection E1. The callouts on Figure 7 for connections E2 and E3 are the reaction forces that were applied to the E2 and E3 surface regions shown in Figure 9.

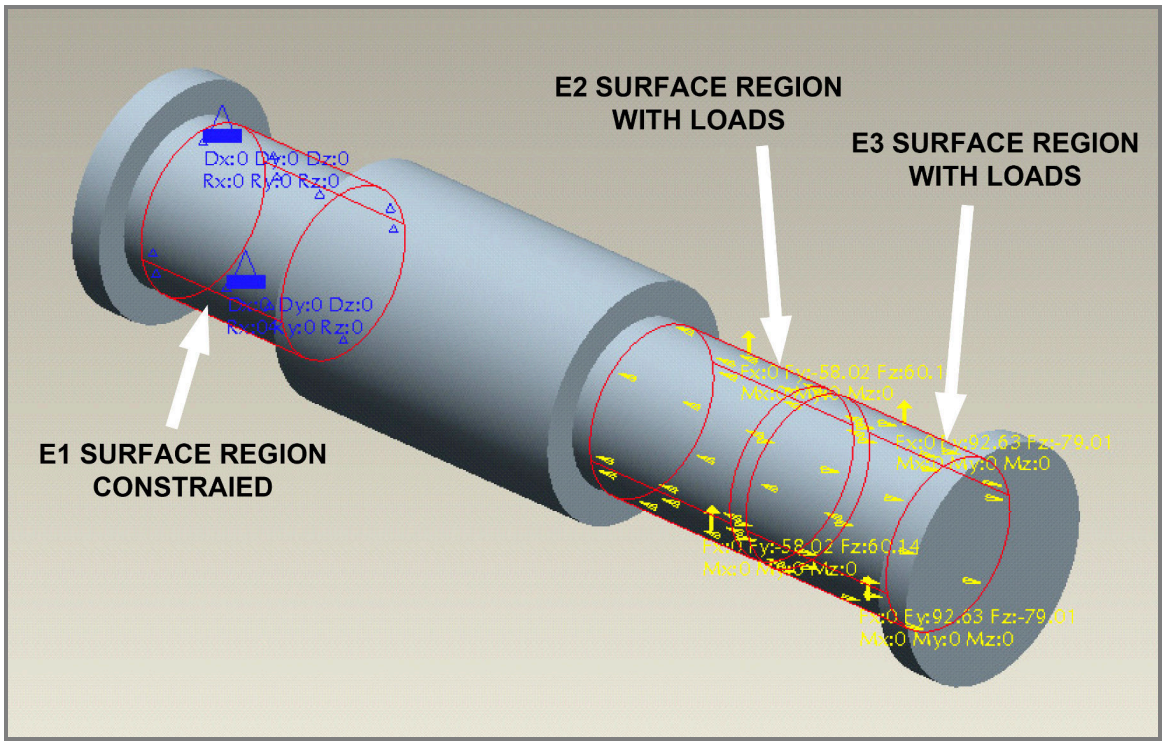

Figure 9 – FEA Constraints and Loads on Pin E

Application of the reaction forces to the E2 and E3 surface regions was straightforward. A distributed load was applied to each region that provided input boxes for the various components of the load. The components of the load in each direction were entered using the X and Y reaction forces from Figure 7. A quirk in *Pro/Engineer* meant that the X and Y reaction forces could not be entered as the X and Y components of the distributed load. By consulting the *Pro/Engineer* help it was revealed that even though the X and Y reaction measures in *Pro/Mechanism* were taken with respect to the coordinate system of the pin, the X and Y reaction measures did not necessarily correspond to the actual X and Y axes of the pin coordinate system. It was evident this mismatch had occurred with Pin E because the Z axis of the pin coordinate system was not the axial axis.

Though this mismatch occurred for nearly every pin, it simply meant that the X reaction forces had to be entered in the boxes for the Y components of the distributed loads, while the Y reaction forces had to be entered in the boxes for the Z components of the distributed loads. The components of the distributed loads were automatically combined and the total resulting loads were automatically distributed over the E2 and E3 surface regions, as shown in Figure 9.

With the displacement constraint and loads applied to Pin E it was possible to run the FEA. Before running the multi-pass FEA a quick check was performed to confirm that the analysis would run properly. The multi-pass FEA was prepared by setting the maximum number of mesh refinement passes to nine (the maximum allowed by *Pro/Mechanica*) and by setting the analysis to converge to within 10% on strain energy. This means that the FEA was set to calculate strain energy during each mesh refinement pass. When the calculated strain energy was within 10% of the previously calculated strain energy the analysis had converged and was complete. If the analysis did not converge after nine passes it was aborted.

Once an FEA is complete the stress results are most easily visualized using a fringe plot. A fringe plot uses a series of filled color regions to represent different ranges of values for the stress quantity being displayed. The stress quantity being displayed depends on which components of the stress are selected. In *Pro/Mechanica* it is possible to display principal stress, normal stress, shear stress, maximum shear stress, or *von Mises* stress.

It was mentioned in the section on *Material Properties* that the yield tensile strength (σ_Y) was used as the maximum allowable stress in the calculation of factor of safety. This means that the stress quantity displayed had to be appropriate for comparing the maximum stress with the yield tensile strength of the pins. Of all the stress quantities available the *von Mises* stress was the most appropriate for this purpose. The *von Mises* criterion was designed to compare multidimensional stress states to the stress state of a one-dimensional test specimen of the same material at yielding. The *von Mises* stress at a particular point is calculated using the principal stresses at that point. In short, this criterion and method of calculation was designed specifically for the application of comparing stress results with yield tensile strengths.

Figure 10 illustrates the fringe plot of *von Mises* stress for Pin E. The maximum stress value (1663 lbf/in^2) appeared at the top of the legend. The FEA results in Figure 10 also clearly illustrated how the design of Pin E impacted the maximum stress. Significant stress concentrations were observed at the boundary between the pin shaft and the enlarged cross section created to act as a spacer between the links at Pin E.

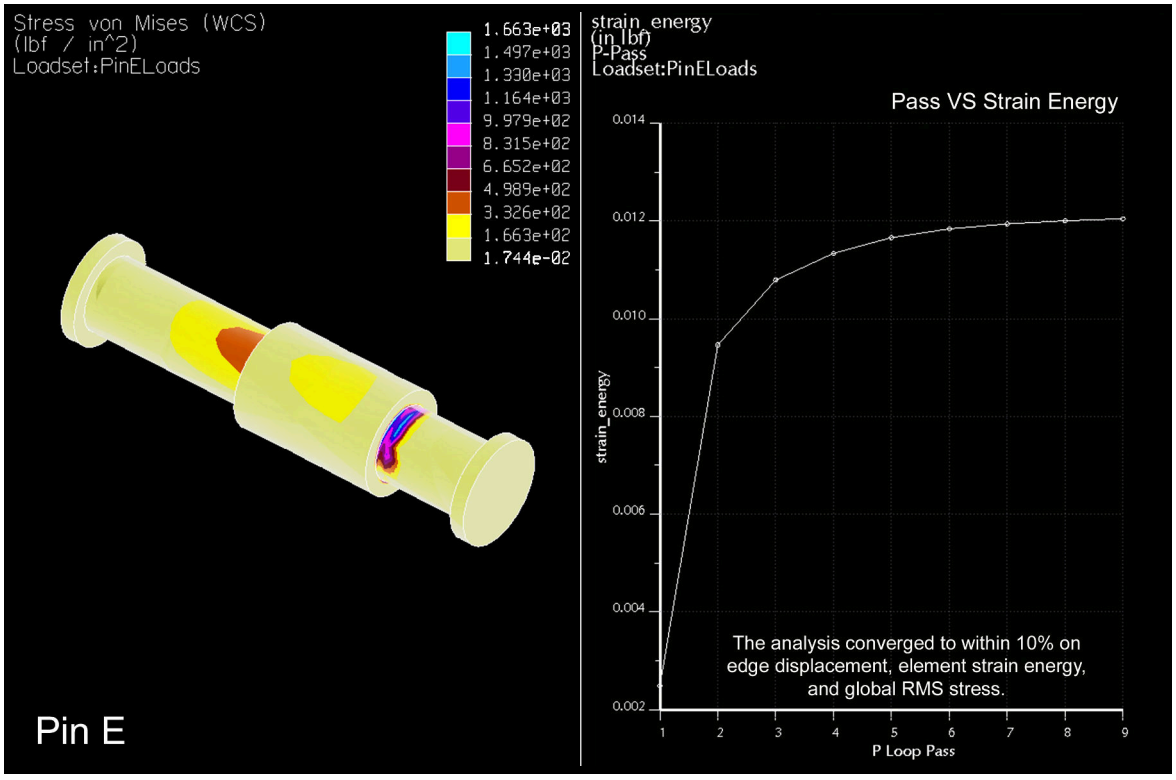

Figure 10 – FEA Results (Pin E)

A measure of strain energy versus the pass number accompanies the FEA results in Figure 10. From the curve it was apparent that the analysis converged because it leveled out around a particular value of strain energy as the number of passes increased. If the analysis did not converge the curve would have continued to grow as the value of strain energy continued to increase with each pass. Strain energy was used as the test for convergence because strain energy incorporates as many variables as possible. Because strain energy is equal to half the product of stress and strain both displacement and force are incorporated in its calculation.

Table 2 lists the maximum *von Mises* stresses obtained for each of the pins in the landing gear mechanism. FEA results for all the pins are located in *Appendix A-4: Gear Retract FEA Results*. Table 2 shows that the highest stresses were experienced by Pins E, J, and G in decreasing order of magnitude. The lowest stresses were experienced by Pins A, F, and B in increasing order of magnitude. The values contained in Table 2 were used to calculate factors of safety for each pin as will be described in the section *Factors of Safety*.

Table 2 – Maximum Pin Stresses (Gear Retract)

Pin	σ_{MAXR}
A	82.86
B	269.8
C	452.7
D	792.1
E	1663
F	236.8
G	1199
H	406.4
J	1354

σ_{MAXR} = Maximum *von Mises* stress (lbf/in^2)

The collection of pin stress data for retracting the landing gear has now been completed. Pin E served as an example for how constraints and loads were applied to the pins. All of the pins except for A, B, D, and H followed the example of Pin E. It was not possible to apply displacement constraints to Pins A, B, and H in the same way as they were applied to Pin E because there was only one connection at each of those pins. Pin D differs from the example of Pin E because it was one of the three pins grounding the landing gear to the frame of the aircraft. Pins A and H also grounded the landing gear to the frame of the aircraft.

Figures 12-13 illustrate the displacement constraints applied to Pins A, B, D, and H. The surfaces constrained in Figures 11 and 12 were assumed to be in complete contact with the frame of the aircraft and were thus made incapable of moving. Note in Figures 11 and 12 that there were displacement constraints applied to both sides of the pins. Pin B is shown in Figure 13 and was actually a part of Link EBJ. For the purposes of the analysis Pin B was modeled as a separate body and the end constrained as if it were fixed to Link EBJ. Note that Pin B could be idealized as a cantilever beam with a distributed load applied (the Pin B reaction force). For this reason Pin B was used to verify the FEA stress results in the section *Stress Verification*.

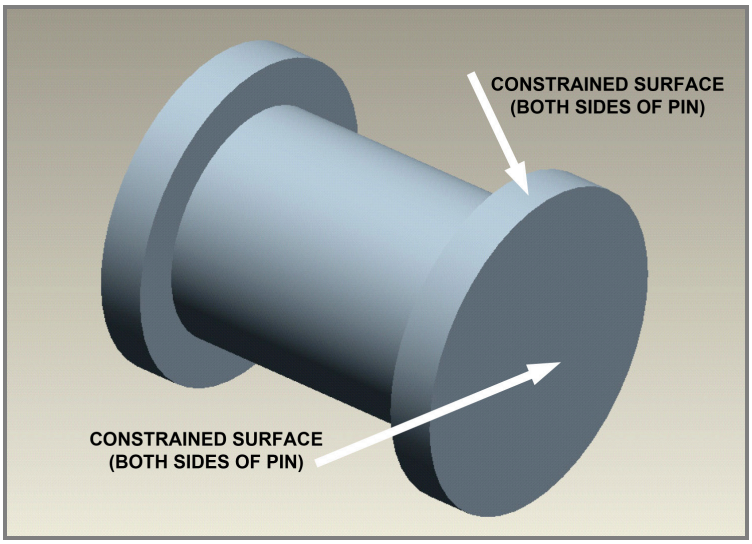

Figure 11 – FEA Constraints (Pins A and H)

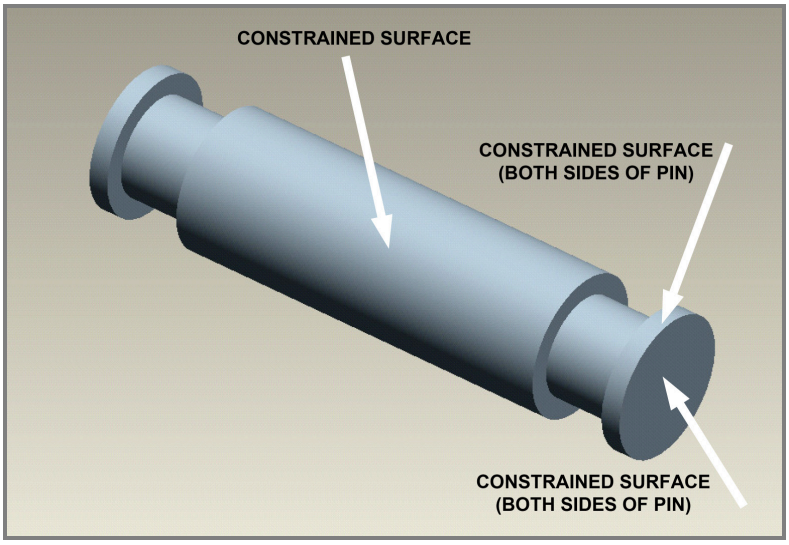

Figure 12 – FEA Constraints (Pin D)

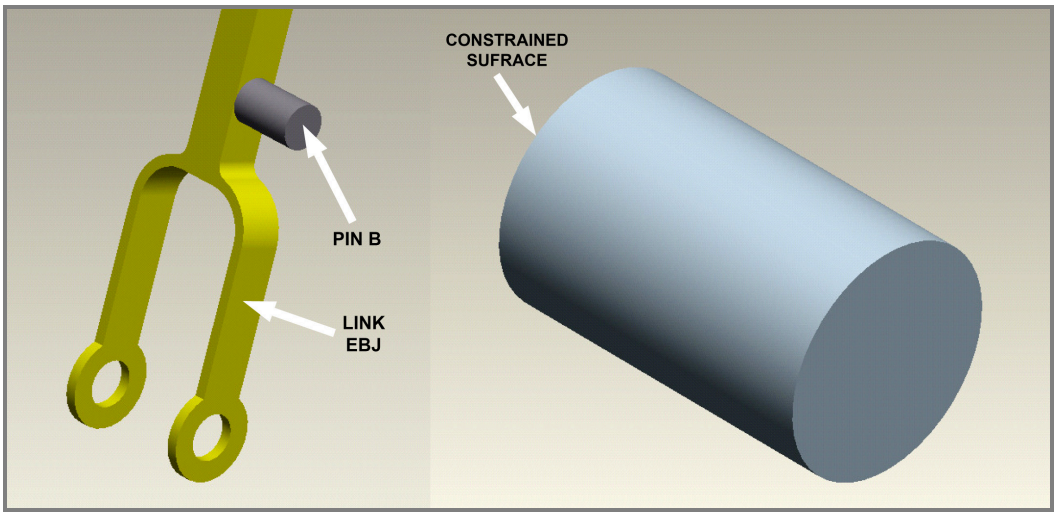

Figure 13 – FEA Constraints (Pin B)

Static Landing Simulation

It was stated in the *Project Description* that a static simulation model was created to determine the forces at each pin resulting from the peak vertical force during the landing of a United States Air Force F-16 Fighting Falcon. As was shown in Figures 7 and 8, a dynamic simulation model was utilized to determine the forces at each pin resulting from the movement of the landing gear piston. As explained in the section *Piston Driver*, the static simulation measured the same connection reaction forces as the dynamic simulation except that the piston position was fixed in its retracted state and a landing force applied to the bottom of the tire. The static simulation results were presented in a table of force values for the fixed position of the piston rather than a plot of force versus piston position. All that was needed to run the static simulation was the approximate peak vertical landing force.

According to the United States Air Force fact sheet on the F-16 Fighting Falcon the maximum takeoff weight of the aircraft is 37,500 pounds. This weight was used to approximate the vertical landing force because the weight of the aircraft decreases during flight as fuel is consumed and weapons are deployed. The impulse equation, as taken from *Introduction to Solid Mechanics* by Shames and Pitaressi, was used to calculate the average force experienced during landing. In Equation L1 F_{avg} is the average vertical landing force, Δt is the landing impulse time, m is the mass of the aircraft, and ΔV is the change in vertical velocity of the aircraft. Rearranging yields Equation L2, in which the only unknowns were ΔV and Δt.

$$(L1) \quad \text{Impulse} = F_{avg} * \Delta t = m * \Delta V$$

$$(L2) \quad F_{avg} = \frac{m * \Delta V}{\Delta t}$$

Research was conducted to establish appropriate values for ΔV and Δt. According to a paper titled *Aircraft Landing Gear Dynamics: Simulation and Control*, “certification process requires that a landing gear sustain a maximum vertical velocity of 10 ft/sec for transport aircraft and up to 25 ft/sec for fighter aircraft on aircraft carriers.” This information could be applied directly to the F-16 Fighting Falcon. In order to calculate an average landing force for the worst case landing scenario ΔV was chosen to be the maximum vertical velocity of 25 ft/sec.

Another paper titled *Dynamic study of Aircraft Gear Behavior in some Unusual Conditions* presents an analysis of aircraft front landing gear behavior. Figure 8 in this paper presents a plot of force versus time for various vertical fall-down velocities. Observation of the landing impulse times on this plot led to the conclusion that an impulse time between .1 and .2 seconds would be appropriate for the approximation being attempted. As a result of this observation Δt was chosen to be .15 seconds. Plugging the chosen values for ΔV and Δt into Equation L2 yielded an average vertical landing force of 194,000 pounds, just over five times the weight of the aircraft. To conduct the static simulation this approximated landing force was applied to the bottom of the tire in *Pro/Mechanism* and the connection reaction forces were measured at each of the pin connections.

As in the dynamic simulation, the X and Y components of the connection reaction forces were separately measured for all of the pin connections except A, B, and H. For pin connections A, B, and H the magnitudes of the net reaction forces were measured. Table 3 lists the X and Y

components of the reaction forces and is the static analog of the Figure 7 that resulted from the dynamic simulation. Table 4 lists the magnitudes of the net reaction forces at each pin connection and is the static analog of the Figure 8 that resulted from the dynamic simulation. With the static simulation complete FEA could be repeated for the connection reaction forces caused by the approximated vertical landing force.

Table 3 – Reaction Components (Landing)

Connection	F_{REA}
A	195584.39
B	988.86
C1X	-928.04
C1Y	-374.37
C2X	930.26
C2Y	378.35
D1X	-13129.92
D1Y	-29865.72
D2X	401.20
D2Y	-3499.34
E1X	13655.93
E1Y	13124.77
E2X	134315.68
E2Y	-141072.35
E3X	-147961.81
E3Y	127937.36
F1X	-18042.83
F1Y	-5761.92
F2X	18044.22
F2Y	5757.58
G1X	-1118.51
G1Y	17008.29
G2X	-2722.06
G2Y	-18961.21
G3X	3830.25
G3Y	1963.75
H	19092.71
J1X	190765.17
J1Y	35576.41
J2X	-190788.17
J2Y	-35580.68
J3X	15.55
J3Y	2.89

F_{REA} = Connection Reaction Force (lbf)

Table 4 – Net Reaction Magnitudes (Landing)

Connection	F_{MAG}
A	195584.39
B	988.86
C1	1000.705
C2*	1004.257
D1	32624.47
D2	3522.267
E1*	18940.54
E2	194787.3
E3	195603.3
F1*	18940.52
F2	18940.53
G1	17045.02
G2	19155.6
G3*	4304.314
H	19092.71
J1	194054.2
J2	194077.6
J3*	15.8138

F_{MAG} = Magnitude of Net Connection Reaction Force (lbf)
*Indicates the connection fixed in the FEA

Landing FEA

As stated in the *Project Description*, data collection was completed by performing FEA in *Pro/Mechanica* to determine the maximum stresses on each pin during landing. The pin stress FEA for the landing simulation was carried out in exactly the same way as the pin stress FEA for the gear retract simulation. Table 4 was utilized exactly as Figure 8 was utilized to determine which connections were constrained in the FEA analyses. The connections fixed in the analyses are identified in Table 4. Table 3 was utilized exactly as Figure 7 was utilized to determine which loads were applied in the FEA analyses. Displacement constraints were applied exactly as described in the section *Gear Retract FEA*. The stress results were also displayed in exactly the same way as described in that section.

The maximum *von Mises* stresses obtained for each of the pins during landing are listed in Table 5. FEA results for all the pins are located in *Appendix A-5: Landing FEA Results*. Table 5 shows that the highest stresses were experienced by Pins J, E, and G in decreasing order of magnitude. The lowest stresses were experienced by Pins B, C, and H in increasing order of magnitude. The values contained in Table 5 were used to calculate factors of safety for each pin as will be described in the section *Factors of Safety*.

Table 5 – Maximum Pin Stresses (Landing)

Pin	σ_{MAX}
A	115200
B	2640
C	3385
D	30970
E	1496000
F	53510
G	215100
H	12430
J	2345000

σ_{MAX} = Maximum *von Mises* stress (lbf/in^2)

Both the dynamic gear retract and the static landing simulations have been completed. The connection reaction forces measured in each simulation were used to conduct FEA analyses to obtain the maximum stresses on each of the pins in the landing gear mechanism. As stated in the *Project Description*, it was necessary to verify that the force and stress results were calculated properly by *Pro/Engineer* for at least one pin. Verification of the force and stress results is conducted in the next section titled *Data Verification.*

DATA VERIFICATION

This section details the mathematical verification of the force and stress data obtained in the *Pro/Mechanism* simulations and the *Pro/Mechanica* stress analyses. For the purposes of the project it was only necessary to verify the results obtained for one pin. Pin F was selected for the verification of the force data and Pin B was selected for the verification of the stress data.

Acceleration Verification

Due to the complexity of the calculations involved it was not possible to verify the forces at the pins directly. Because force is related to acceleration by mass it was possible to verify the forces at a pin by verifying the acceleration of that pin. It was assumed that *Pro/Engineer* correctly manipulated the masses in its calculation of forces. Pin F was selected as the subject of the acceleration verification because its rotation about Pin D could be easily related to the change in length of the piston, for which a drive equation was known. In fact, acceleration verification could have been carried out easily for nearly any point on Link CDFG because its rotation was directly relatable to the change in length of the piston.

Verifying the acceleration of Pin F was also desirable because it was equivalent to verifying the acceleration of Pin E about Pin A. The fact that the distance from Pin A to Pin E and from Pin D to Pin F were both the same meant that the position, velocity, and acceleration of Pins F and E were identical about their respective axes. Recall the names and locations of the pins in the landing gear mechanism by referring to Figure 2 in the section *Landing Gear Design.*

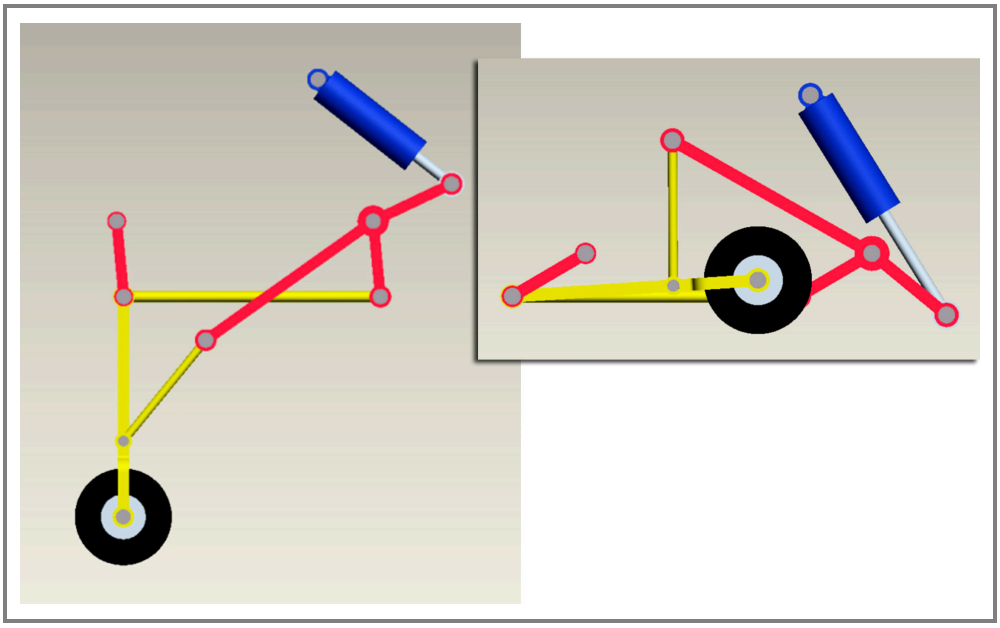

Figure 14 – Landing Gear Deployed and Retracted

The first step in the acceleration verification of Pin F was the derivation of an equation that related the change in length of the piston to the rotation of Link CDFG. The dimensions critical to this derivation are illustrated in Figure 15. The piston positions illustrated in Figure 15 can be compared to the positions of the landing gear mechanism illustrated in Figure 14. As stated in the section *Piston Driver*, the retracted state of the piston corresponded to the deployed state of the landing gear. It is important to note that θ in Figure 15 was defined to be the angle between the line segments HD and DG in both the retracted and deployed states of the piston.

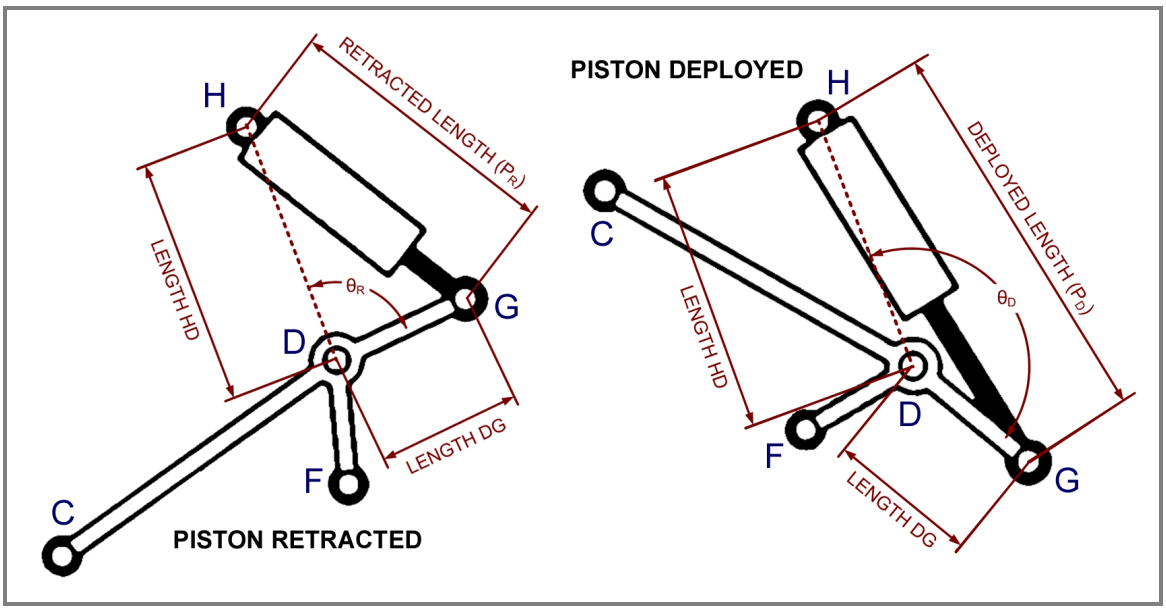

Figure 15 – Piston Retracted and Deployed with Rotation of Link CDFG

As shown in equations A1 and A2, the law of cosines was used to develop expressions for θ_R and θ_D. The R corresponds to the retracted state of the piston and the D to the deployed state. The change in angular position of Link CDFG from its starting position is shown in equation A3. Substituting equations A1 and A2 into equation A3 yielded equation A4.

$$(A1) \quad Cos(\theta_R) = \frac{HD^2 + DG^2 - P_R^2}{2 * HD * DG}$$

$$(A2) \quad Cos(\theta_D) = \frac{HD^2 + DG^2 - P_D^2}{2 * HD * DG}$$

$$(A3) \quad \Delta\theta = \theta_R - \theta_D$$

$$(A4) \quad \Delta\theta = Cos^{-1}\left(\frac{HD^2 + DG^2 - P_R^2}{2 * HD * DG}\right) - Cos^{-1}\left(\frac{HD^2 + DG^2 - P_D^2}{2 * HD * DG}\right)$$

The HD and DG terms in equation A4 were easily determined using the geometry of Link CDFG and the layout of the ground pins. The P_R and P_D terms, corresponding to the retracted and deployed lengths of the piston, were easily determined using the maximum and minimum positions of the piston and the geometry of the piston and cylinder components. The dimensions of the piston and cylinder are illustrated in Figure 16. Recall that the minimum and maximum piston positions relate back to the start and end of the drive profile in Figure 4.

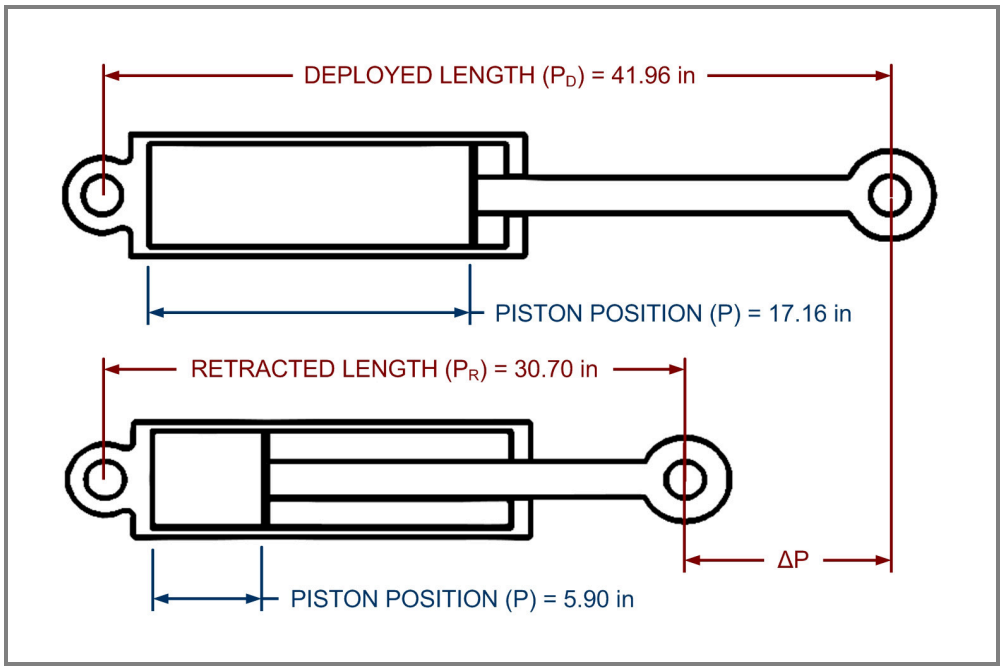

Figure 16 – Piston Dimensions

Referring to Figure 16 and equation A5, it can be seen that even though P_R and P_D were constants either of those constants could be expressed in terms of ΔP, the change in length of the piston. Recall that an equation for the *piston position* as a function of time was described in detail in the section *Piston Driver*. The drive equation taken from Figure 4 was used to derive an equation for the *change in length* of the piston as a function of time. This was accomplished by translating the drive profile in Figure 4 downward until the minimum value of the cosine function was zero. This made sense because ΔP at time zero was zero and ΔP at four seconds was equal to the difference between the two piston positions shown in Figure 16, also known as the maximum value of ΔP. The resulting function for ΔP is shown in equation A6.

$$(A5) \quad P_D = P_R + \Delta P$$

$$(A6) \quad \Delta P = -5.63 * Cos\left(\frac{2 * \pi * t}{8}\right) + 5.63$$

Once equations for P_D and ΔP were derived they were inserted into the equation for the change in rotation of Link CDFG as it relates to the piston position. Inserting equation A5 into equation A4 yielded equation A7. Inserting equation A6 into equation A7 yielded equation A8.

$$(A7) \quad \Delta\theta = Cos^{-1}\left(\frac{HD^2 + DG^2 - (P_R + \Delta P)^2}{2 * HD * DG}\right) - Cos^{-1}\left(\frac{HD^2 + DG^2 - P_D^2}{2 * HD * DG}\right)$$

$$(A8) \quad \Delta\theta = Cos^{-1}\left(\frac{HD^2 + DG^2 - \left(P_R + \left(-5.63 * Cos\left(\frac{2 * \pi * t}{8}\right) + 5.63\right)\right)^2}{2 * HD * DG}\right) - Cos^{-1}\left(\frac{HD^2 + DG^2 - P_D^2}{2 * HD * DG}\right)$$

A review of velocity and acceleration in cylindrical coordinates was carried out using *Engineering Mechanics: Dynamics* by Irving Shames. The vector equations A9-A13 are the equations encountered during the review as simplified for the two dimensional verification of the acceleration of Pin F. As shown in Figure 17, the terms ε_R and ε_θ represent unit vectors in the radial and tangential directions of the path traced by Pin F. Because Pin F was the subject of the verification the length DF appears in equations A9, A11, and A12. The substitution of length CD for DF and the adjustment of the unit vectors would have been the basis of an acceleration verification for Pin C had one been carried out.

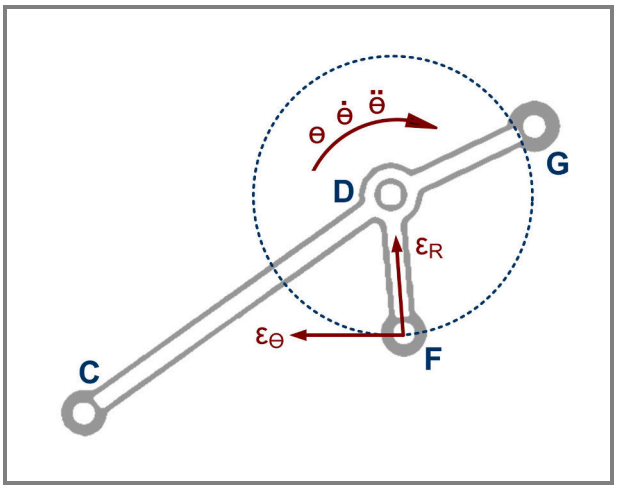

Figure 17 – Link CDFG Unit Vectors

$$(A9) \quad \vec{V} = DF * \dot{\theta} * \varepsilon_\theta$$

$$(A10) \quad \vec{A} = \vec{A}_\theta + \vec{A}_R$$

$$(A11) \quad \vec{A}_R = -DF * \dot{\theta}^2 * \varepsilon_R$$

$$(A12) \quad \vec{A}_\theta = DF * \ddot{\theta} * \varepsilon_\theta$$

$$(A13) \quad \left|\vec{A}\right| = \sqrt{\left|A_R\right|^2 + \left|A_\theta\right|^2}$$

It is important to note that the velocity vector for Pin F has only one component in the tangential direction while the acceleration vector has one component in the tangential direction and one component in the radial direction. It is also important to note that the velocity and acceleration equations for Pin F include the first and second derivatives of θ, also known as angular velocity and angular acceleration. This meant that an expression for θ, the angular position, was needed to calculate the velocity and acceleration of Pin F.

Recall that the movement of the piston in the dynamic gear retract simulation always began from the retracted state of the piston. This meant that Δθ in equation A8 referred simply to the angular position of Link CDFG and could be directly referred to as θ. This interpretation is shown in equation A14. Because θ was a function ΔP, which was a function of time, θ was also a function of time and could be differentiated with respect to time to yield the angular velocity and angular acceleration of Link CDFG as shown in equations A15 and A16. The positive directions of the angular position, velocity, and acceleration are shown in Figure 17.

$$(A14) \quad \theta = \Delta\theta$$

$$(A15) \quad \dot{\theta} = \frac{d\theta}{dt}$$

$$(A16) \quad \ddot{\theta} = \frac{d\dot{\theta}}{dt} = \frac{d^2\theta}{dt^2}$$

Once the equations had been derived for the angular position, the velocity, and the acceleration of Pin F a MATLAB program was written to symbolically differentiate equation A8 and to calculate and plot arrays of the velocity and acceleration of Pin F versus time. Measures were used in *Pro/Mechanism* to create plots of the velocity and acceleration of Pin F. Because it was only possible to measure the magnitude of the acceleration in *Pro/Mechanism* equation A13 was used in MATLAB to calculate and plot the magnitude of the acceleration rather than the individual components. Even though it was not necessary to verify the velocity of Pin F it was measured, calculated, and plotted simply because of the ease with which it could be done.

The velocity plots obtained from *Pro/Mechanism* and MATLAB are shown in Figures 19 and 20 while the acceleration plots are shown in Figures 21 and 22. The callouts on the plots in Figures 19-22 allow direct comparison of the velocity and acceleration values at the three times illustrated in Figure 18. By comparing the plots obtained from *Pro/Mechanism* and MATLAB it was clear that both the velocity and the acceleration of Pin F had been verified.

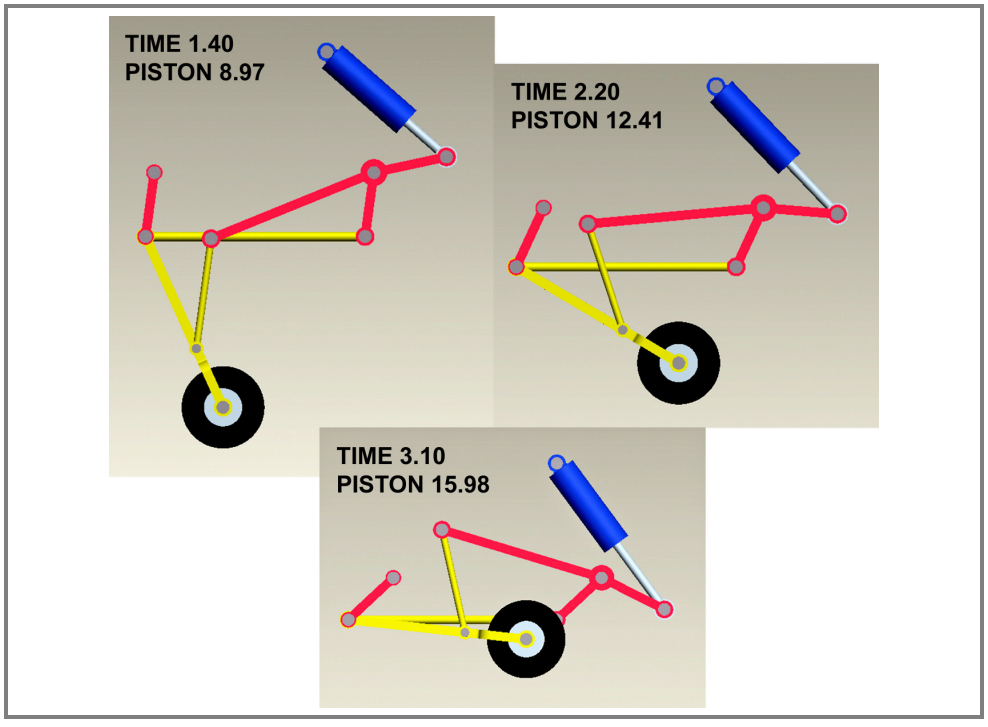

Figure 18 – Verification Positions

This concludes the acceleration verification of Pin F. The velocity and acceleration plots can be found on the following two pages. The MATLAB code written to perform the calculations and create the plots can be found in *Appendix A-5: Acceleration Verification MATLAB Code*.

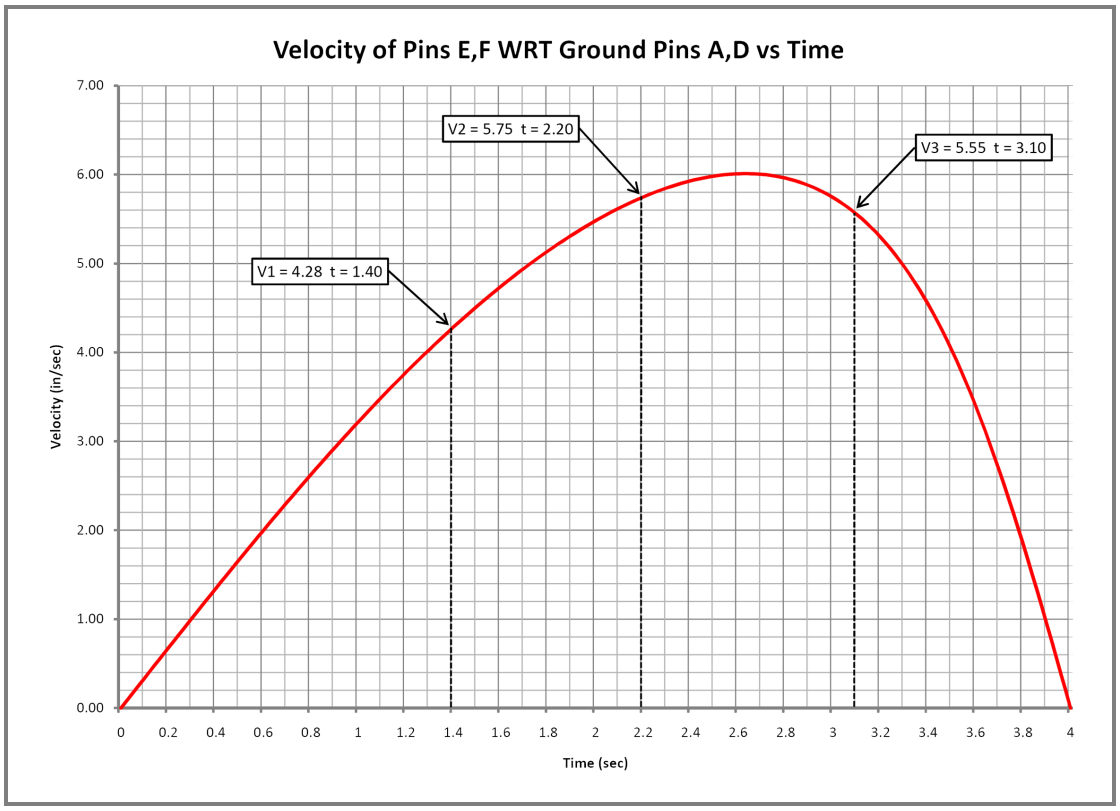

Figure 19 – Velocity Measured in Pro/Mechanism

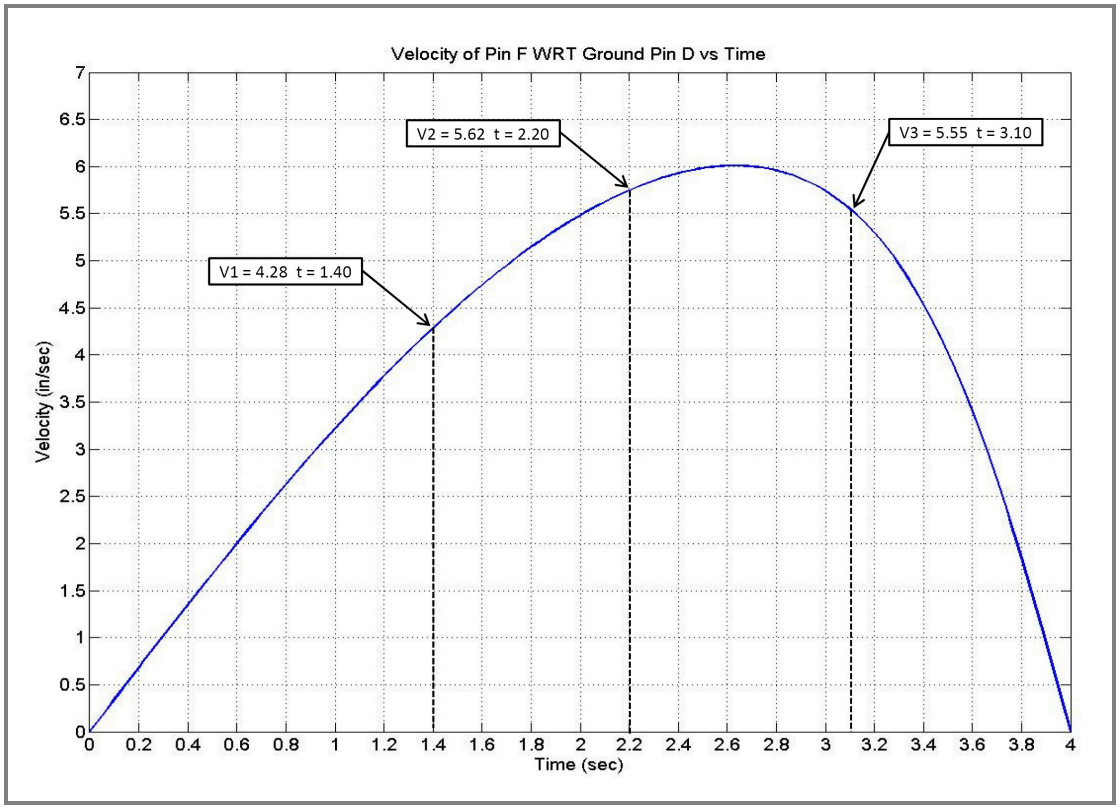

Figure 20 – Velocity Calculated in MATLAB

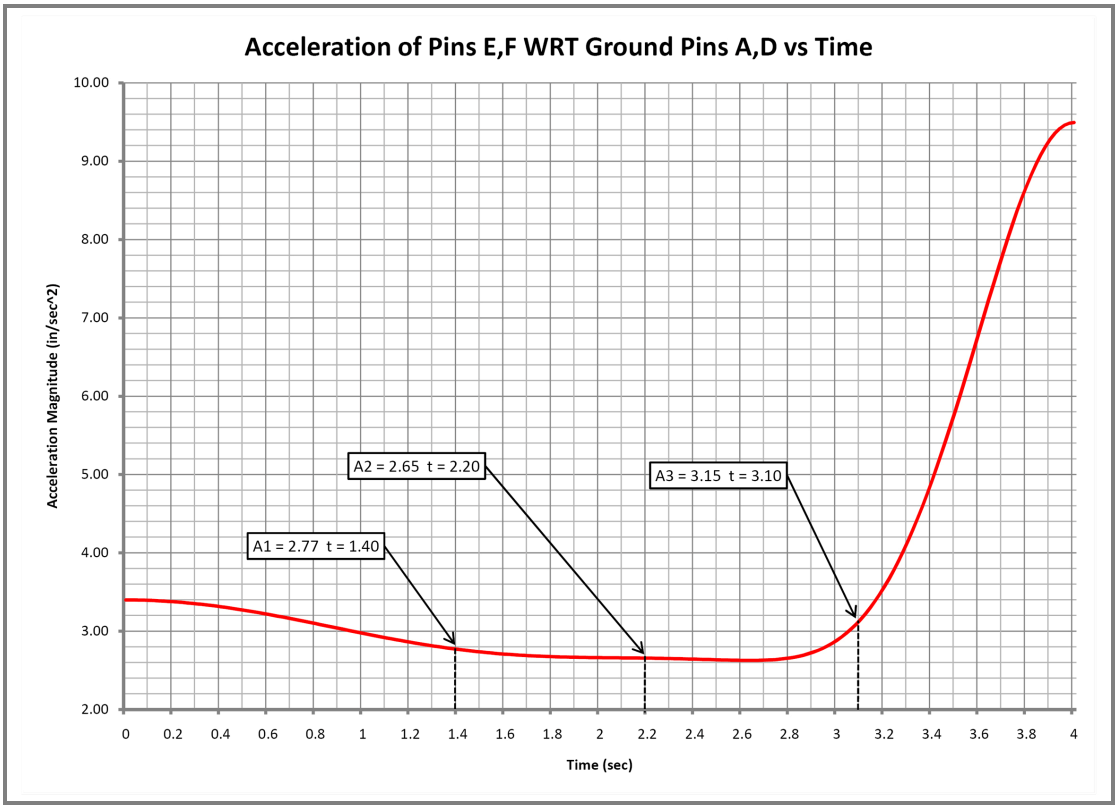

Figure 21 – Acceleration Measured in Pro/Mechanism

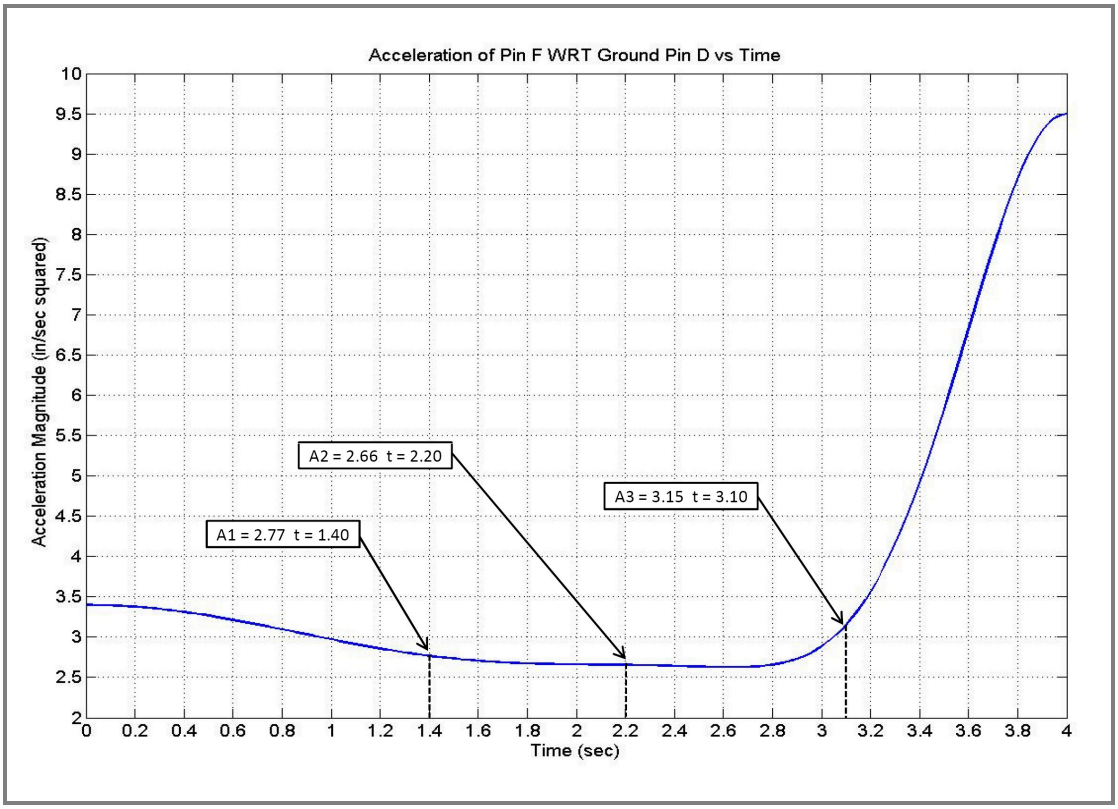

Figure 22 – Acceleration Calculated in MATLAB

Stress Verification

In the section *Gear Retract FEA* it was mentioned that Pin B could be idealized as a cantilever beam with a distributed load applied. The distributed load would be equal in magnitude to the Pin B connection reaction force measured in *Pro/Mechanism*. Figure 13 illustrated the ease with which such an idealization could be made; Pin B was a simple cylindrical pin fixed to the side of Link EBJ. For this reason Pin B was the subject of the stress verification.

To verify the stress results for Pin B it was necessary to manually calculate one of the stress components and compare the values to the same stress component displayed from the *Pro/Mechanica* FEA results. The stress component verified was the normal stress in the axial direction of Pin B. Equation S1 represents the axial normal stress in a beam (σ_{ZZ}) and is dependent on the bending moment (M_X), the distance from the neutral axis of the beam (y), and the second moment of the area of the beam cross section (I_{XX}).

Figure 23 illustrates the directions of the normal stress, the bending moment, and the distance from the neutral axis in a beam element. The z position is the position along the beam length at which the normal stress is being calculated. The y position is the distance from the neutral axis at which the normal stress is being calculated. The neutral axis is the z-axis. M_X is the value of the bending moment about the x axis and depends on the z position and on the loads applied to the beam. The normal stress for a given z and y position is considered to be constant for any values of x that are within the cross section of the beam. The coordinate system shown in Figure 23 is consistent with the coordinate system used for Pin B. Because Pin B had a circular cross section the value of I_{XX} is given by equation S2.

$$(S1) \quad \sigma_{ZZ} = \frac{-M_X * y}{I_{XX}}$$

$$(S2) \quad I_{XX} = \frac{\pi}{4} r^4$$

$$(S2) \quad \frac{dV_y}{dz} = -w_y$$

$$(S3) \quad V_2 = V_1 - \int_1^2 w_y dz$$

$$(S4) \quad \frac{dM_x}{dz} = V_y$$

$$(S5) \quad M_2 = M_1 + \int_1^2 V_y dz$$

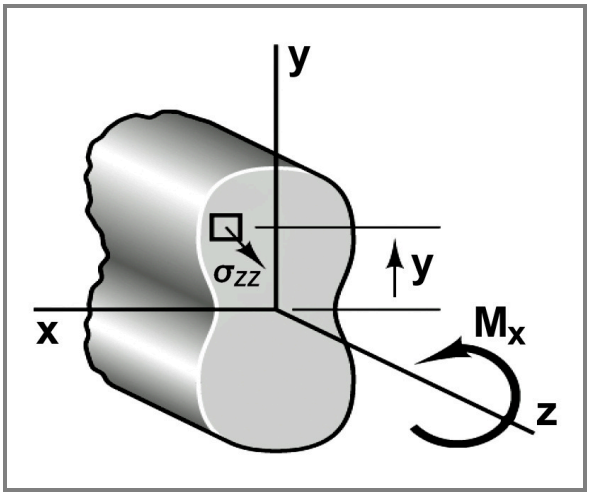

Figure 23 – Normal Stress in Z Direction

The calculation of M_X was carried out using equations S2-S5. Equations S2 and S3 relate the shear force in the beam (V_Y) to the loads applied to the beam (w_Y). Both V_Y and w_Y are parallel to the y axis and are functions of the z position along the neutral axis of the beam. Equations S4 and S5 relate the shear force (V_Y) in the beam to the bending moment in the beam (M_X). Both V_Y and M_X are functions of the z position along the neutral axis of the beam.

The total load applied to Pin B was the magnitude of the connection reaction force at Pin B. The application of the total load was achieved as shown in the Figure 24 loading diagram labeled *W*. A distributed load of 50.52 pounds per inch was applied over the 2 inch section of the beam that would have been in contact with Link BC. The reaction force at the cantilever support confirmed that the total load was the desired 101 pound connection reaction force at Pin B. The application of equations S2 and S3 to the distributed load yielded the Figure 24 shear force plot labeled *V*. The application of equations S4 and S5 to the shear force plot yielded the Figure 24 bending moment plot labeled *M*. By this method the values of M_X were derived from the distributed load that was applied to Pin B. Figure 24 was created using a combination of manual calculation and *Dr. Beam Pro* software.

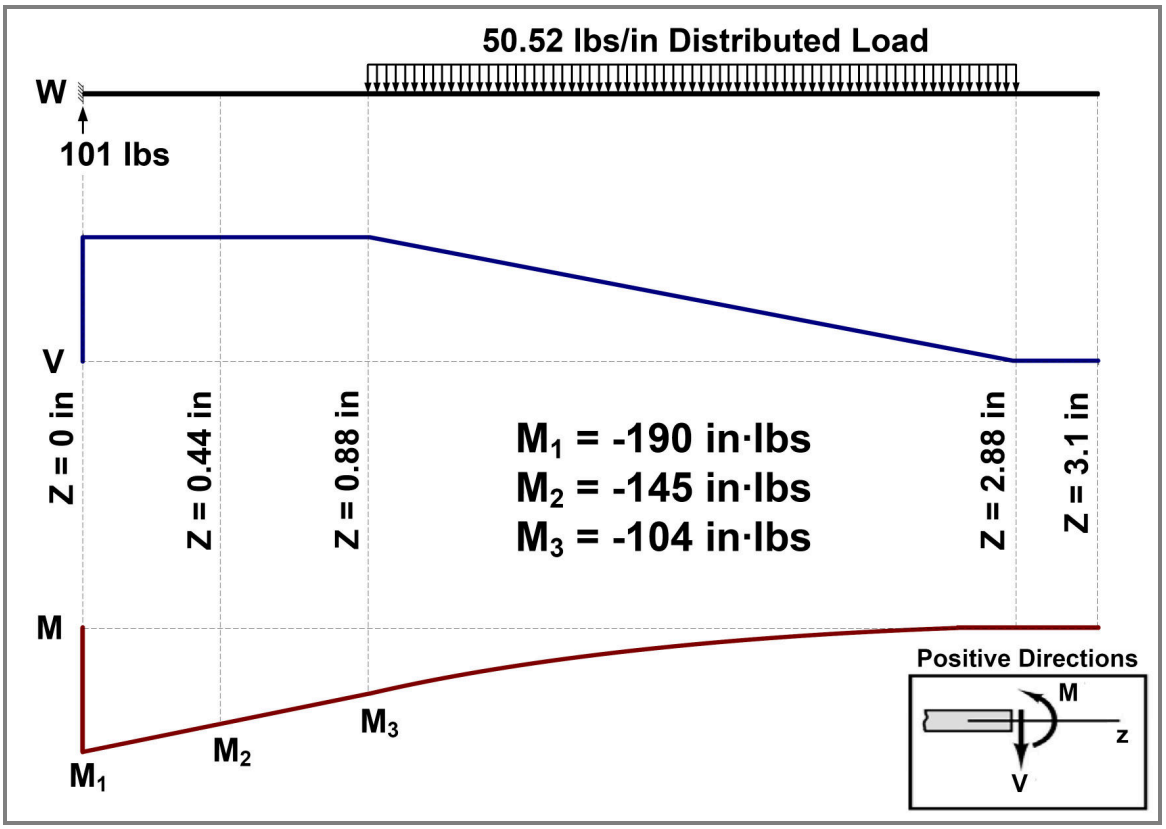

Figure 24 – Shear Force and Bending Moment Diagrams for Pin B

With I_{XX} calculated from equation S2 and M_X calculated using equations S3-S5 it was necessary to choose a value of *y* in order to calculate σ_{ZZ} as a function of the z position along the neutral axis. Because the cross section of Pin B was a circle with a 2 inch diameter the maximum allowable value of *y* was 1 inch (the maximum distance between the neutral axis and the surface of the pin). This maximum allowable value for *y* was used to calculate the normal stress as a function of the z position along the neutral axis. Because an explicit equation was not derived for M_X it was not possible to derive an explicit equation for σ_{ZZ}. Instead of deriving the explicit equations a table of z positions was created and the corresponding values of M_X at were obtained from the bending moment plot in Figure 24. The normal stress was calculated according to equation S1 for each z position in the table and the resulting data pairs were plotted. The red curve in Figure 27 illustrates the calculated values of the normal stress as a function of the z position along the neutral axis of Pin B.

The next step in the stress verification was to repeat the Finite Element Analysis for Pin B in *Pro/Mechanica* using the idealized loading employed in the manual calculation. Recall that in the *Gear Retract FEA* the load was distributed over a surface region that represented the portion of the pin in contact with the link. For the manual calculations the load was distributed over a segment of the neutral axis of the pin. Every attempt to duplicate the idealized loading in *Pro/Mechanica* by applying a load to a datum curve on the neutral axis failed. The reason for the failure could not be determined from the error message encountered which stated that one or more forces were applied to curves that were not part of any elements in the mesh. Because datum curves could not be utilized an alternative approach was attempted. In the alternative approach, shown in Figure 25, a cylindrical cutout was made around the neutral axis at the core of the pin and the load was distributed over the resulting surface. The diameter of the cylinder was made as small as possible to minimize adverse effects on the analysis. A cylindrical shape was chosen for the cutout to minimize stress concentrations that would cause extreme distortions in the legend contours. The results of the FEA carried out using the alternative method are shown in Figure 26. For comparison with the manual calculations the stress component displayed in Figure 26 is the z direction normal stress rather than the *Von Mises* stress that was displayed in the previous FEA results.

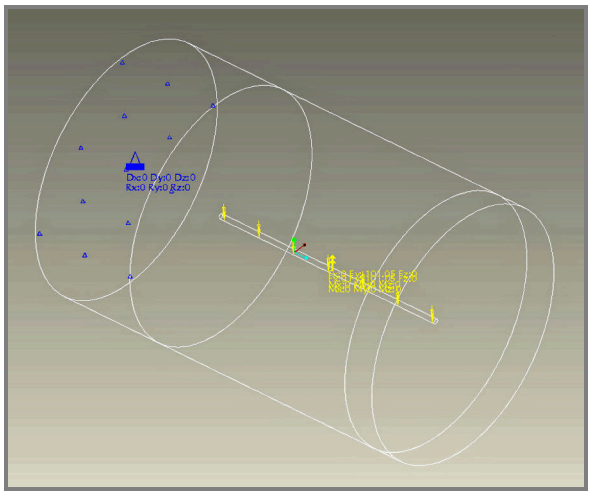

Figure 25 – Pin B Idealization Cutout

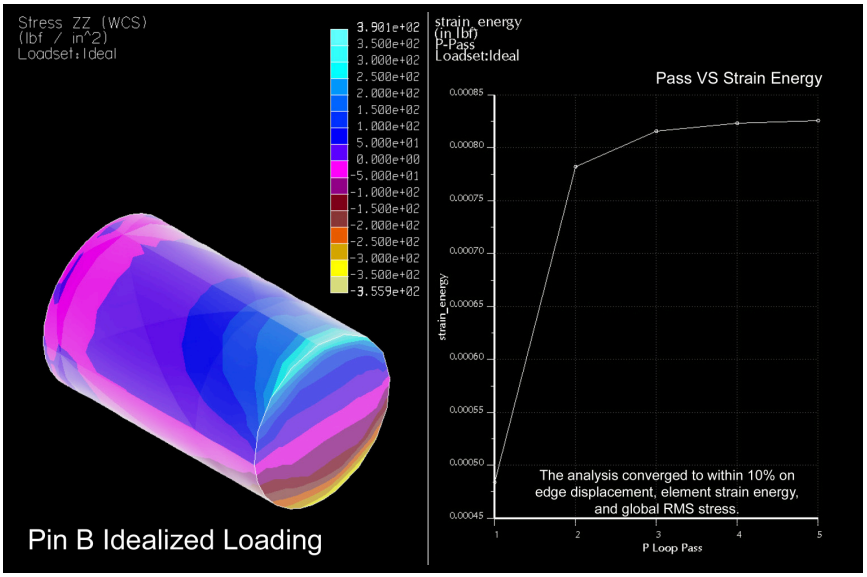

Figure 26 – Pin B Stress Verification FEA

The results shown in Figure 26 seemed appropriate in that the stresses observed above the neutral axis were positive and the stresses observed below the neutral axis were negative. The positive values indicated tension caused by the bending of the pin and the negative values indicated compression. As expected there were no normal stresses at the neutral axis. The neutral axis is indicated in Figure 26 by the straight contour boundary running through the middle of the fixed end of the pin. The end of the pin visible in Figure 26 is the fixed end.

Figure 26 was not particularly useful for comparing how closely the FEA results match the results of the manual calculations. Because the manual calculations were carried out using a value of *y* equal to 1 inch it was necessary to determine from the FEA results the stresses along the top edge of the pin where *y* was equal to 1 inch. The dynamic query tool in *Pro/Mechanica* could have been used to read stress values along the top edge of the pin but the exact z position of each reading could not be queried along with the stress value.

It was most desirable to create a plot of normal stress versus z position along the neutral axis as was created for the manual calculation results. To do this, a datum curve was inserted in *Pro/Mechanica* and a dummy load of zero pounds was applied in order to make the curve selectable in the results window. A graph of the normal stress along the datum curve was created, the data was exported to Excel, and the values were plotted alongside those obtained from the manual calculations. The blue curve in Figure 27 illustrates the values obtained from *Pro/Mechanica* for the normal stress as a function of the z position along the neutral axis.

Figure 27 – ZZ Normal Stress vs Z Position Along Pin B Axis*

*Though this plot is labeled as the *normal stress* along the Pin B axis it is more precisely the *maximum normal stress* along the Pin B axis because the value of *y* used in the calculations was the maximum allowed.

It is apparent in Figure 27 that there was significant variation in the first half inch along the neutral axis between the manually calculated values and those obtained from *Pro/Mechanica*. It is possible that the variation was attributed to the alternative approach used to apply the load in *Pro/Mechanica*. Despite the initial variation it was apparent over the majority of the neutral axis that the manual calculations verified the stress results of the FEA carried out.

CONCLUSIONS

This section includes a review of the maximum stresses on each pin, the calculation of factors of safety for each pin, and recommendations concerning the results and the potential impact those results have on the design of the landing gear mechanism.

Factors of Safety

The final result of the data collection carried out during the project was a set of maximum stresses on each pin of the landing gear mechanism that resulted from the dynamic gear retract simulation and the static landing simulation. The maximum stresses on each pin are shown in Table 6. During the retract of the landing gear, the highest stresses were experienced by Pins E, J, and G in decreasing order of magnitude and the lowest stresses by Pins A, F, and B in increasing order of magnitude. In response to the approximated landing force applied to the tire, the highest stresses were experienced by Pins J, E, and G in decreasing order of magnitude, and the lowest stresses by Pins B, C, and H in increasing order of magnitude. Comparison of these results indicated that Pins E, G, and J experienced the highest stresses during both the retract of the landing gear and during landing.

Table 6 – Pin Factors of Safety (Gear Retract and Landing)

Pin	σ_{MAXR}	σ_{MAXL}	FoS_R	FoS_L
A	82.86	115200	2715	1.95
B	269.8	2640	834	85.23
C	452.7	3385	497	66.47
D	792.1	30970	284	7.27
E	1663	1496000	135	0.15
F	236.8	53510	950	4.20
G	1199	215100	188	1.05
H	406.4	12430	554	18.10
J	1354	2345000	166	0.10

σ_{MAXR} = Maximum *von Mises* stress during retract (lbf/in^2)
σ_{MAXL} = Maximum *von Mises* stress during landing (lbf/in^2)
FoS_R = Pin factor of safety during retract FoS_L = Pin factor of safety during landing

To evaluate the likelihood that the pins in the landing gear mechanism would fail in response to the maximum stresses it was necessary to calculate the factor of safety for each pin. Factor of safety, denoted *FoS*, is calculated according to equation F1 where σ_{max} is the maximum allowable stress and σ_{exp} is the experienced stress. As mentioned in the section *Material Properties* it was not desirable for any of the pins to yield so the yield tensile strength of the pin material, 225 ksi for AISI 4340 steel, was used for σ_{max}. The maximum stress values in Table 6 represent the σ_{exp} for each pin during retract and landing. Using equation F1 the factors of safety shown in Table 6 were calculated for each pin during retract and landing.

$$(F1) \quad FoS = \frac{\sigma_{\max}}{\sigma_{\exp}}$$

According to the structure of equation F1 if the factor of safety for a pin was greater than one that pin was not yielding. If the factor of safety for a pin was less than one that pin had undergone yielding. A factor of safety of one indicated that a pin was at the point of yielding. Yielding was considered the point of failure and was used in the calculation of factor of safety because it was undesirable for any of the pins to experience nonreversible changes in geometry. This means that any strain (change in geometry) experienced by a pin while forces were applied would be completely reversed when there was no force applied.

Recommendations

Based on the factors of safety calculated from the dynamic gear retract simulation it is apparent that the design of the landing gear mechanism is adequate for retracting the landing gear at the rate specified by the drive profile in Figure 4. The lowest factor of safety calculated for retracting of the landing gear was 135 for Pin E. The highest factor of safety calculated for retracting of the landing gear was 2715 for Pin A. The factors of safety calculated from the static landing simulation are more troubling. Pins E and J had factors of safety significantly less than one, which indicates that they yielded in response to the approximated vertical landing force applied to the bottom of the tire. This is understandable because Pins E and J are the first two Pins encountered along the vertical from the tire. Pins G and A also had troubling factors of safety in that Pin G had a factor of safety very near the point of yielding and Pin A had a factor of safety just under two.

To determine the factor of safety that should be present it is necessary to consider the nature of the force that was applied to the bottom of the tire and the consequences of failure of any of the pins in the mechanism. The vertical landing force was approximated using the impulse equation and resulted from a .15 second change in velocity from 25 feet per second to zero. This sudden shock is important when considering the factor of safety. EngineersEdge.com states that when components “are subjected to repeated shock loading the factor should not be less than 10.” Based on the fact that the landing gear mechanism does not incorporate any type of shock absorber and must be able to endure repeated landings a factor of 10 is a desirable value for the factor of safety. A factor of safety of at least 10 is also desirable given that 1) the total cost of the F-16 Fighting Falcon and payload could easily exceed 20 million dollars and 2) considerable harm could be caused to the pilot or others on the ground should the front landing gear collapse during landing.

Given that the desired factor of safety is 10 it is recommended that Pins A, D, E, F, G, and J all be redesigned to achieve the desired factor of safety and provide adequate assurance that the pins will not fail during landing of the F-16 Fighting Falcon. It is likely that this would be most easily achieved by increasing the typical diameter of the pins. It is also recommended that more extensive redesign take place in order to reduce stress concentrations, especially on Pins D, E, G, and J. During the redesign it should be considered whether Pins D, E, and G should incorporate enlarged cross sections that act as spacers or if separate spacers should be employed. Finally, even though the links of the landing gear mechanism were outside the scope of the project, it is recommended that a shock absorber be employed somewhere beneath Pin B on Link EBJ to help reduce the stresses on the pins during landing and increase the ease with which the desired factor of safety is achieved.

REFERENCES

EngineersEdge.com. *"Engineering and Applications: Factor of Safety Review."* www.engineersedge.com/analysis/factor-of-safety-review.htm. 5 Dec, 2008.

GoodyearAviation.com. *Aircraft Tire Data Book.* www.goodyearaviation.com/tiredatabook.html. Ohio: The Goodyear Tire & Rubber Company, 2002.

Kruger, W., I. Besselink, D. Cowling, D.B. Doan, W. Kortum, and W. Krabacher. *"Aircraft Landing Gear Dynamics: Simulation and Control."* *Vehicle System Dynamics* 28 (1997): 119-158. Swets & Zeitlinger, 1997.

Matweb.com. *"AISI 4340 Steel, oil quenched 855°C (1570°F), 230°C (450°F) temper for 4 hrs., tested at 26°C."* www.matweb.com. 5 Nov, 2008.

Matweb.com. *"Aluminum 6061-T6; 6061-T651."* www.matweb.com. 5 Nov, 2008.

Matweb.com. *"AK Steel 316L Austenitic Stainless steel."* www.matweb.com. 5 Nov, 2008.

Moran, Michael, and Howard Shapiro. *Fundamentals of Engineering Thermodynamics, Sixth Edition.* New Jersey: John Wiley & Sons, Inc, 2008.

Shames, Irving. *Engineering Mechanics: Dynamics, Fourth Edition*. New Jersey: Prentice-Hall, Inc, 1997.

Shames, Irving, and James Pitarresi. *Introduction to Solid Mechanics, Third Edition.* New Jersey: Prentice-Hall, Inc, 2000.

Tadeusz, Niezgoda, Malachowski Jerzy, and, Budzynski Adam. *"Dynamic Study of Aircraft Gear Behaviour in Some Unusual Conditions."*

APPENDIX A-1: DESIGN DRAWINGS

Drawing 1 – Landing Gear Assembly 38
Drawing 2 – Links EF, BC, and AE 40
Drawing 3 – Link EBJ 42
Drawing 4 – Links FDG and CDG 44
Drawing 5 – Pins A, C, D, and E 46
Drawing 6 – Pins F, G, H, and J 48
Drawing 7 – Tire Subassembly 50
Drawing 8 – Piston Subassembly 52
Drawing 9 – Ground Pin Layout 54

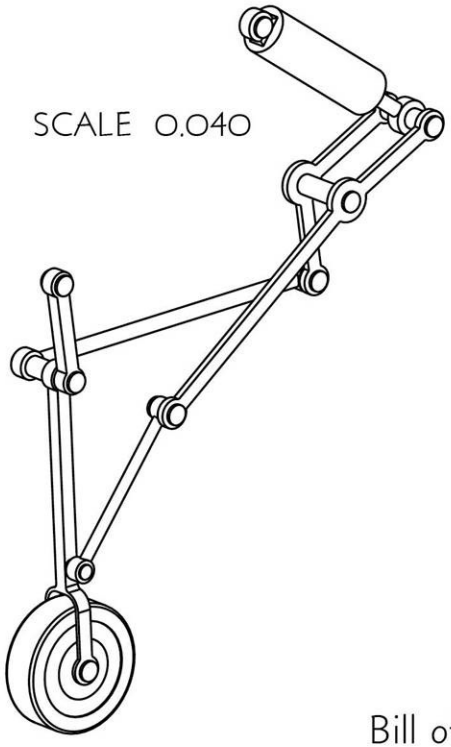

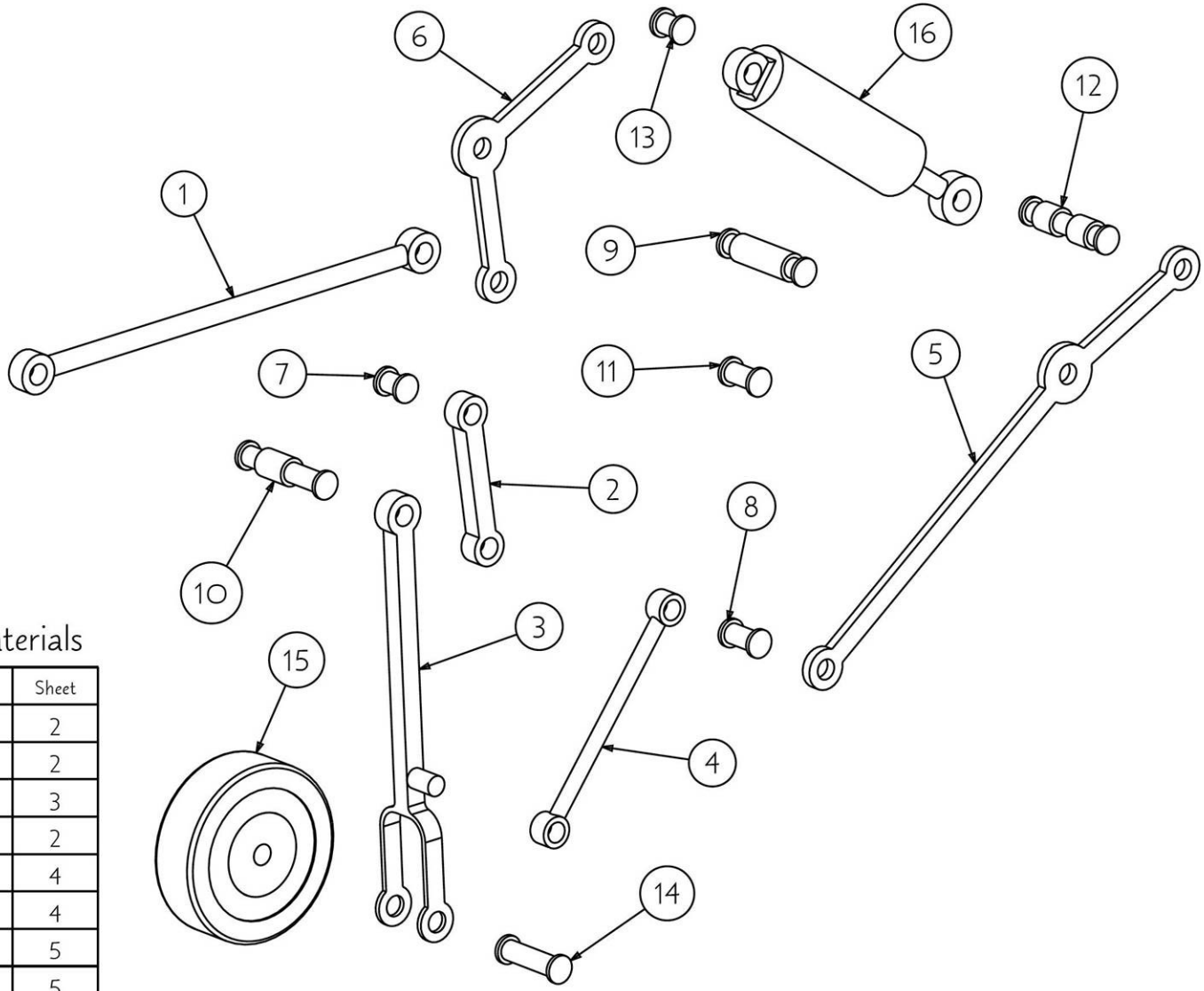

Bill of Materials

Item	Part Name	Materials	Qty	Sheet
1	Link EF	4340 Q&T	1	2
2	Link AE	4340 Q&T	1	2
3	Link EBJ	4340 Q&T	1	3
4	Link BC	4340 Q&T	1	2
5	Link CDG	4340 Q&T	1	4
6	Link FDG	4340 Q&T	1	4
7	Pin A	4340 Q&T	1	5
8	Pin C	4340 Q&T	1	5
9	Pin D	4340 Q&T	1	5
10	Pin E	4340 Q&T	1	5
11	Pin F	4340 Q&T	1	6
12	Pin G	4340 Q&T	1	6
13	Pin H	4340 Q&T	1	6
14	Pin J	4340 Q&T	1	6
15	Tire Subassembly	S-SBR & 6061-T651	1	7
16	Piston Subassembly	316L-SS	1	8

PART AND DRAWING NOTES

DRAWING SHEET NUMBERS ARE LISTED IN THE BOM
DRAWING SHEET 9 ILLUSTRATES THE LAYOUT OF THE GROUND PINS
MEANINGFUL TOLERANCES ARE SHOWN WHERE NECESSARY
GLOBAL DRAWING TOLERANCES ARE UNDEFINED

All dimensions shown in inches

DRAWN: Matthew Grenier

Binghamton University Watson School of Engineering
ME 481 Computer Aided Engineering - Project 3

TITLE: Landing gear assembly

SIZE	FSCM NO.	DWG NO.	REV
A	N/A	GRENIER-DWG01	A

DATE	SCALE	SHEET
12/4/08	0.063 Inch = 1 Inch	1 OF 9

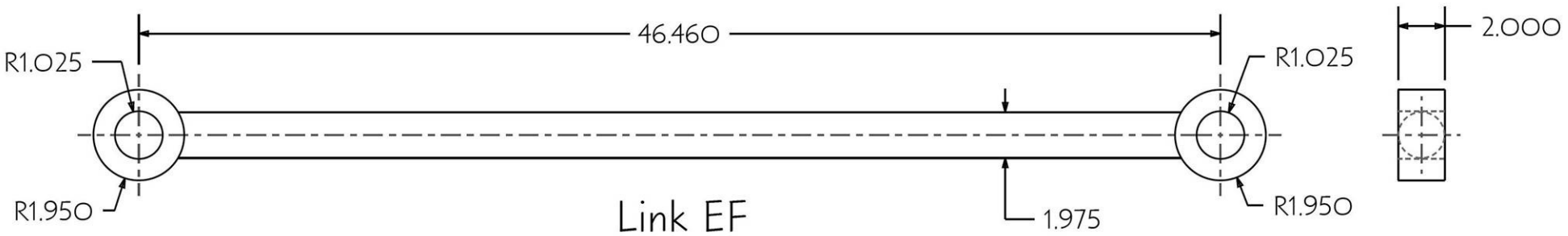

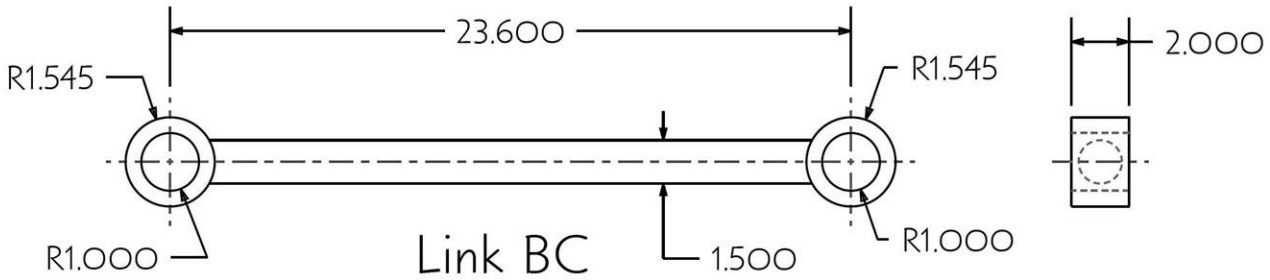

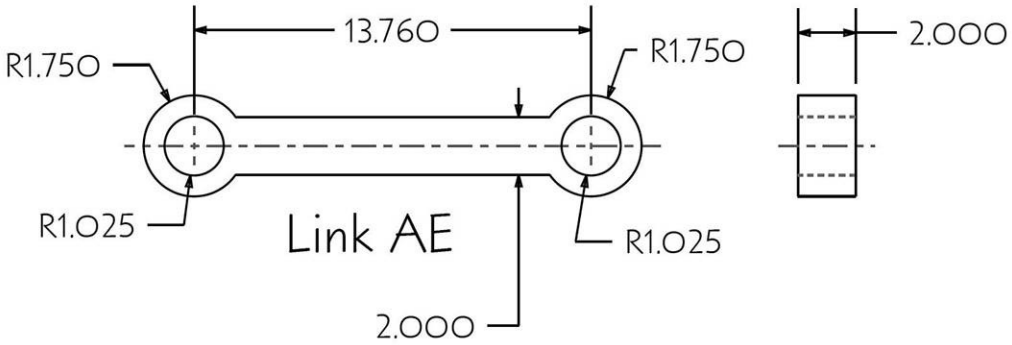

PART AND DRAWING NOTES MATERIAL - 4340 Q&T STEEL MEANINGFUL TOLERANCES ARE SHOWN WHERE NECESSARY GLOBAL DRAWING TOLERANCES ARE UNDEFINED	Binghamton University Watson School of Engineering ME 481 Computer Aided Engineering - Project 3			
	TITLE Links EF, BC, and AE			
All dimensions shown in inches	SIZE A	FSCM NO. N/A	DWG NO. GRENIER-DWG02	REV A
DRAWN Matthew Grenier	DATE 12/4/08	SCALE 0.15 Inch = 1 Inch	SHEET 2 OF 9	

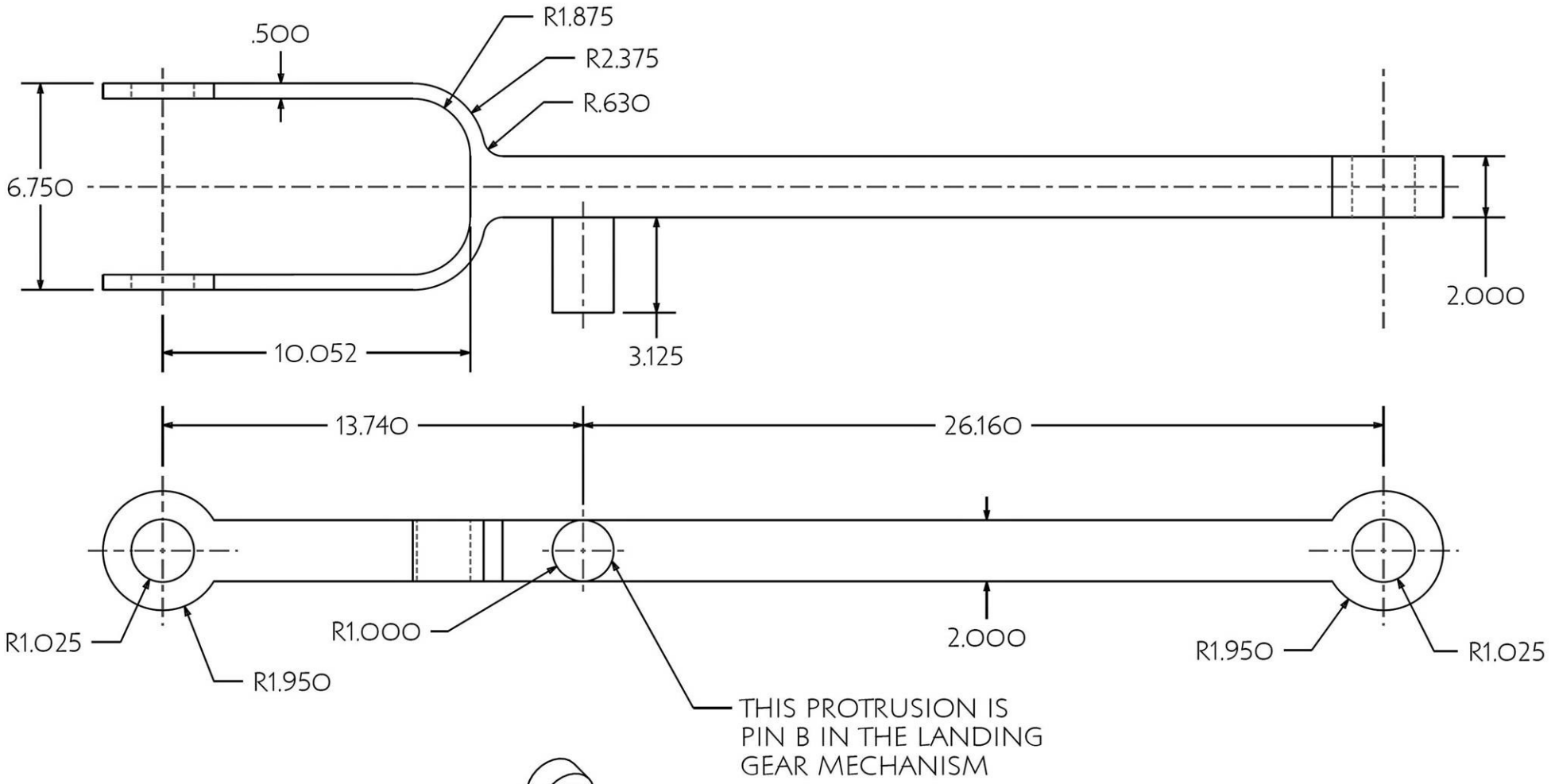

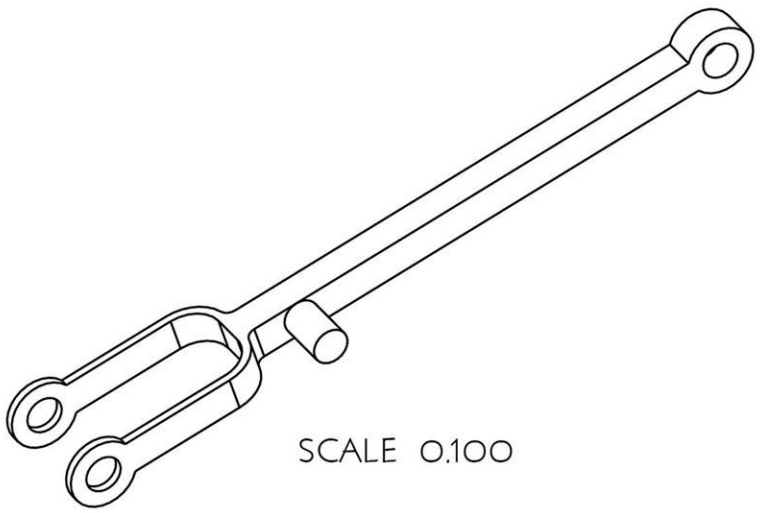

SCALE 0.100

PART AND DRAWING NOTES MATERIAL - 4340 Q&T STEEL MEANINGFUL TOLERANCES ARE SHOWN WHERE NECESSARY GLOBAL DRAWING TOLERANCES ARE UNDEFINED	Binghamton University Watson School of Engineering ME 481 Computer Aided Engineering - Project 3			
	TITLE Link EBJ			
All dimensions shown in inches	SIZE A	FSCM NO. N/A	DWG NO. GRENIER-DWG03	REV A
DRAWN Matthew Grenier	DATE 12/4/08	SCALE 0.2 Inch = 1 Inch	SHEET 3 OF 9	

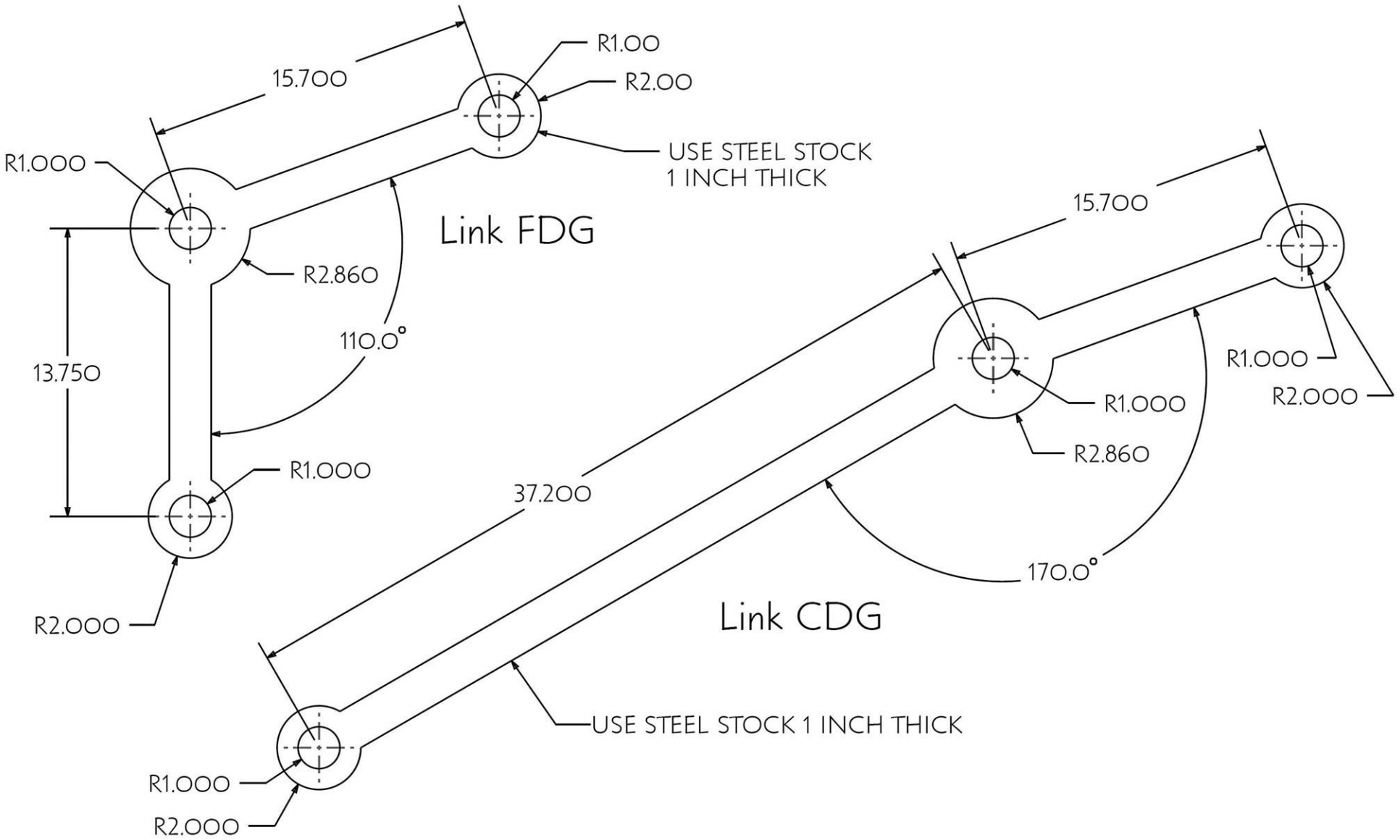

PART AND DRAWING NOTES MATERIAL - 4340 Q&T STEEL MEANINGFUL TOLERANCES ARE SHOWN WHERE NECESSARY GLOBAL DRAWING TOLERANCES ARE UNDEFINED	Binghamton University Watson School of Engineering ME 481 Computer Aided Engineering - Project 3			
	TITLE Links FDG and CDG			
All dimensions shown in inches	SIZE A	FSCM NO. N/A	DWG NO. GRENIER-DWG04	REV A
DRAWN Matthew Grenier	DATE 12/4/08	SCALE 0.15 Inch = 1 Inch	SHEET 4 OF 9	

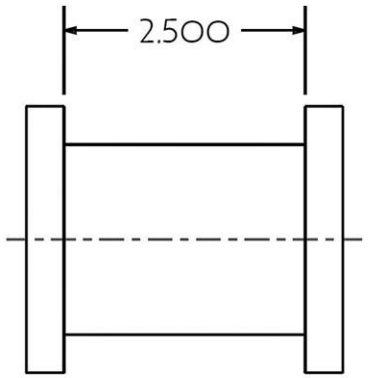

Pin A

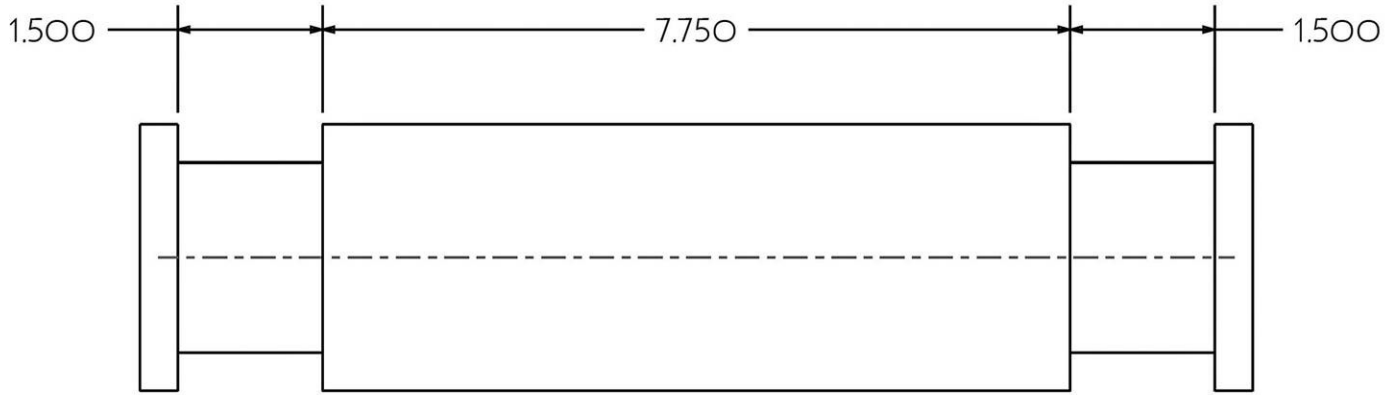

Pin D

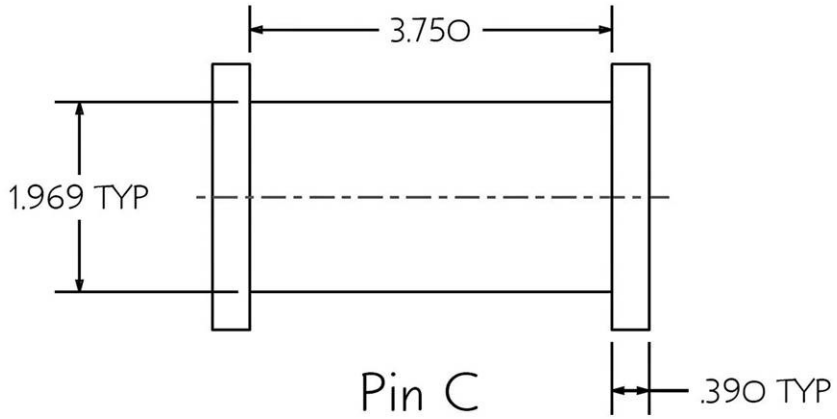

Pin C

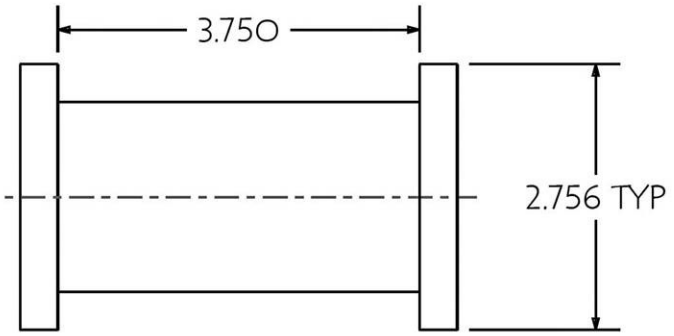

Pin E

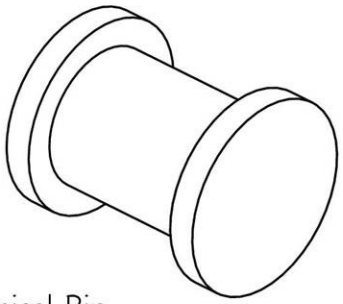

Typical Pin
SCALE 0.400

PART AND DRAWING NOTES MATERIAL - 4340 Q&T STEEL VALUES MARKED TYP ARE TYPICAL OF ALL PINS MEANINGFUL TOLERANCES ARE SHOWN WHERE NECESSARY GLOBAL DRAWING TOLERANCES ARE UNDEFINED	Binghamton University Watson School of Engineering ME 481 Computer Aided Engineering - Project 3			
	TITLE Pins A,C, D and E			
All dimensions shown in inches	SIZE A	FSCM NO. N/A	DWG NO. GRENIER-DWG05	REV A
DRAWN Matthew Grenier	DATE 12/4/08	SCALE 0.5 Inch = 1 Inch	SHEET 5 OF 9	

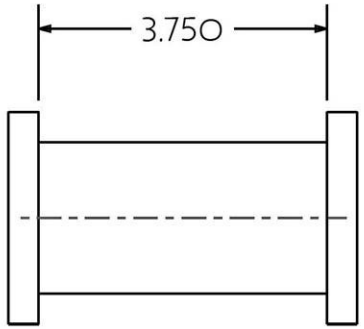

Pin F

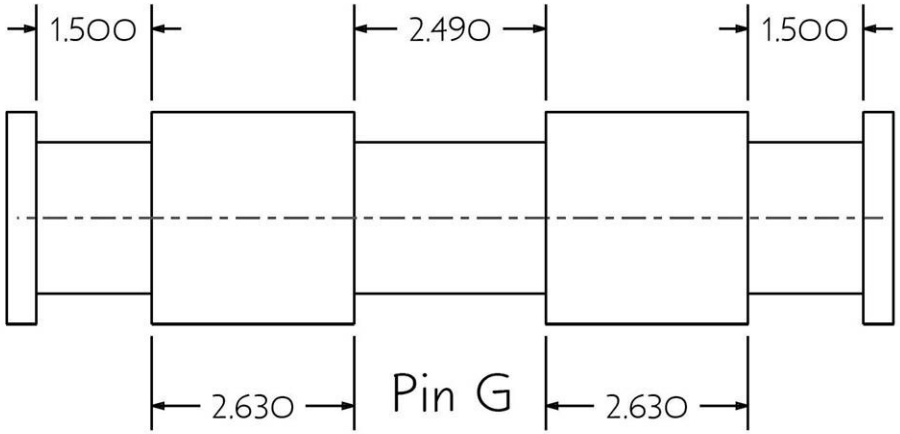

Pin G

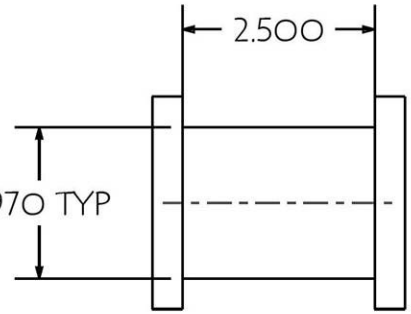

Pin H

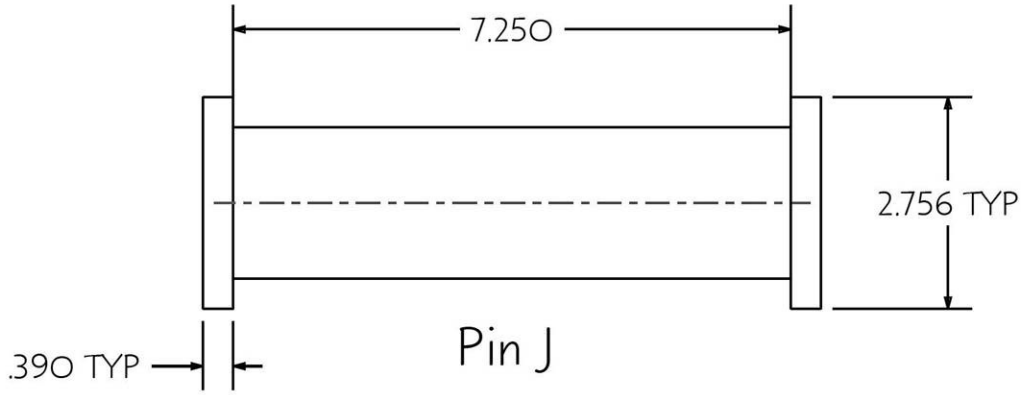

Pin J

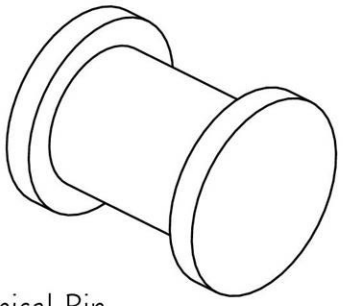

Typical Pin
SCALE 0.400

PART AND DRAWING NOTES MATERIAL - 4340 Q&T STEEL VALUES MARKED TYP ARE TYPICAL OF ALL PINS MEANINGFUL TOLERANCES ARE SHOWN WHERE NECESSARY GLOBAL DRAWING TOLERANCES ARE UNDEFINED	Binghamton University Watson School of Engineering ME 481 Computer Aided Engineering - Project 3			
	TITLE Pins F, G, H and J			
All dimensions shown in inches	SIZE A	FSCM NO. N/A	DWG NO. GRENIER-DWG06	REV A
DRAWN Matthew Grenier	DATE 12/4/08	SCALE 0.4 Inch = 1 Inch	SHEET 6 OF 9	

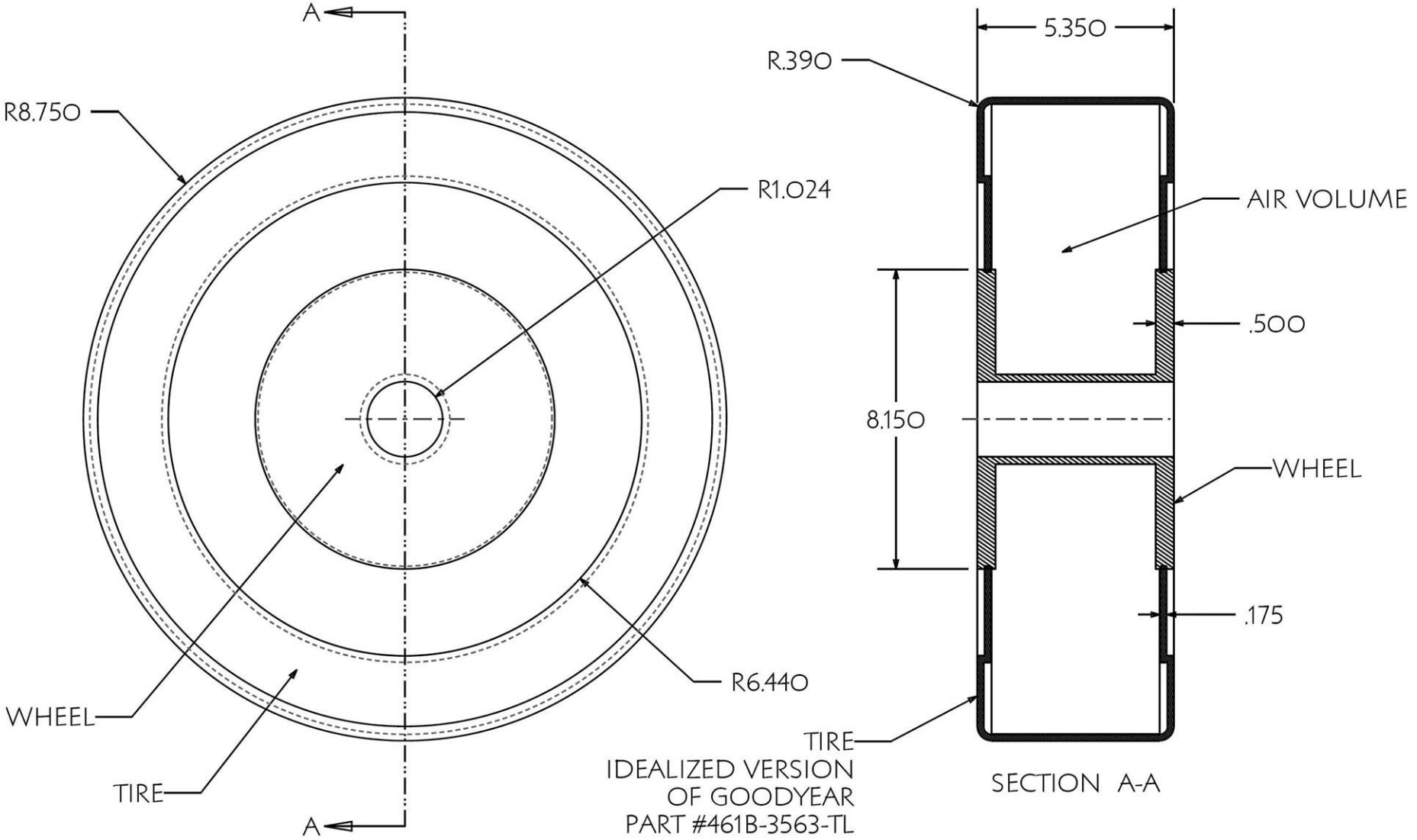

PART AND DRAWING NOTES WHEEL MATERIAL - 6061-T651 TIRE MATERIAL - S-SBR MEANINGFUL TOLERANCES ARE SHOWN WHERE NECESSARY GLOBAL DRAWING TOLERANCES ARE UNDEFINED	Binghamton University Watson School of Engineering ME 481 Computer Aided Engineering - Project 3			
	TITLE Tire subassembly			
All dimensions shown in inches	SIZE A	FSCM NO. N/A	DWG NO. GRENIER-DWG07	REV A
DRAWN Matthew Grenier	DATE 12/4/08	SCALE .25 Inch = 1 Inch	SHEET 7 OF 9	

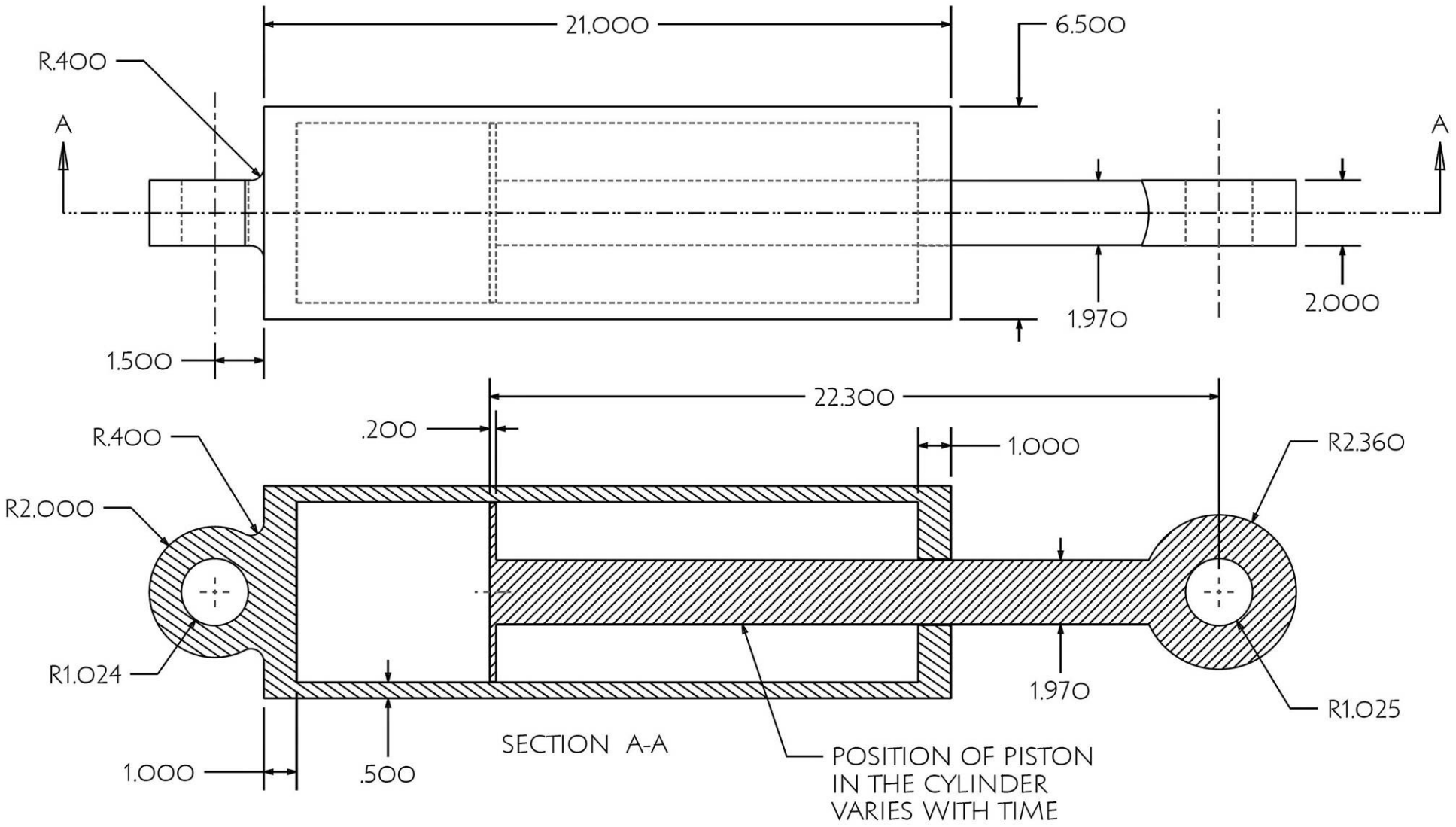

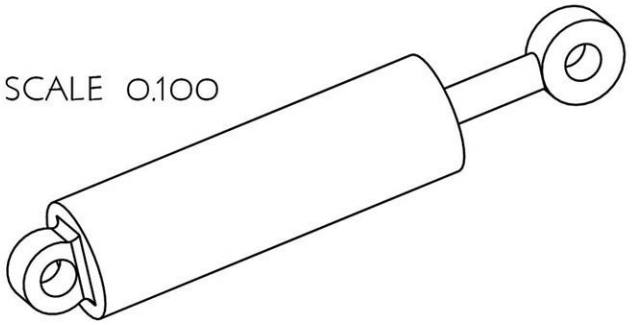

PART AND DRAWING NOTES MATERIAL - 316L STAINLESS STEEL MEANINGFUL TOLERANCES ARE SHOWN WHERE NECESSARY GLOBAL DRAWING TOLERANCES ARE UNDEFINED	Binghamton University Watson School of Engineering ME 481 Computer Aided Engineering - Project 3			
	TITLE Piston subassembly			
All dimensions shown in inches	SIZE A	FSCM NO. N/A	DWG NO. GRENIER-DWG08	REV A
DRAWN Matthew Grenier	DATE 12/4/08	SCALE .225 Inch = 1 Inch	SHEET 8 OF 9	

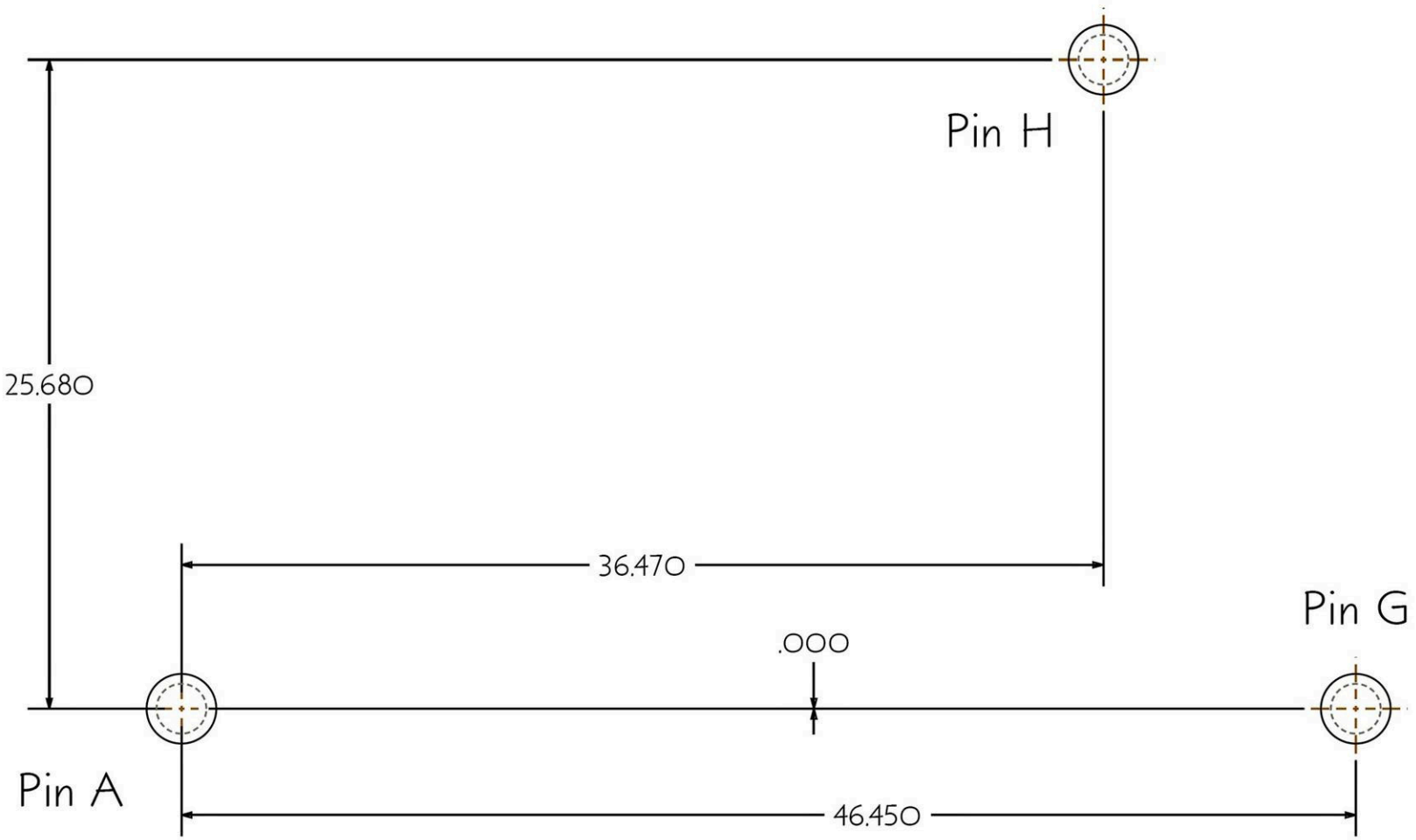

PART AND DRAWING NOTES PINS A, H, AND G SERVE AS THE GROUND CONNECTIONS TO THE AIRCRAFT FRAME MEANINGFUL TOLERANCES ARE SHOWN WHERE NECESSARY GLOBAL DRAWING TOLERANCES ARE UNDEFINED	Binghamton University Watson School of Engineering ME 481 Computer Aided Engineering - Project 3			
	TITLE Ground pin layout			
All dimensions shown in inches	SIZE A	FSCM NO. N/A	DWG NO. GRENIER-DWG09	REV A
DRAWN Matthew Grenier	DATE 12/4/08	SCALE .225 Inch = 1 Inch	SHEET 9 OF 9	

APPENDIX A-2: PIN CONNECTION REACTION FORCES

Appendix A-2 Figure 1 – Pins A,B,H Connection Reactions 58
Appendix A-2 Figure 2 – Pin C Connection Reactions 59
Appendix A-2 Figure 3 – Pin C Net Magnitudes 59
Appendix A-2 Figure 4 – Pin D Connection Reactions 60
Appendix A-2 Figure 5 – Pin D Net Magnitudes 60
Appendix A-2 Figure 6 – Pin E Connection Reactions 61
Appendix A-2 Figure 7 – Pin E Net Magnitudes 61
Appendix A-2 Figure 8 – Pin F Connection Reactions 62
Appendix A-2 Figure 9 – Pin F Net Magnitudes 62
Appendix A-2 Figure 10 – Pin G Connection Reactions 63
Appendix A-2 Figure 11 – Pin G Net Magnitudes 63
Appendix A-2 Figure 12 – Pin J Connection Reactions 64
Appendix A-2 Figure 13 – Pin J Net Magnitudes 64

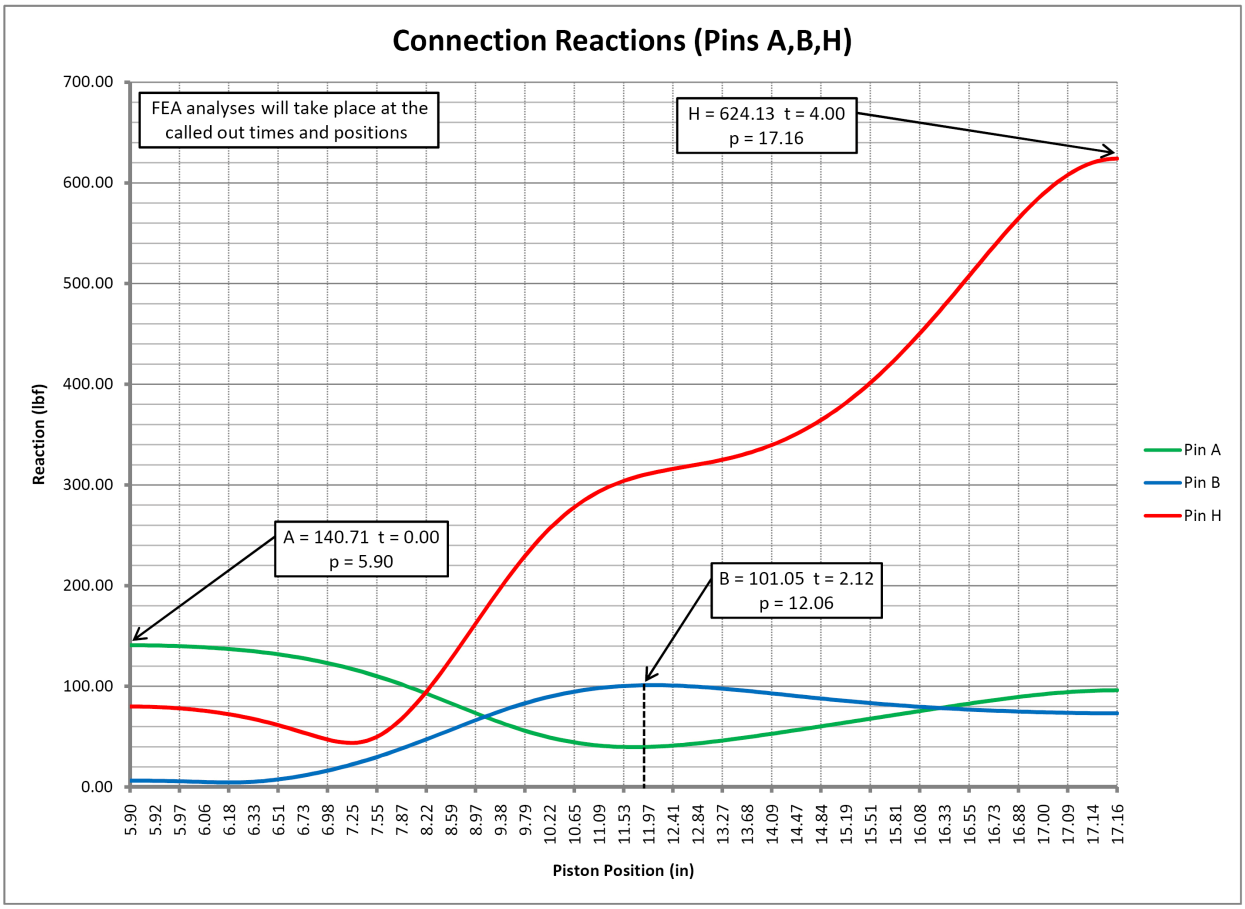

Appendix A-2 Figure 1 – Pins A,B,H Connection Reactions

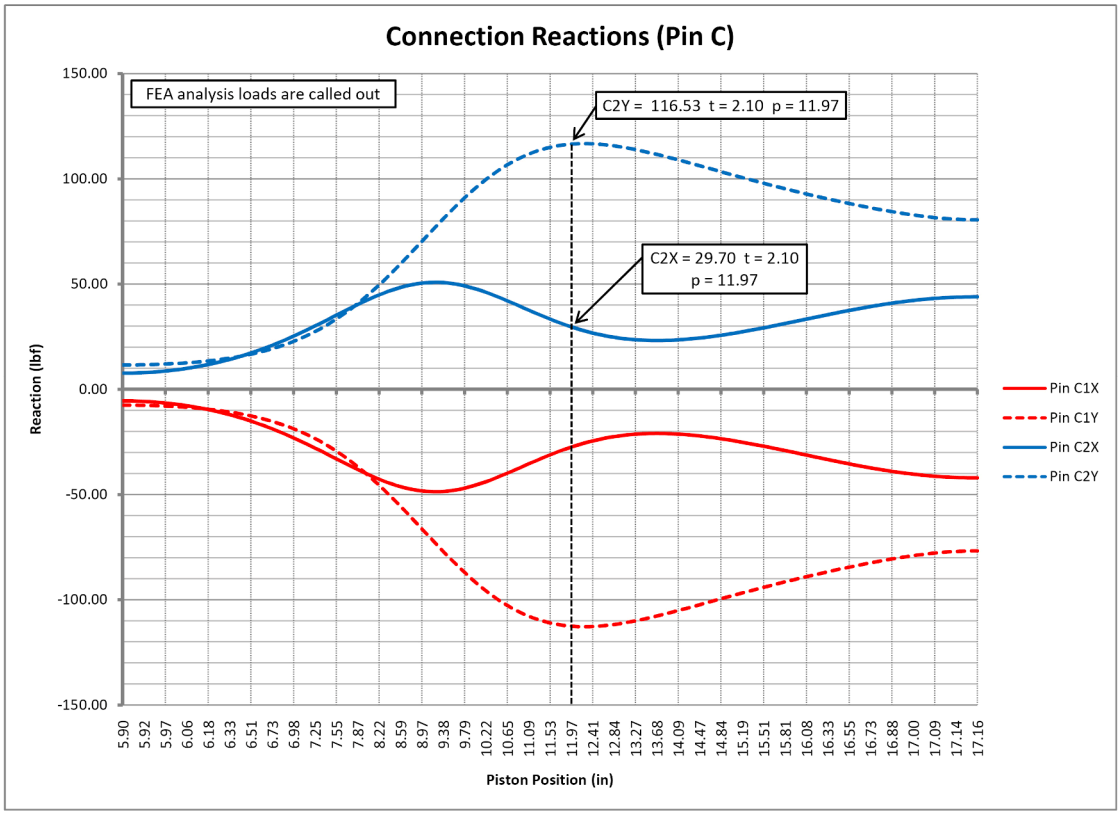

Appendix A-2 Figure 2 – Pin C Connection Reactions

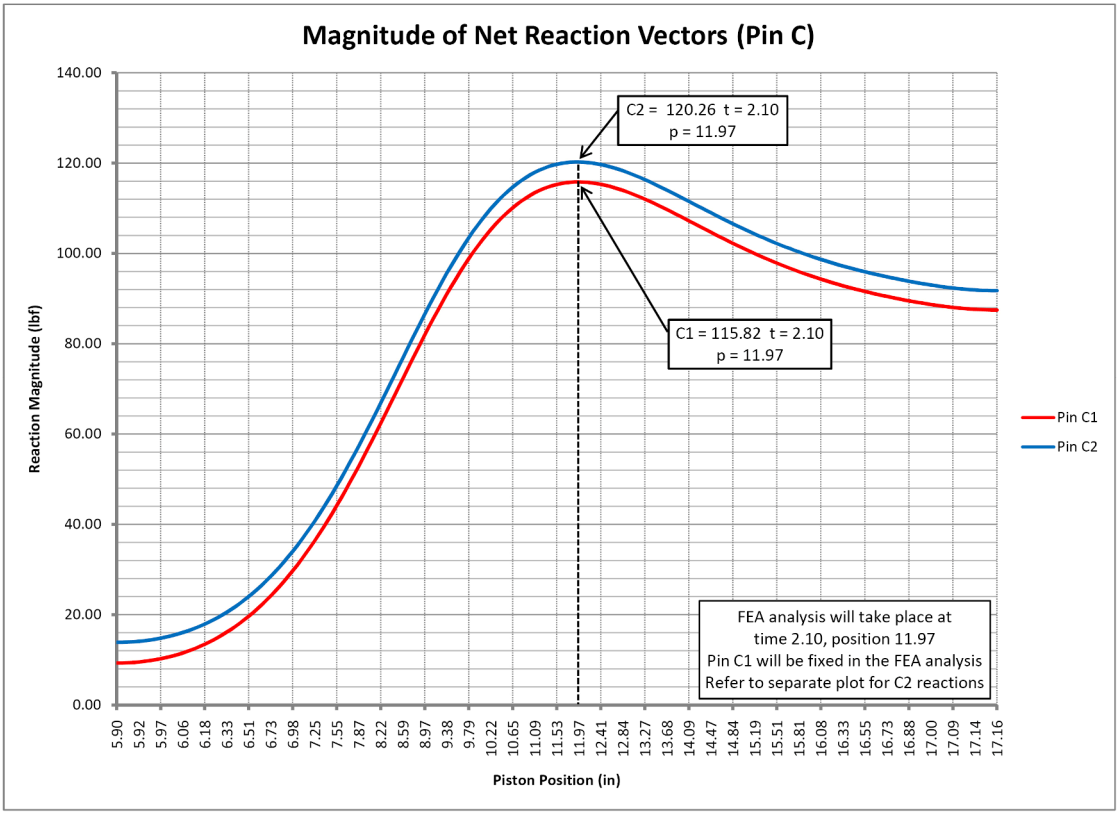

Appendix A-2 Figure 3 – Pin C Net Magnitudes

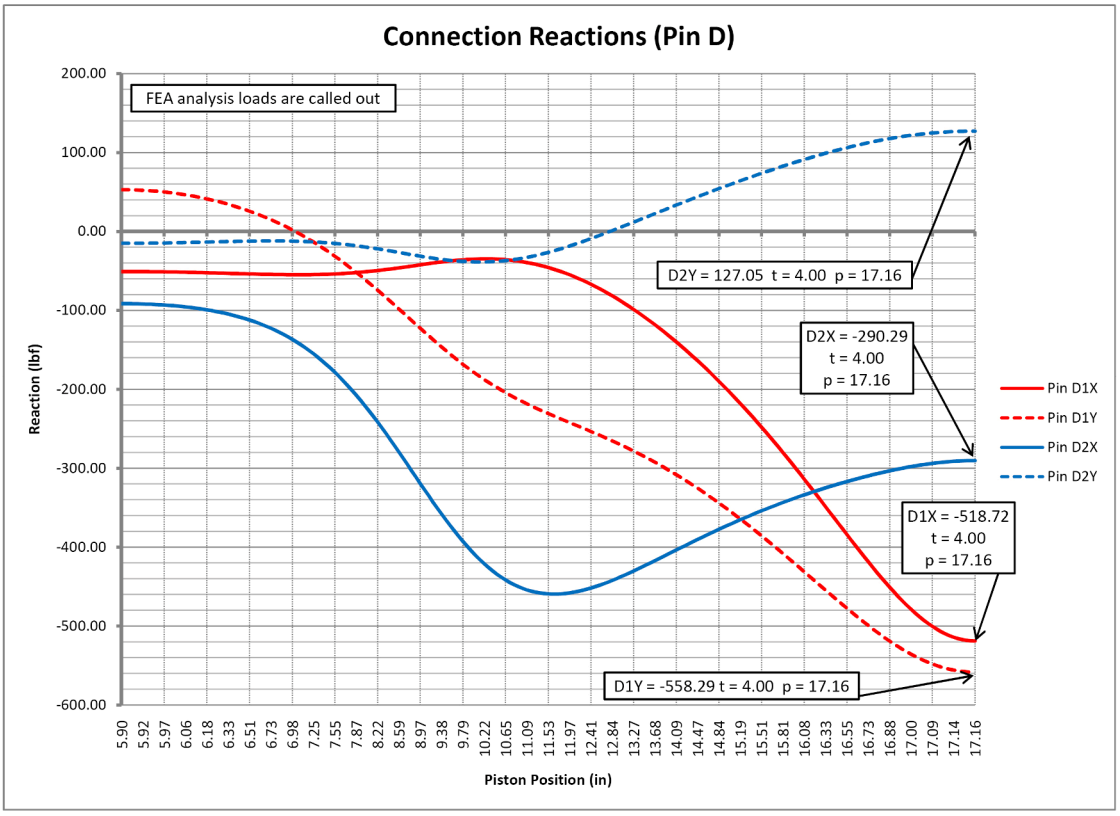

Appendix A-2 Figure 4 – Pin D Connection Reactions

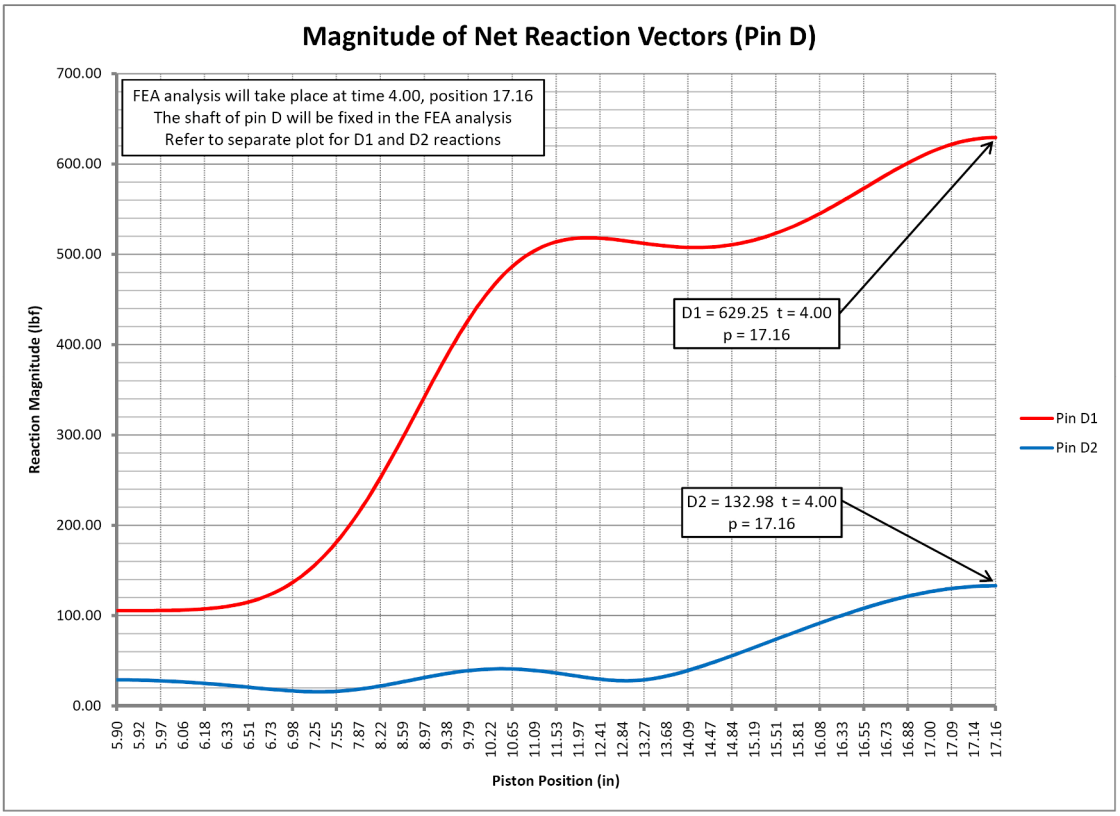

Appendix A-2 Figure 5 – Pin D Net Magnitudes

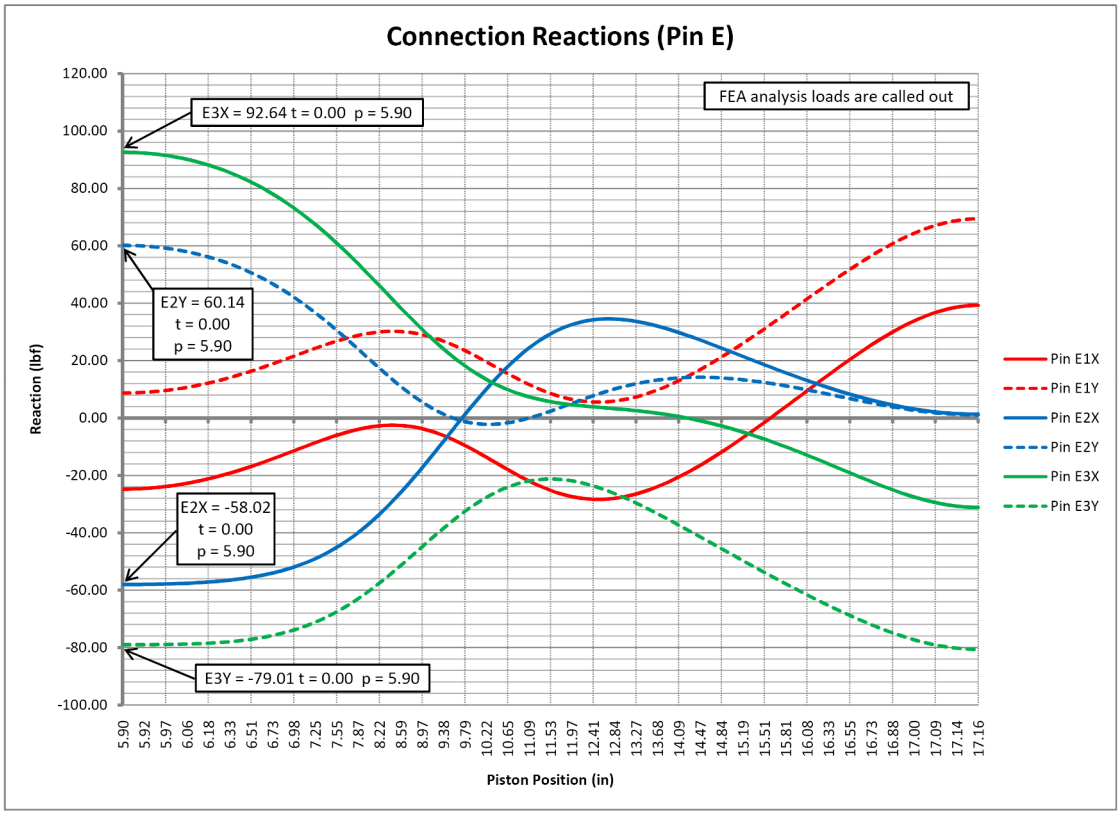

Appendix A-2 Figure 6 – Pin E Connection Reactions

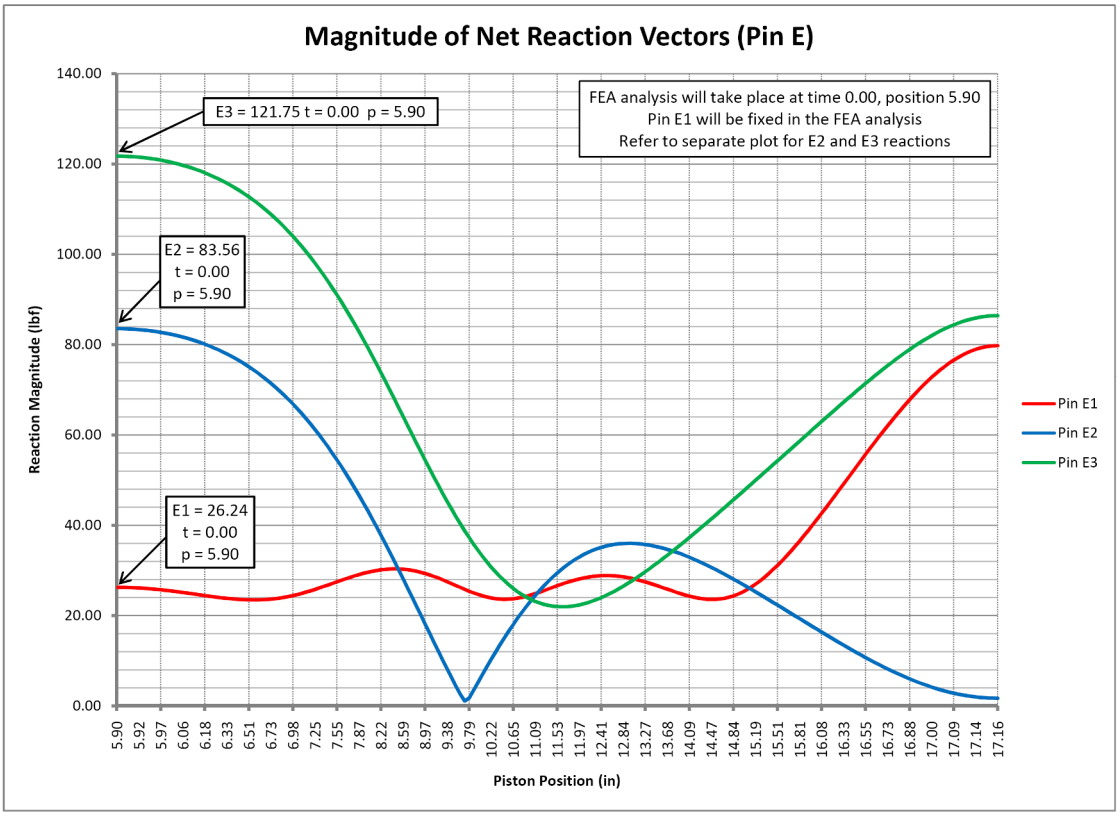

Appendix A-2 Figure 7 – Pin E Net Magnitudes

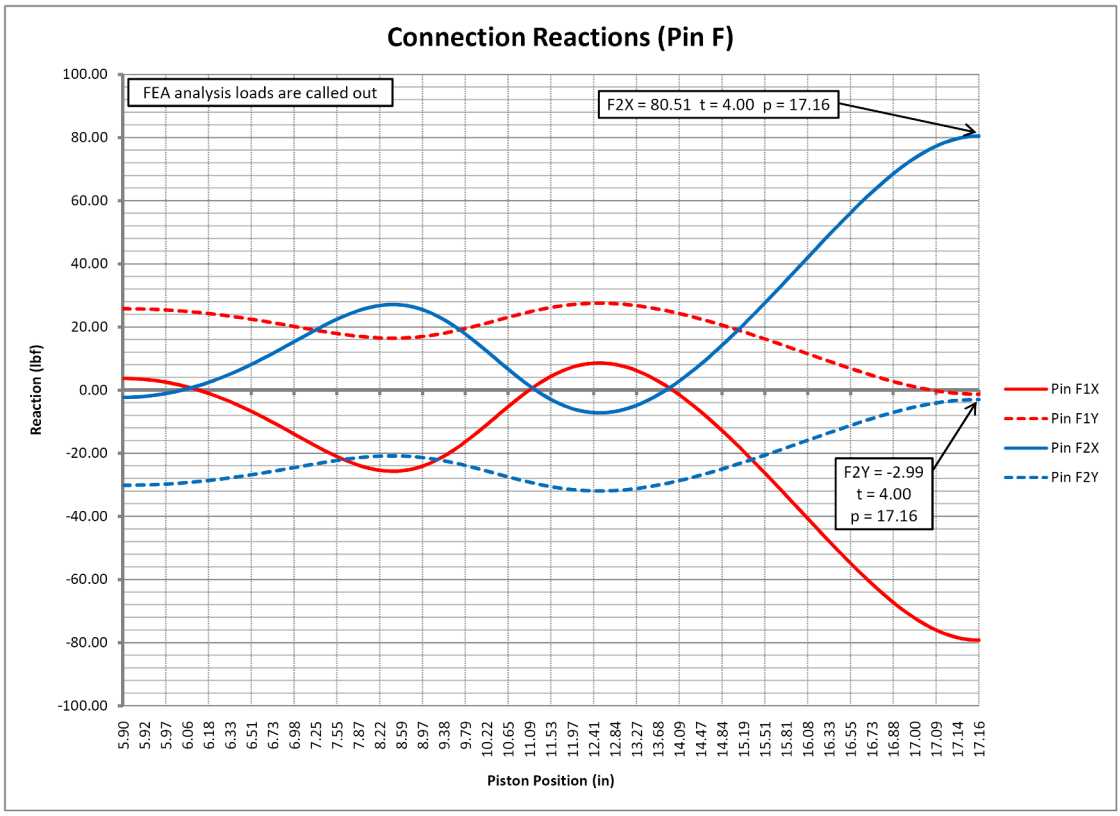

Appendix A-2 Figure 8 – Pin F Connection Reactions

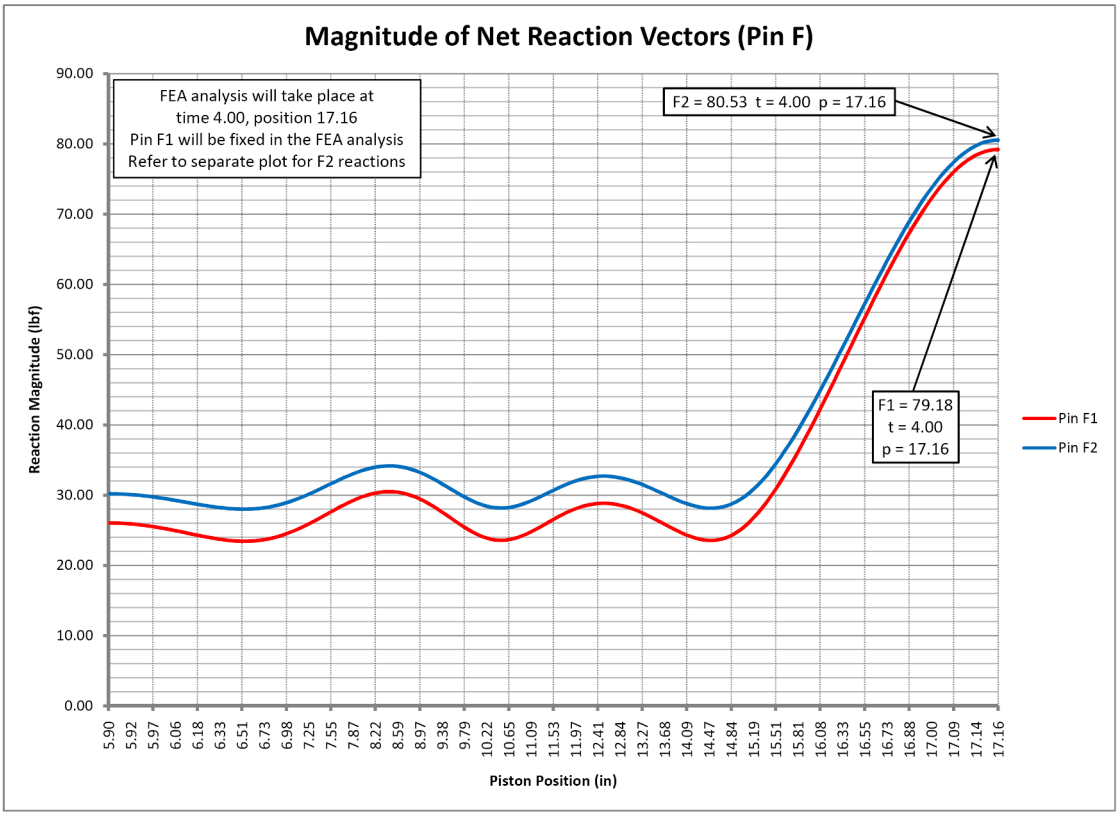

Appendix A-2 Figure 9 – Pin F Net Magnitudes

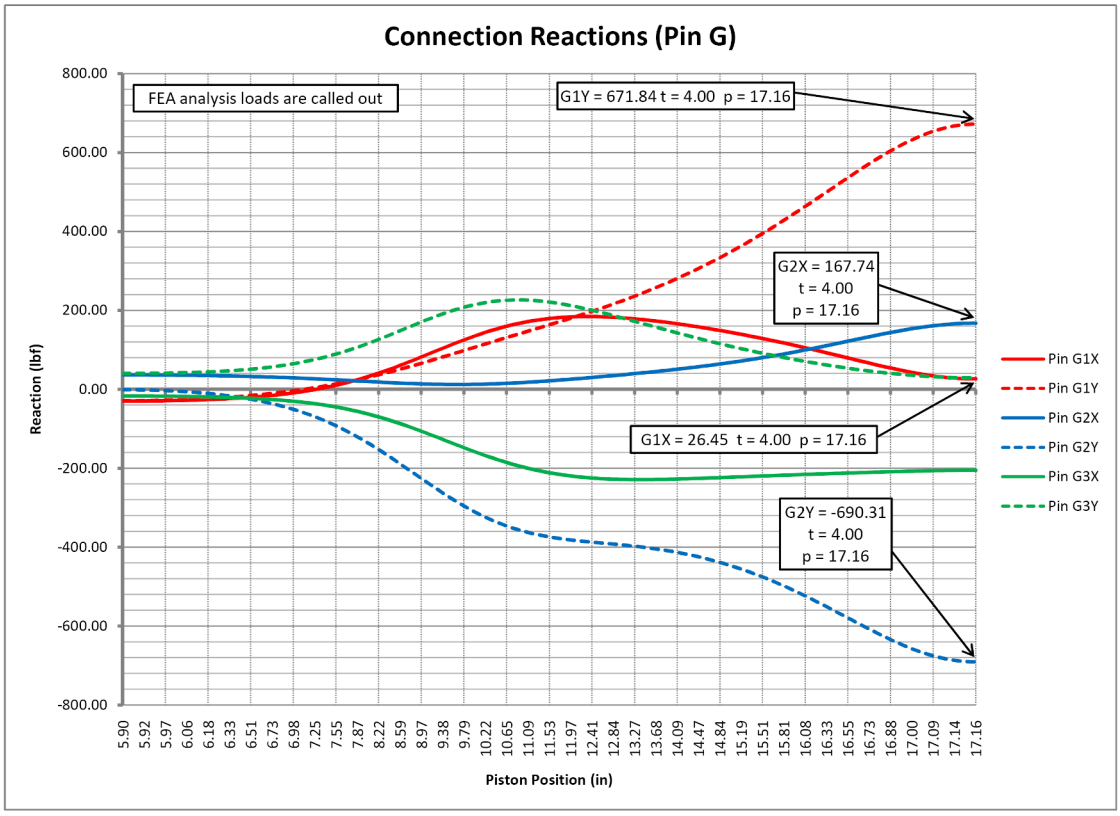

Appendix A-2 Figure 10 – Pin G Connection Reactions

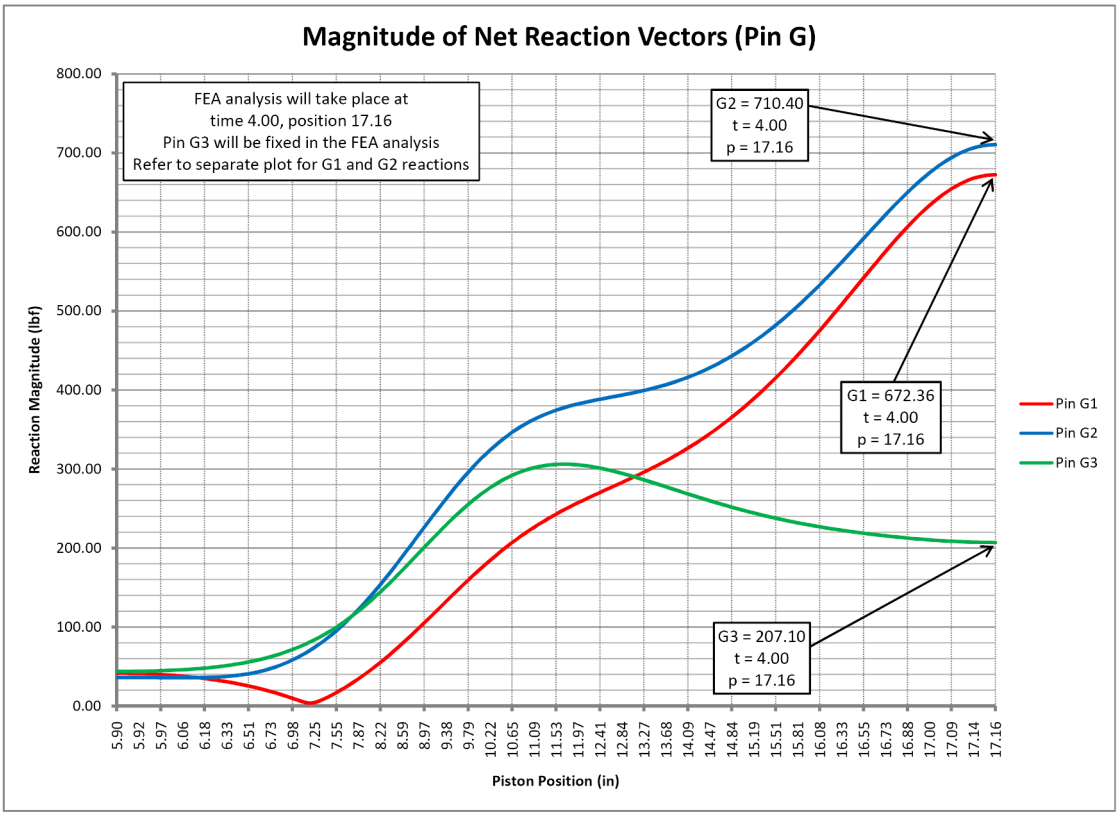

Appendix A-2 Figure 11 – Pin G Net Magnitudes

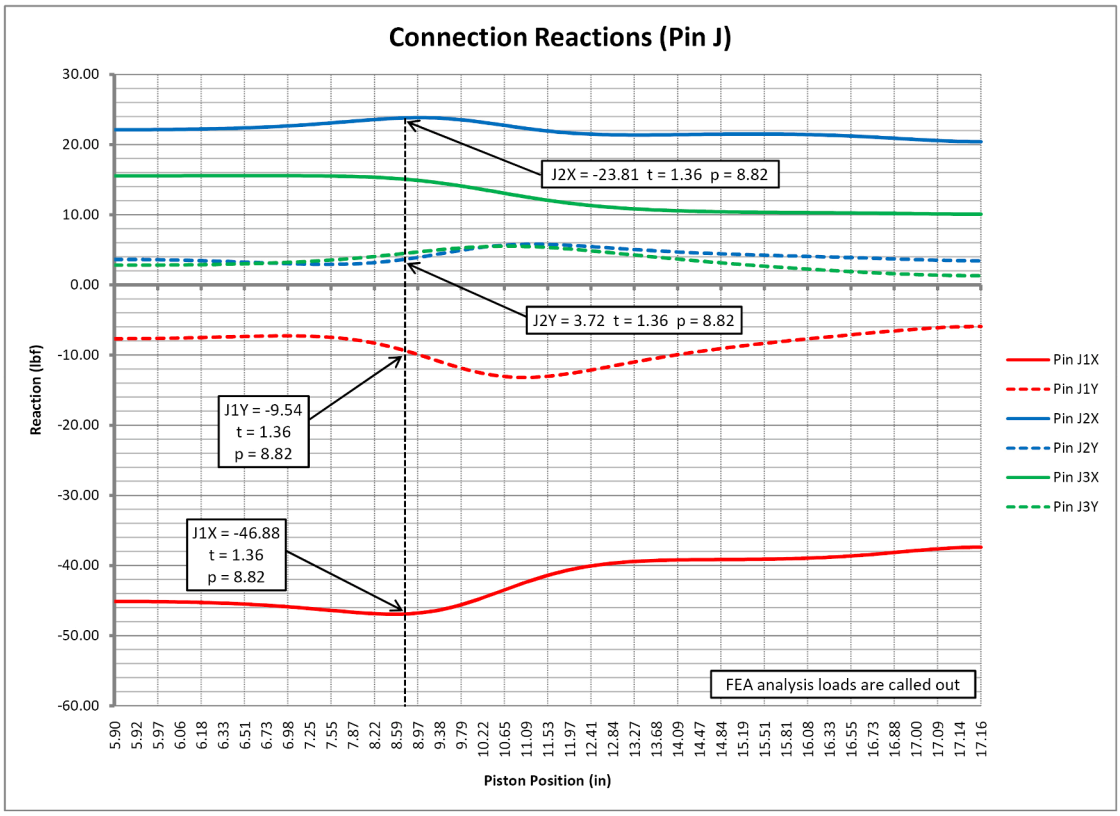

Appendix A-2 Figure 12 – Pin J Connection Reactions

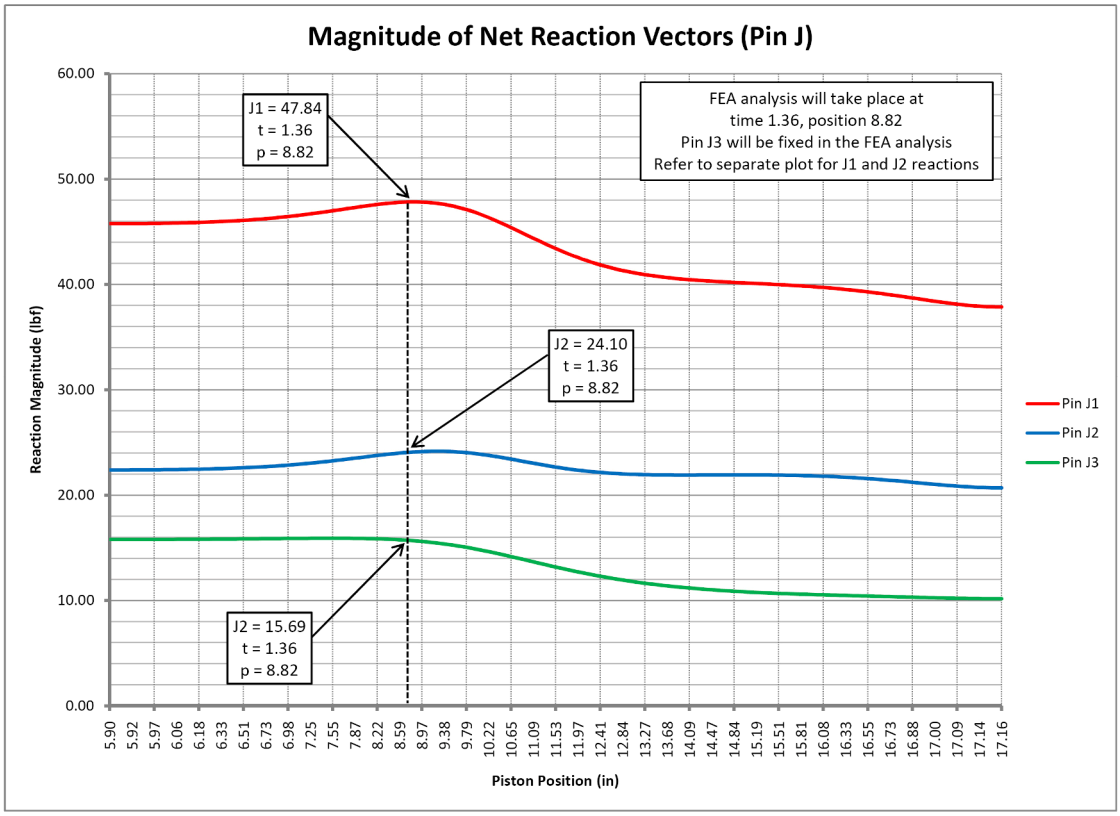

Appendix A-2 Figure 13 – Pin J Net Magnitudes

APPENDIX A-3: GEAR RETRACT FEA RESULTS

Appendix A-3 Figure 1 – Pin A Gear Retract 68
Appendix A-3 Figure 2 – Pin B Gear Retract 68
Appendix A-3 Figure 3 – Pin C Gear Retract 69
Appendix A-3 Figure 4 – Pin D Gear Retract 69
Appendix A-3 Figure 5 – Pin E Gear Retract 70
Appendix A-3 Figure 6 – Pin F Gear Retract 70
Appendix A-3 Figure 7 – Pin G Gear Retract 71
Appendix A-3 Figure 8 – Pin H Gear Retract 71
Appendix A-3 Figure 9 – Pin J Gear Retract 72

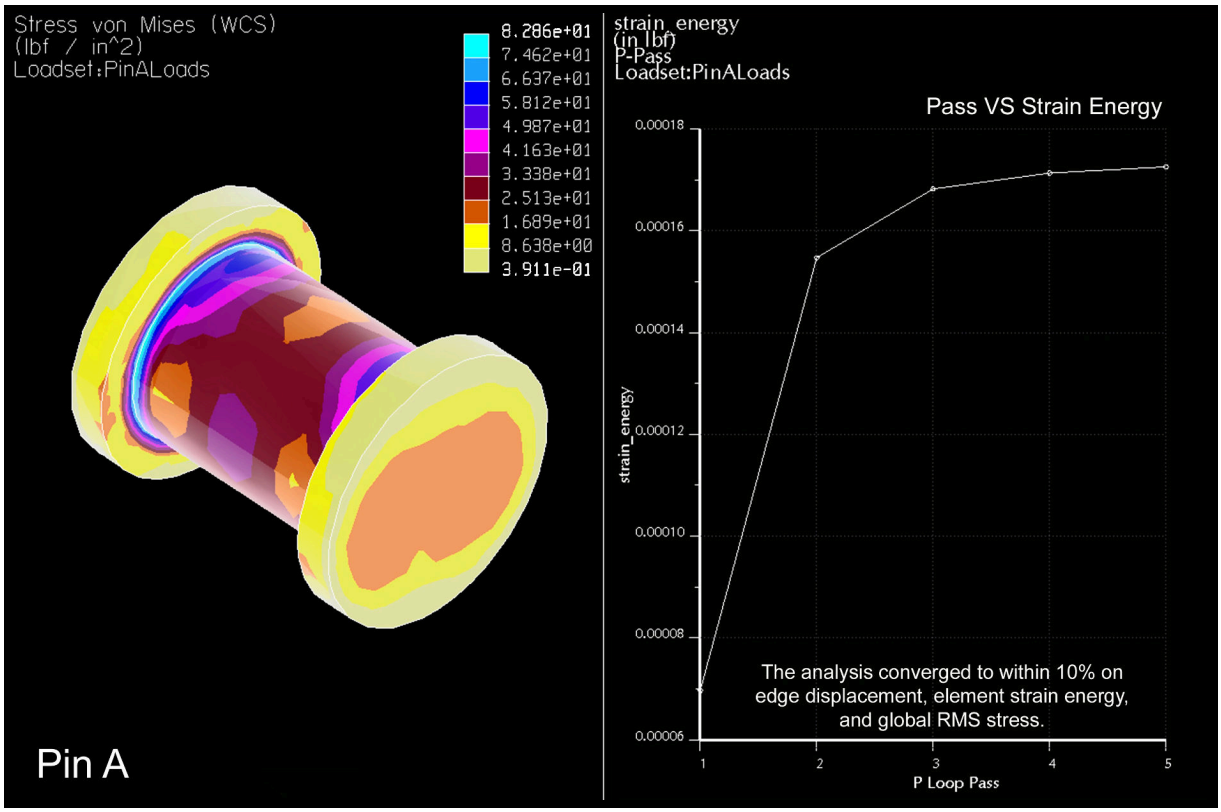

Appendix A-3 Figure 1 – Pin A Gear Retract

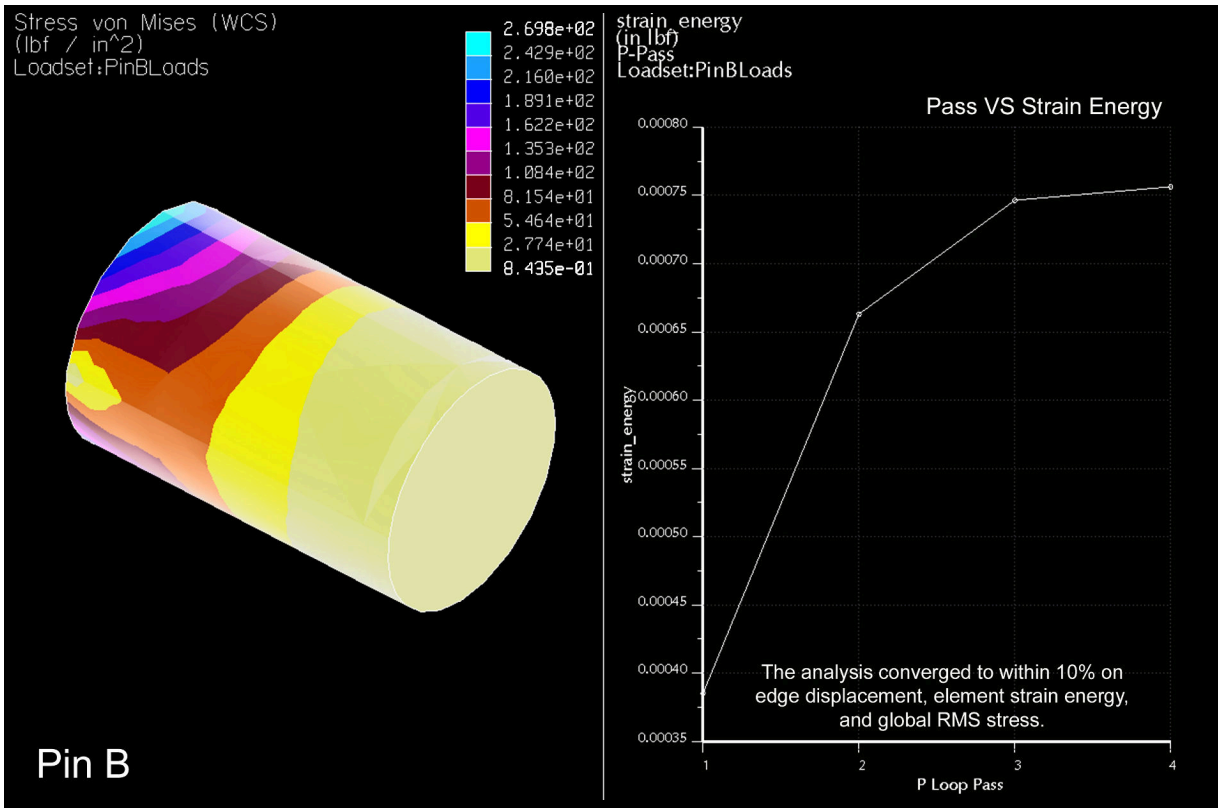

Appendix A-3 Figure 2 – Pin B Gear Retract

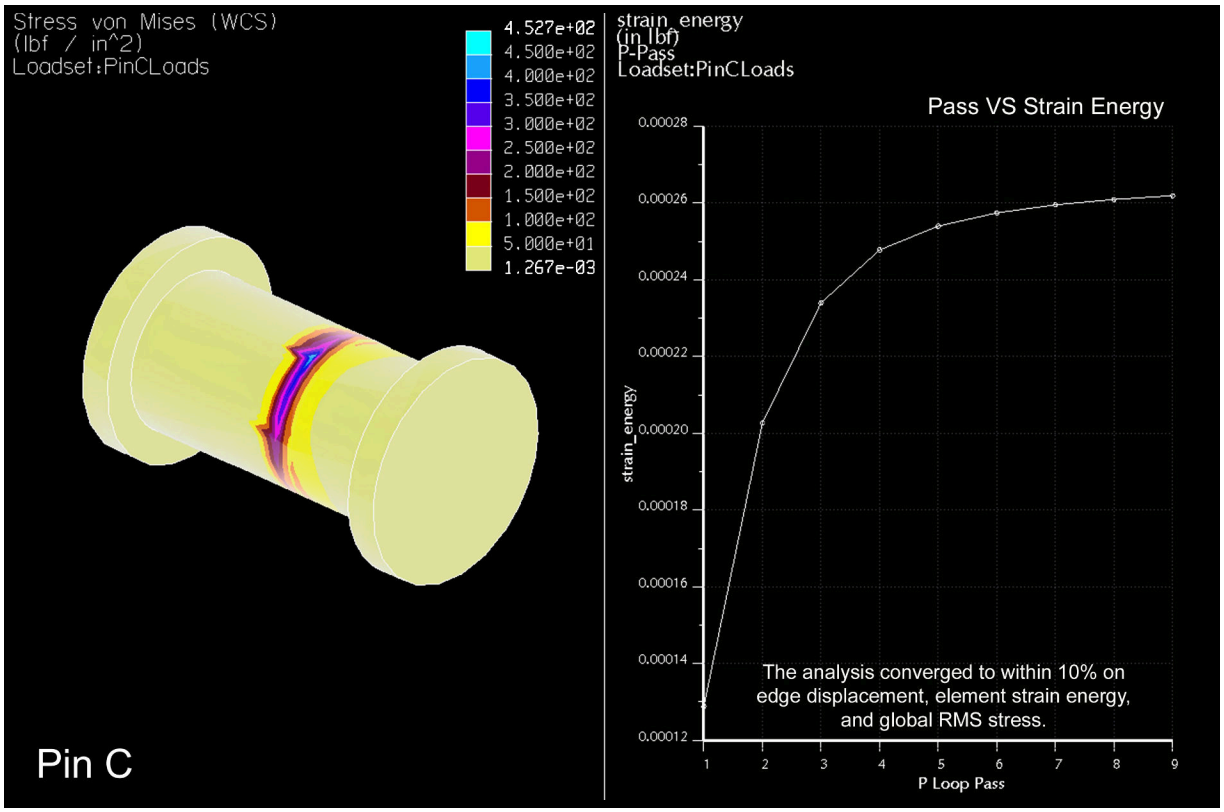

Appendix A-3 Figure 3 – Pin C Gear Retract

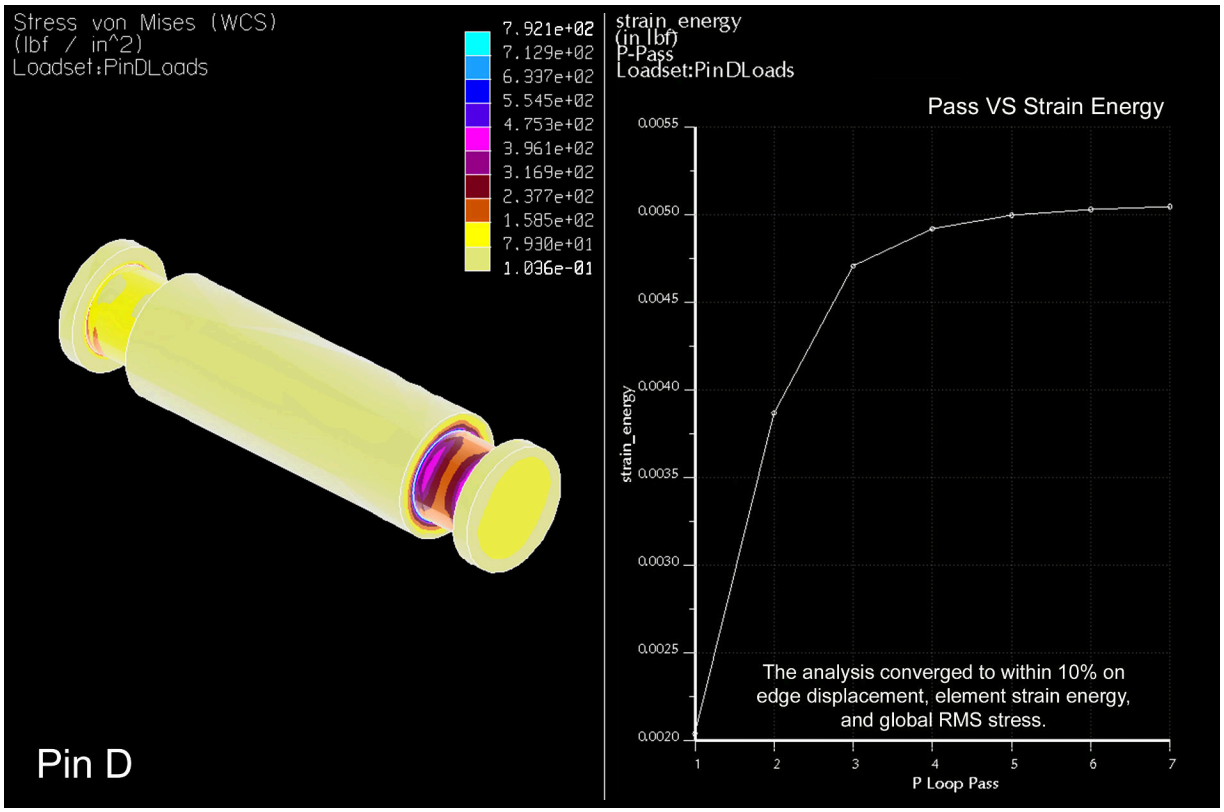

Appendix A-3 Figure 4 – Pin D Gear Retract

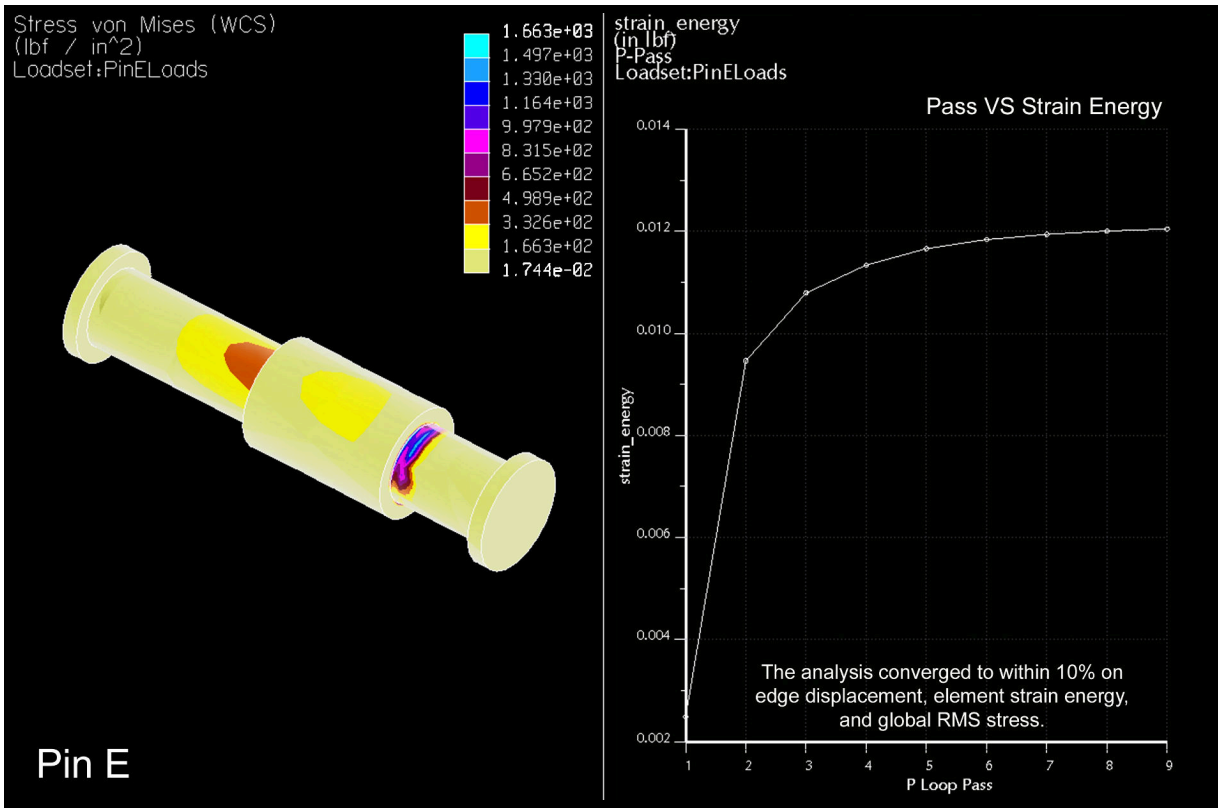

Appendix A-3 Figure 5 – Pin E Gear Retract

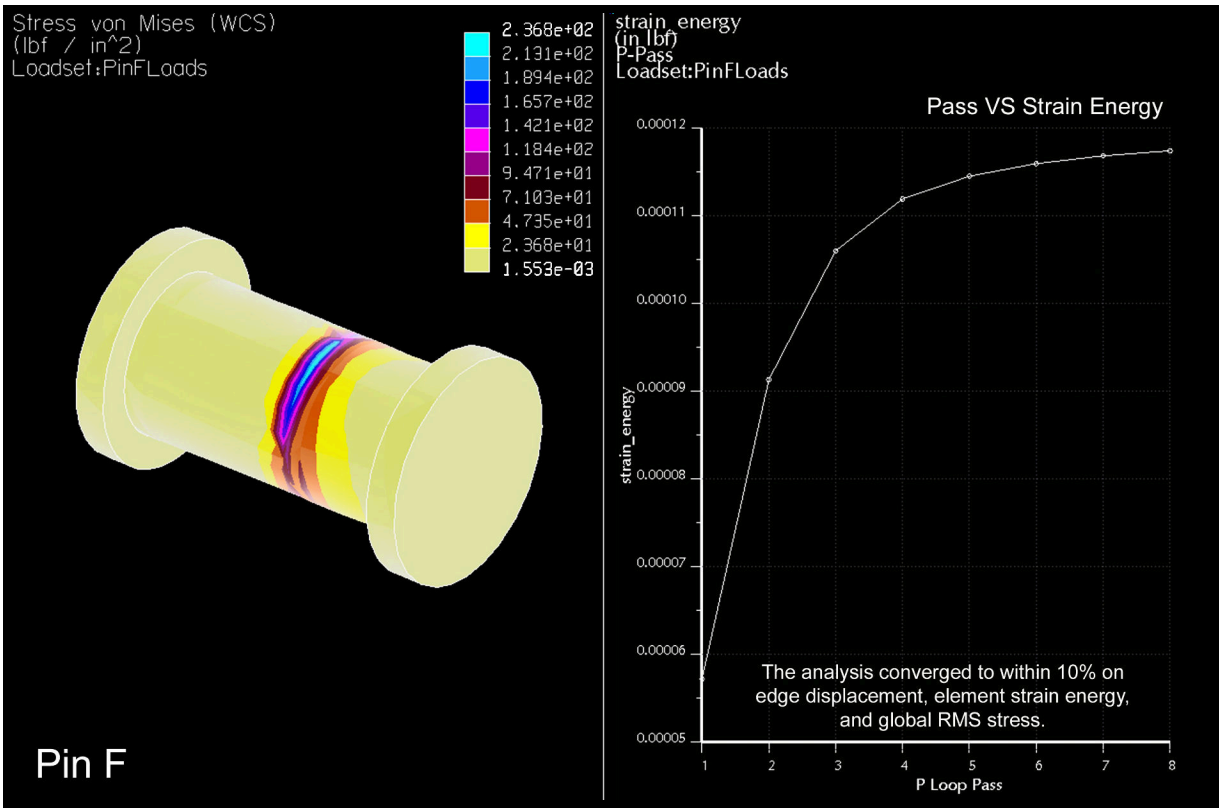

Appendix A-3 Figure 6 – Pin F Gear Retract

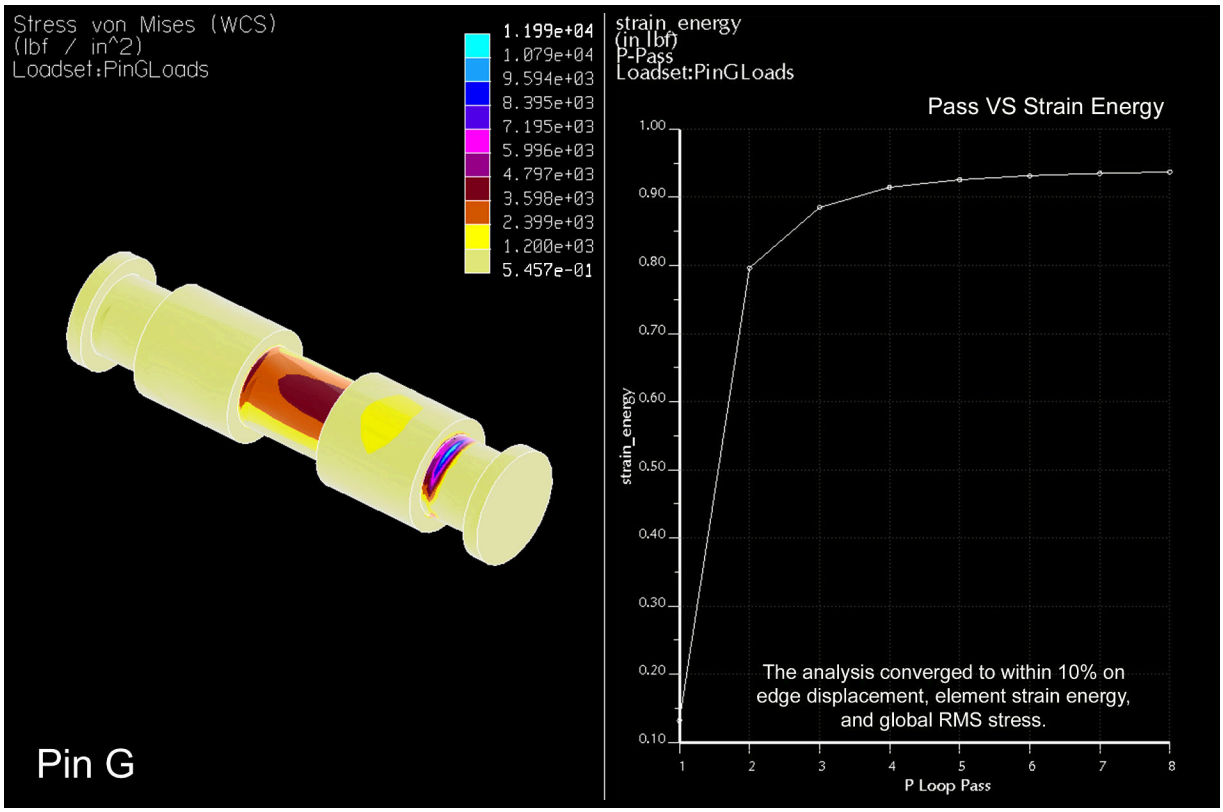

Appendix A-3 Figure 7 – Pin G Gear Retract

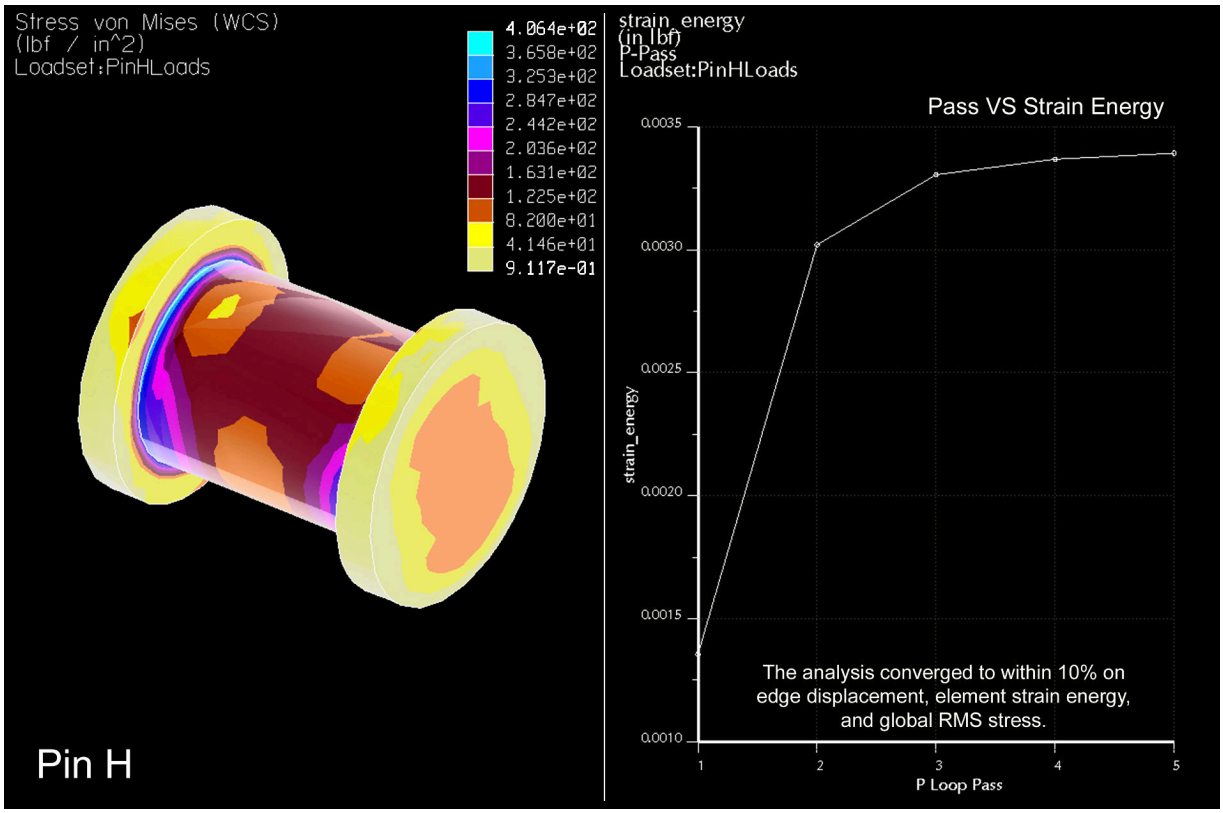

Appendix A-3 Figure 8 – Pin H Gear Retract

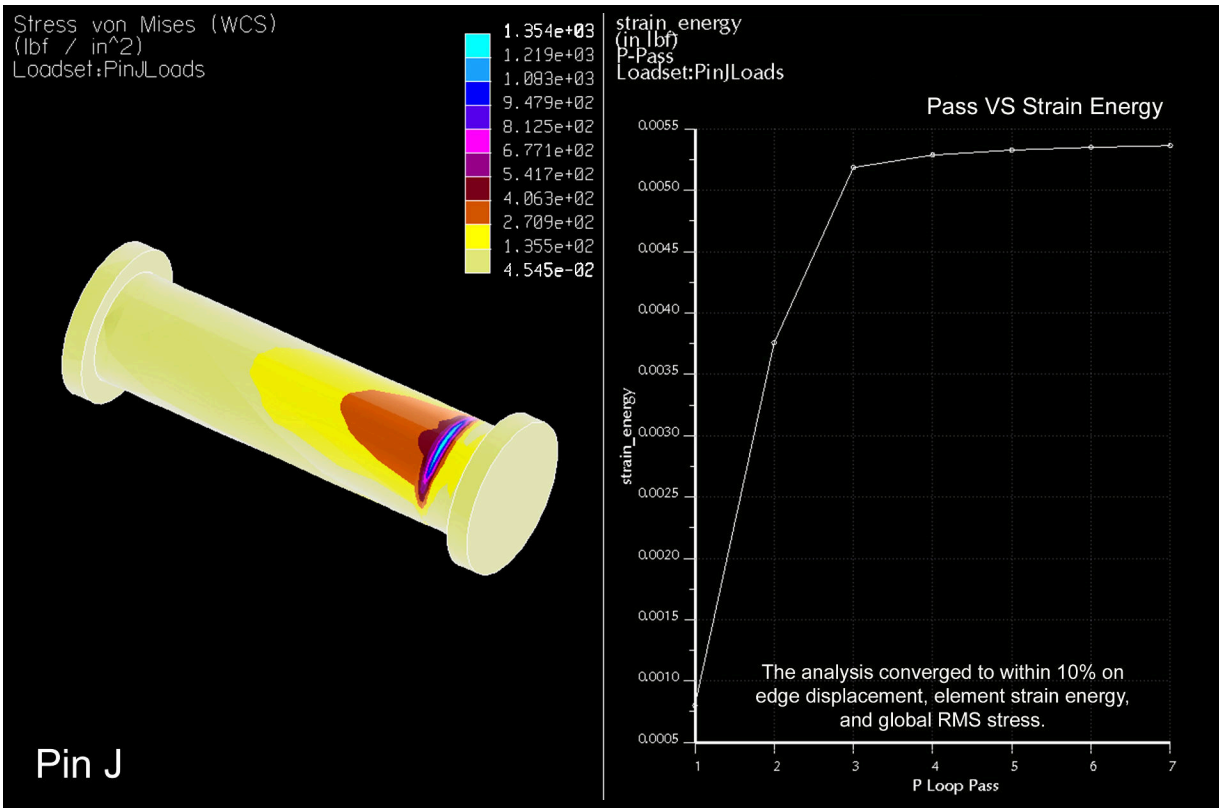

Appendix A-3 Figure 9 – Pin J Gear Retract

APPENDIX A-4: LANDING FEA RESULTS

Appendix A-4 Figure 1 – Pin A Landing 76
Appendix A-4 Figure 2 – Pin B Landing 76
Appendix A-4 Figure 3 – Pin C Landing 77
Appendix A-4 Figure 4 – Pin D Landing 77
Appendix A-4 Figure 5 – Pin E Landing 78
Appendix A-4 Figure 6 – Pin F Landing 78
Appendix A-4 Figure 7 – Pin G Landing 79
Appendix A-4 Figure 8 – Pin H Landing 79
Appendix A-4 Figure 9 – Pin J Landing 80

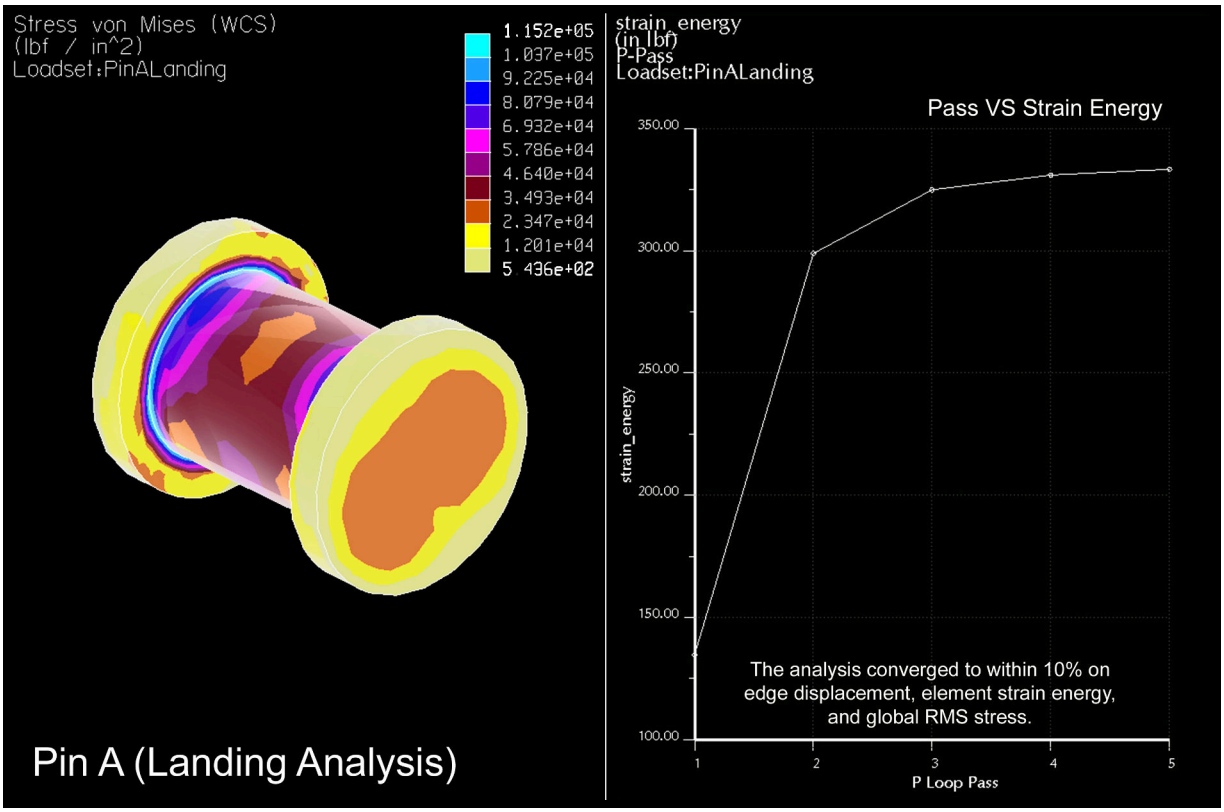

Appendix A-4 Figure 1 – Pin A Landing

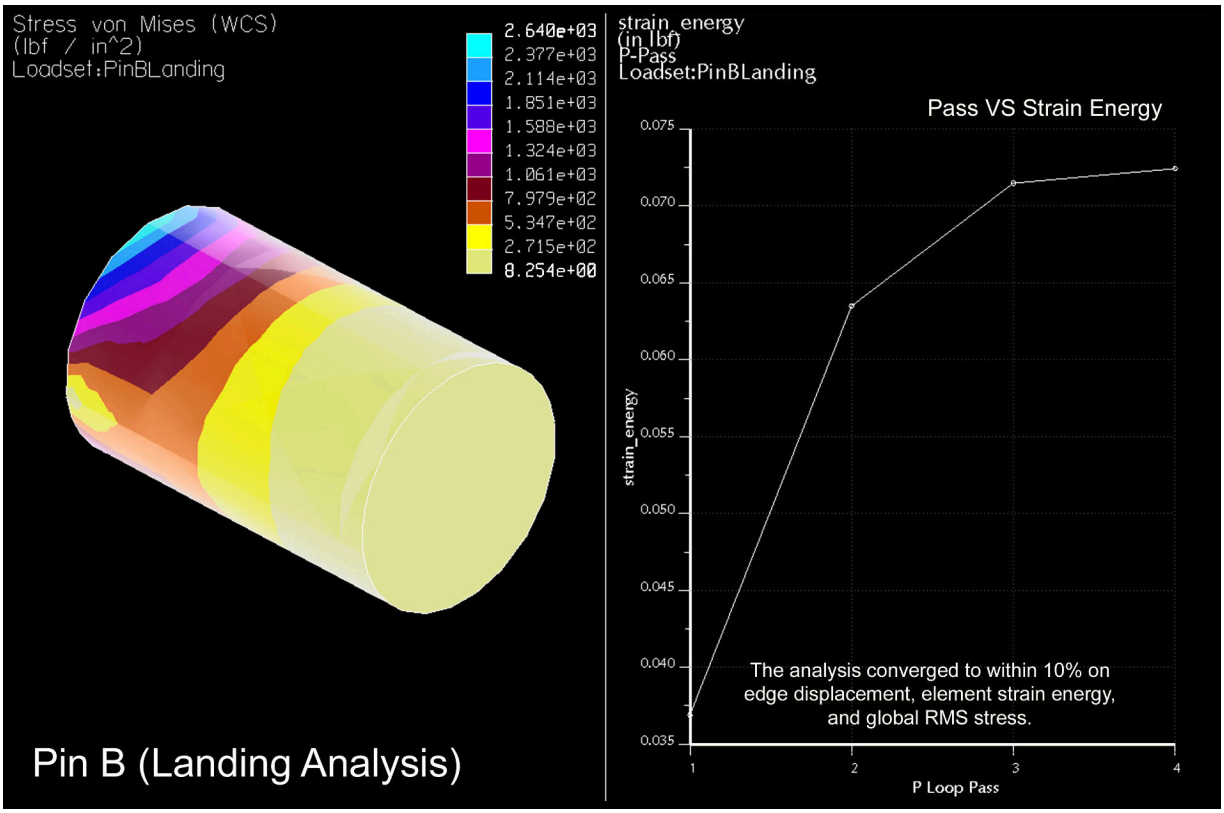

Appendix A-4 Figure 2 – Pin B Landing

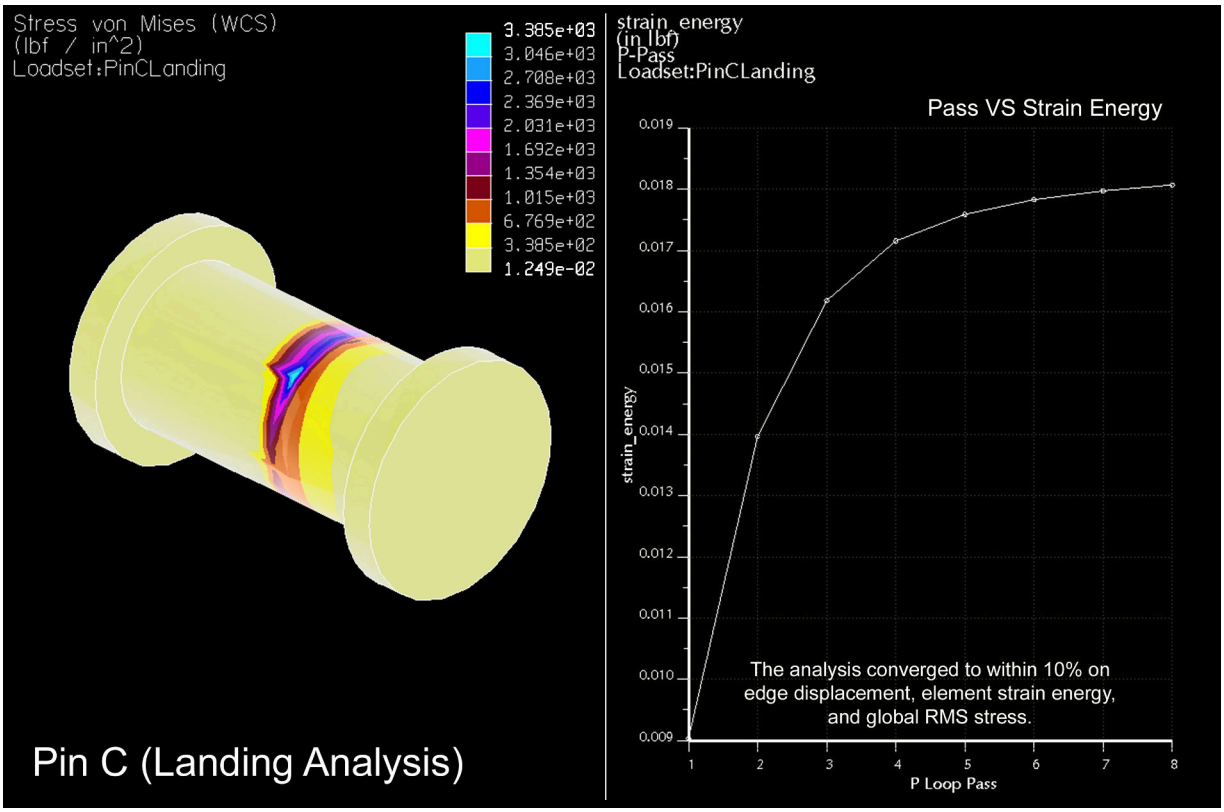

Appendix A-4 Figure 3 – Pin C Landing

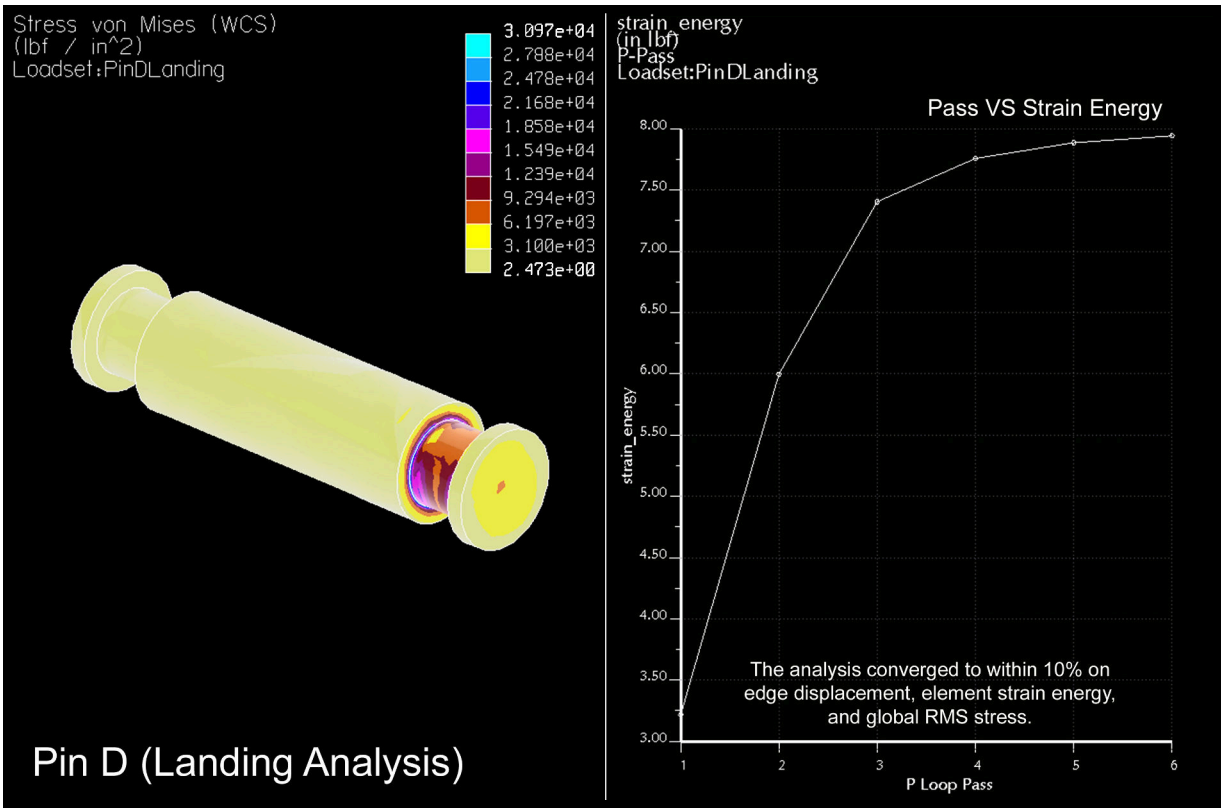

Appendix A-4 Figure 4 – Pin D Landing

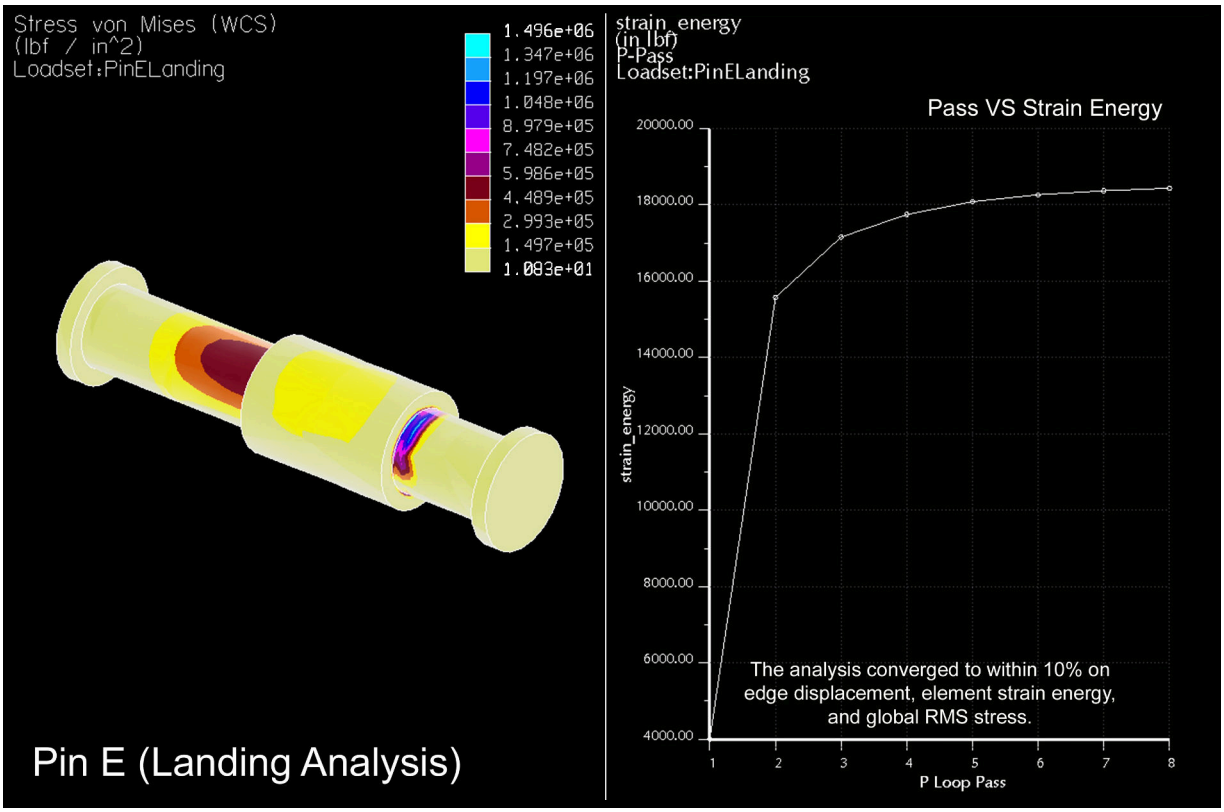

Appendix A-4 Figure 5 – Pin E Landing

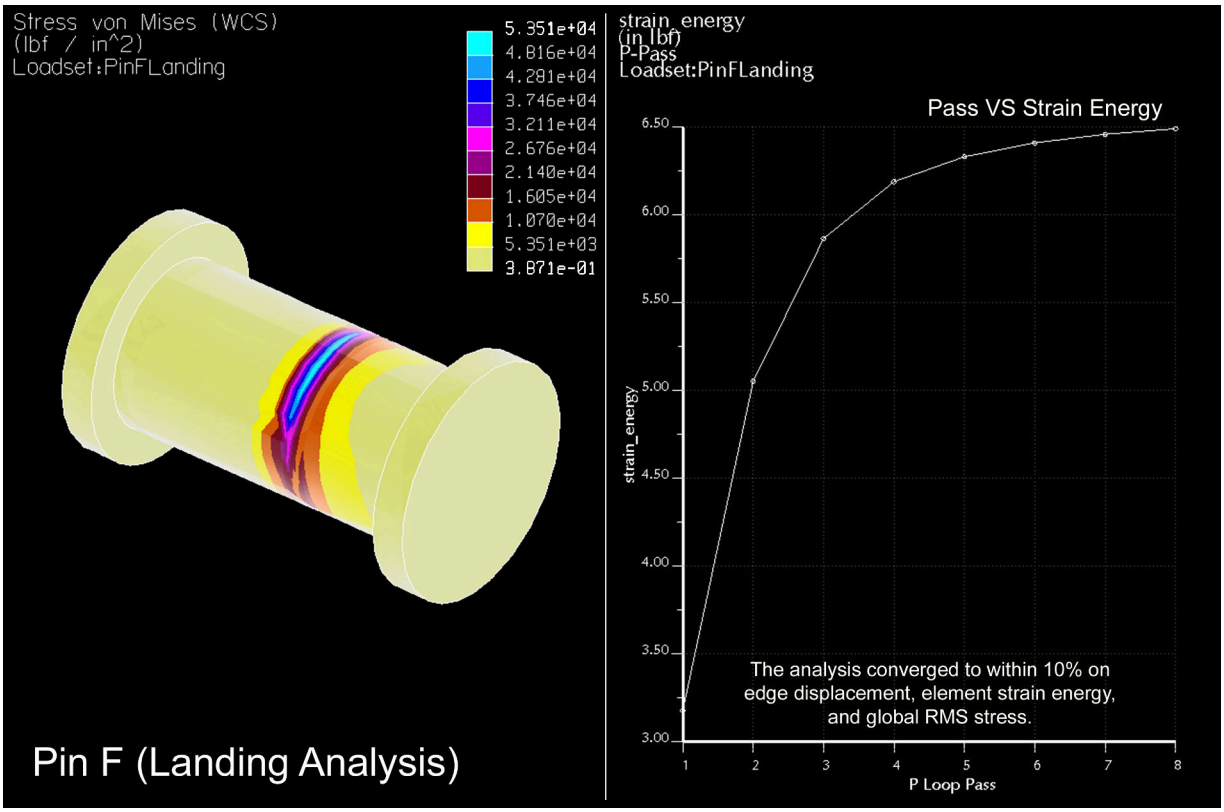

Appendix A-4 Figure 6 – Pin F Landing

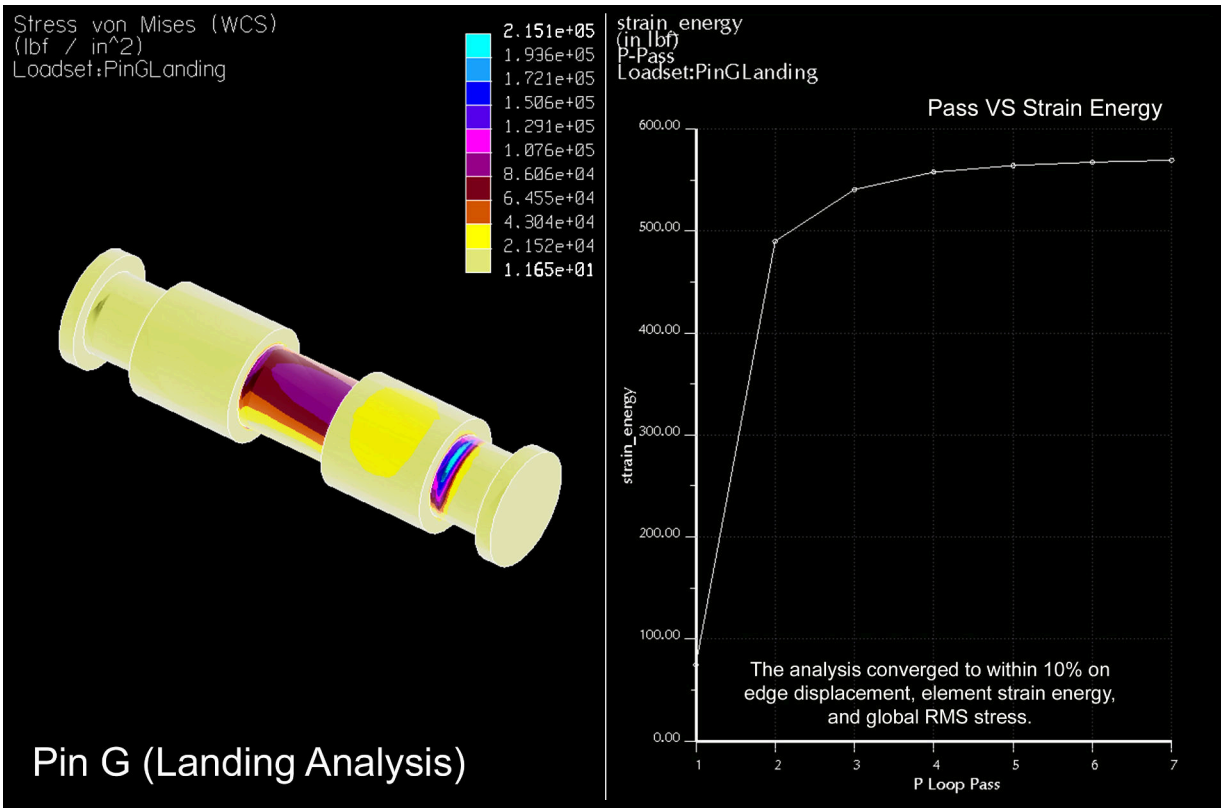

Appendix A-4 Figure 7 – Pin G Landing

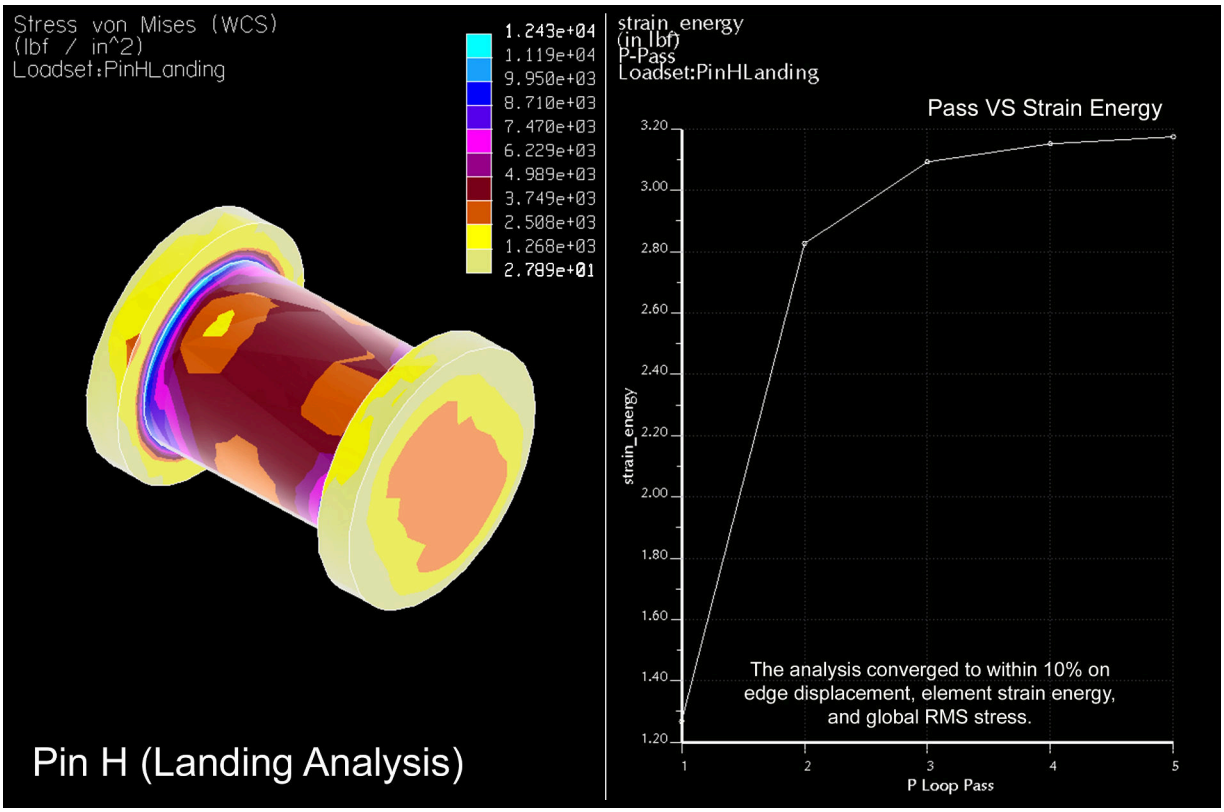

Appendix A-4 Figure 8 – Pin H Landing

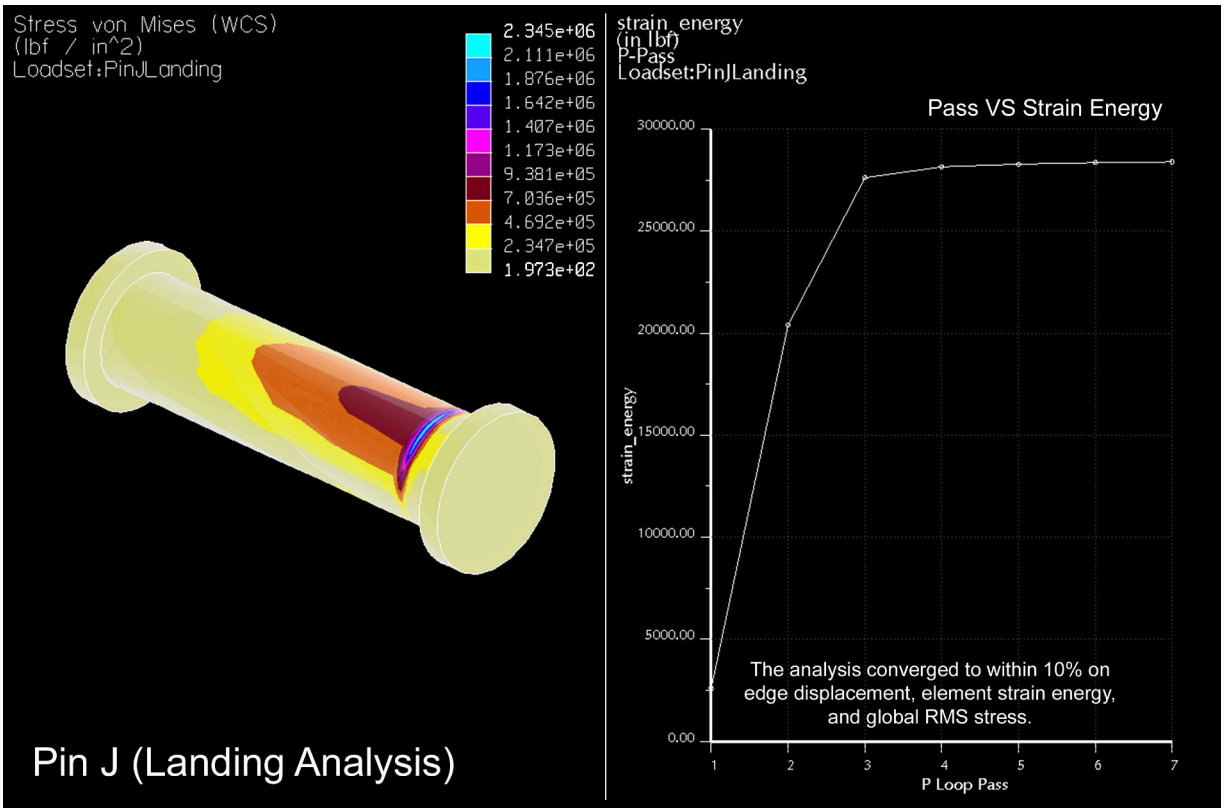

Appendix A-4 Figure 9 – Pin J Landing

APPENDIX A-5: ACCELERATION VERIFICATION MATLAB CODE

```
%Velocity and acceleration check for pin F

clear all
close all

%Declare variables
Pr=30.70; DG=15.70; DF=13.75;

%Declare symbolic variables
syms tsym Pp Pd theta;

%Create symbolic equation for theta
Pp=-5.63*cos(2*pi*tsym/8)+5.63;
Pd=Pr+Pp;
theta=acos((759+DG^ 2-Pd^ 2)/(55.1*DG))-acos((759+DG^ 2-Pr^ 2)/(55.1*DG));

%Symbolically calculate the derivatives of theta
thetadot=diff(theta,tsym);
thetadotdot=diff(thetadot,tsym);

%Create the time domain exactly as it was created in Pro/Engineer
t=0:.02:4;

%Create arrays for the velocity and acceleration magnitude of pin F
for it=1:length(t)
    tsym=t(it);
    velocity(it)=eval(thetadot)*DF;
    accelnorm(it)=(eval(thetadot)^ 2)*DF;
    acceltang(it)=eval(thetadotdot)*DF;
    accelmag(it)=sqrt((accelnorm(it)^ 2)+(acceltang(it)^ 2));
end

set (0,'defaultaxesfontsize',14); % Set default font size for all plots

%Plot velocity and acceleration magnitude of pin F
figure(1)
plot(t,velocity,'LineWidth',2);
title('Velocity of Pin F WRT Ground Pin D vs Time');
xlabel('Time (sec)');
ylabel('Velocity (in/sec)');
grid on
figure(2)
plot(t,accelmag,'LineWidth',2);
title('Acceleration of Pin F WRT Ground Pin D vs Time');
xlabel('Time (sec)');
ylabel('Acceleration Magnitude (in/sec squared)');
grid on
```

```
%Print velocity and acceleration magnitude at time of interest
disp('1st Point of Interest');
T1=t(71)
V1=velocity(71)
A1=accelmag(71)
disp('2nd Point of Interest');
T2=t(106)
V2=velocity(106)
A2=accelmag(106)
disp('3rd Point of Interest');
T3=t(156)
V3=velocity(156)
A3=accelmag(156)
```

Resulting Output

```
1st Point of Interest

T1 =
   1.4000

V1 =
   4.2827

A1 =
   2.7672

2nd Point of Interest

T2 =
   2.1000

V2 =
   5.6243

A2 =
   2.6588

3rd Point of Interest

T3 =
   3.1000

V3 =
   5.5502

A3 =
   3.1508
```